Site Characterisation for Geological Storage of Carbon Dioxide: Examples of Potential Sites from the North West Shelf, Australia

Catherine M. Gibson-Poole

B.Sc. (Hons.) Geology – Royal Holloway University of London, UK

M.Sc. Micropalaeontology – University of Southampton, UK

Australian School of Petroleum

The University of Adelaide

This thesis is submitted in fulfilment of the requirements of Doctor of Philosophy in the Faculty of Science, The University of Adelaide

August 2009

CHAPTER 1. INTRODUCTION

1.1 RATIONALE

Carbon dioxide (CO_2) is one of the gases in the atmosphere that contribute to the 'greenhouse effect', the natural phenomenon that keeps the Earth's climate hospitable and conducive to life (Commonwealth Bureau of Meteorology, 2003). However, in recent years there has been increasing international concern that anthropogenic greenhouse gas emissions to the atmosphere are enhancing the natural greenhouse effect, resulting in global warming with a projection that will have adverse consequences for humanity (Houghton, 2004). The combustion of fossil fuels over the last century has been blamed in particular as one of the major contributors to increased anthropogenic emissions of CO_2 (Houghton, 2004). Thus, practical and economic solutions are being sought by industry to combat this problem. Geological storage of CO_2 is one possible method for reducing large volumes of greenhouse gas emissions.

1.1.1 CO_2 and Climate Change: the Debate

Carbon dioxide concentrations in the atmosphere have increased 31% since the year 1750, from about 280 ppm to almost 370 ppm (Figure 1.1). The large increase is attributed to anthropogenic emissions during the industrial era (IPCC, 2001). The combustion of fossil fuels is the main contributor, although studies indicate that 25% of anthropogenic CO_2 emissions during the past 20 years are also due to land-use change, especially deforestation (IPCC, 2001).

NOTE:
This figure is included on page 1 of the print copy of the thesis held in the University of Adelaide Library.

Figure 1.1 Change in global atmospheric concentration of carbon dioxide over the past 1000 years. The symbols indicate ice core and fern data for several different Antartica and Greenland sites and the line represents direct atmospheric samples taken over the past few decades (after IPCC, 2001).

The global average surface temperature has increased by approximately 0.6°C since the year 1861. Studies have also shown that the rate and duration of warming during the Twentieth Century in the Northern Hemisphere has been much greater than in any of the previous nine centuries (Figure 1.2) (IPCC, 2001).

NOTE:
This figure is included on page 2 of the print copy of the thesis held in the University of Adelaide Library.

Figure 1.2 Variations of the Earth's surface temperature. (a) The past 140 years. The red bars indicate year by year values (with the thin black bars representing the 95 % confidence range) and the black curve indicates the aproximate decade by decade values. (b) The past 1000 years. The blue curve indicates year by year values (with the grey region representing the 95 % confidence range) and the black curve the 50-year average (the red data as per part (a)) (after IPCC, 2001).

Whilst these data are interpreted to indicate that the Earth's climate is warming, other researchers argue that when compared with geological history, the Twentieth Century warming is no greater in rate or magnitude than many natural variations that have occurred in the geological past (Bluemle *et al.*, 2001; Davis & Bohling, 2001; Jenkins, 2001). In addition, the current perception of warming may also be an artefact of the scale of analysis (Gerhard & Hanson, 2001). For example, a 20-year average record of $\delta^{18}O$ values from Greenland ice cores indicates both cooling and warming trends, dependent on the timescale investigated (Figure 1.3). The time since the industrial revolution (~100 years before present) is a rapid warming trend, but the period since the start of the 'Little Ice Age' (~700 years before present) is constant, whilst at larger timescales the entire Christian era (~2,000 years before present) exhibits a cooling trend, as does the whole of the Holocene (~10,000 years before present) (Davis & Bohling, 2001). If, however, the recent warming trend is 'real', then global warming is a significant environmental concern. The most recent findings from the Intergovernmental Panel on Climate Change (IPCC) state that warming of the climate system is unequivocal, based on the evidence of observations of increases in global average air and ocean temperatures, widespread melting of snow and ice, and rising global average sea level (IPCC, 2007).

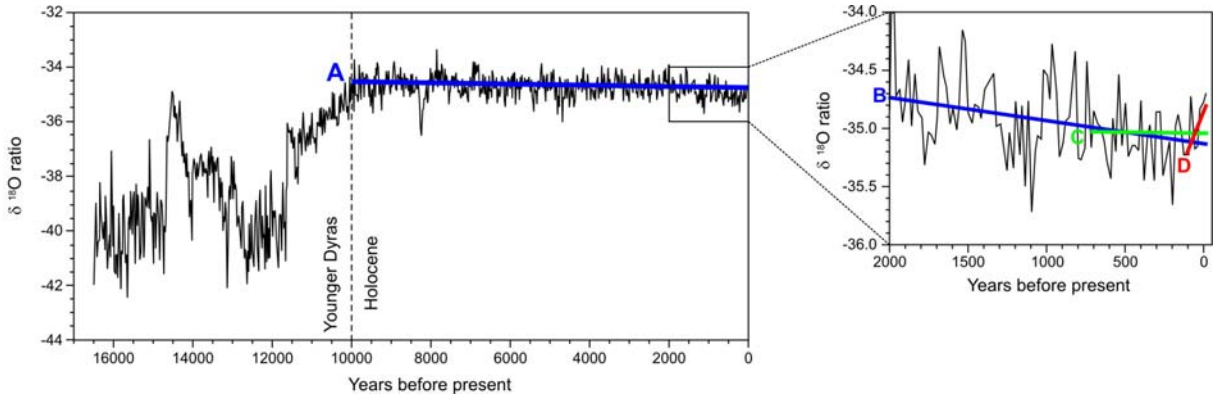

Figure 1.3 Long-term trends in 20-year $\delta^{18}O$ ratios measured on the GISP2 Greenland ice core: A = cooling trend since start of Holocene (10,000 B.P.); B = cooling trend since start of Christian era (2,000 B.P.); C = constant trend since start of Little Ice Age (700 B.P.); D = warming trend since start of industrial revolution (100 B.P.) (modified after Davis & Bohling, 2001).

If global warming is occurring, then the more important question is whether anthropogenic increases in CO_2 emissions are responsible for the rise in global temperature. Calculations by Idso (1998) indicated that a doubling of the atmosphere's CO_2 concentration (300 ppm to 600 ppm) would raise the Earth's average surface temperature by about 0.4°C. Current observations show that the increase in global average surface temperature has already exceeded 0.4°C but CO_2 emissions have only increased by less than a third of the estimated required value, suggesting that other factors, such as solar energy output, may be responsible (Idso, 1998). Recent studies by the IPCC, however, state that most of the observed increase in global average temperatures since the mid-Twentieth Century is very likely (>90% probability) due to the observed increase in anthropogenic greenhouse gas concentrations (IPCC, 2007). Simulated Earth temperature variations compared with measured results (Figure 1.4) show that natural forcings alone (i.e. solar irradiance and volcanic eruptions) do not adequately represent the trends seen in the Twentieth Century. Anthropogenic forcings (i.e. greenhouse gases and sulphate aerosols) provide a much improved estimate, particularly in the second half of the Twentieth Century, although the best match is obtained when both natural and anthropogenic forcings are included (IPCC, 2001, 2007). It is this type of evidence that clearly indicates anthropogenic increases in CO_2 are having a detrimental effect on the global climate, and that measures need to be taken to reduce anthropogenic CO_2 emissions to atmosphere.

Figure 1.4 Simulated annual global mean surface temperature variations of the Earth compared to measured changes, for: (a) natural forcings only – solar variation and volcanic activity; (b) anthropogenic forcings only – greenhouse gases and sulphate aerosols; and (c) both natural and anthropogenic forcings (after IPCC, 2001).

1.1.2 Geological Storage of CO_2: a Potential Solution

The science of climate change is still being actively researched and debated; however, enough scientific evidence has been accumulated for the international community to begin taking precautionary steps to reduce anthropogenic CO_2 emissions (Cook *et al.*, 2000; Gerhard & Hanson, 2001; Bachu, 2003). Fuel switching, improvement in energy efficiency and use of renewable sources of energy in place of fossil fuels are some of the measures that have been proposed to reduce anthropogenic greenhouse gas emissions. The first two options are measures that can be put in place in the short- to medium-term; however, the production of energy from non-carbon sources will require a significant change in the global energy system and is a longer-term solution. Thus, storage of carbon dioxide is an option that could be implemented in the short-term to achieve significant reductions in anthropogenic emissions whilst zero-emission renewable energy technologies are improved (Bradshaw & Cook, 2001; Gale *et al.*, 2001; Lewis & Shinn, 2001).

There are numerous options for storage of CO_2, the most significant of which are ocean storage, geological storage and biological storage (e.g. forestry) (Freund & Ormerod, 1997). Ocean storage has the greatest potential storage capacity (upwards of 1000 Gt), but there are major concerns regarding the impact this may have on the marine environment and the resolution required on the considerable legal and jurisdictional issues (Freund & Ormerod, 1997). Forestry is currently very low in cost, but a large area of land is required with maintenance for several hundred years for just one single power plant (e.g. 1400 km^2 for one 500 MW coal-fired power plant), thus may not be suitable for many economic, social and political situations (Freund & Ormerod, 1997). Geological storage of CO_2, the concept of 'putting it back where it came from', is potentially a very suitable solution to the problem of reducing anthropogenic greenhouse gas emissions (Cook *et al.*, 2000; Bradshaw & Cook,

2001). Potential storage capacity is high (100s of Gt), it utilises well-established technology and knowledge developed in the petroleum industry, and can be implemented immediately (pending legislation) (Freund & Ormerod, 1997; Bradshaw & Cook, 2001).

1.1.3 The GEODISC™ Research Program

The Australian Petroleum Cooperative Research Centre (APCRC) coordinated the GEODISC™ Program, which was designed to investigate the technological, environmental and commercial feasibility of geological storage of carbon dioxide in Australia. The collaborative GEODISC™ research program comprised a four-year study undertaken by the research organisations and universities associated with the APCRC and sponsored by members of the petroleum industry and Government (Cook *et al.*, 2000; Bradshaw & Rigg, 2001).

Part of this wide-ranging research involved regional assessment of sedimentary basins across Australia, identifying, screening and ranking potential CO_2 storage sites. A potential site is termed an Environmentally Sustainable Site for CO_2 Injection or 'ESSCI' (Bradshaw & Rigg, 2001; Rigg *et al.*, 2001; Bradshaw *et al.*, 2002). The new term was devised to encompass all the various components of a CO_2 injection site (such as reservoir, seal and trap) in a similar manner to a hydrocarbon prospect or play. The ESSCIs were assessed in terms of their location logistics, injectivity potential, containment security, storage capacity and existing natural resources (Bradshaw & Rigg, 2001; Rigg *et al.*, 2001; Bradshaw *et al.*, 2002). After reviewing over 100 ESSCIs, four were selected by the GEODISC™ Program for further detailed studies. The conceptual sites comprised one depleted gas field and three deep saline formations, each with varying geographical, geological and technical characteristics. Two of the deep saline formation sites, in the Petrel and Barrow sub-basins, are the focus for this PhD study.

1.2 AIMS AND OBJECTIVES

The primary aim of this PhD study is to utilise the principles of sequence stratigraphy and reservoir characterisation to develop detailed geological models of two possible sites for geological storage of carbon dioxide on the North West Shelf of Australia. The conceptual sites to be investigated are located offshore in the Petrel Sub-basin and the Barrow Sub-basin. Two non-hydrocarbon-bearing stratigraphic intervals are to be considered in the Petrel Sub-basin: the Jurassic Plover and Elang formations, sealed by the Frigate Formation, and the

overlying Cretaceous Sandpiper Sandstone, sealed by the Bathurst Island Group. The Plover and Elang formations are the primary injection target but the Sandpiper Sandstone will also be assessed as a secondary target in case of communication between the two ESSCIs. In the Barrow Sub-basin, the interval of interest is the Cretaceous Flag Sandstone, sealed by the overlying Muderong Shale. This interval is a major hydrocarbon-producing zone, but any injection wells will be sited within the water-leg (saline part) of the system, down-dip of any existing oil and gas fields. The objectives for each site are to:

- Define the structural and stratigraphic framework of the injection horizon and overlying seal;
- Assess the likely geometry, connectivity and injection quality of the reservoir units;
- Assess the likely distribution, continuity and containment security of the seal units;
- Identify the potential CO_2 migration pathways and trapping mechanisms;
- Calculate the pore volume and likely CO_2 storage capacity achievable; and
- Integrate petrological, geomechanical and hydrodynamic analyses to assess their impact on injectivity, containment and capacity.

1.3 PREVIOUS WORK

Research into geological storage of CO_2 was first published in the public domain in the early 1990s, following the First International Conference on Carbon Dioxide Removal held 4–6 March, 1992, in Amsterdam (Blok *et al.*, 1992). Initially, many papers were concerned only with calculating potential CO_2 geological storage capacity for various countries or globally, e.g. Koide *et al.* (1992), Hendriks and Blok (1993), Tanaka *et al.* (1995) and Hendriks and Blok (1995). These estimates were highly variable due to the considerable differences in the parameters used and the assumptions made about the likely storage concept and the volumes of storage space available. The topic of geological CO_2 storage picked up interest through the 1990s, with the publication of some key landmark papers, e.g. Gunter *et al.* (1993), Holloway and Savage (1993), van der Meer (1993), Bachu *et al.* (1994), Holloway (1997) and Rochelle *et al.* (1999). The first operational CO_2 geological storage project commenced in late 1996 at the Sleipner Field in the Norwegian sector of the North Sea (Korbøl & Kaddour, 1995; Baklid *et al.*, 1996). Interest in geological storage of CO_2 accelerated in the new millennium. International research projects of note include: the IEA GHG Weyburn CO_2 Monitoring and Storage Project, which studied the CO_2 enhanced oil

recovery project at the Weyburn Field in Saskatchewan, Canada (Wilson & Monea, 2004); the joint industry partners CO_2 Capture Project (CCP), which researched new technologies to reduce the cost of capturing CO_2 from combustion sources and safely store it underground (Thomas & Benson, 2005); and the Saline Aquifer Carbon Dioxide Storage (SACS) project, which monitored the storage of CO_2 at the Sleipner Field in the North Sea (Torp & Gale, 2004).

Applying the concept of geological storage of CO_2 to areas in Australia is new research that was undertaken by the GEODISC™ Program, for which this PhD study was a component. It involved using existing techniques and knowledge from the petroleum industry, but applying that experience to the concept of storage, rather than exploration, to sedimentary basins around Australia. Key outcomes from the GEODISC™ Program research have been a series of published papers on a wide range of topics, for example: regional assessment and source-to-sink matching (Bradshaw *et al.*, 2004), detailed site characterisation (Gibson-Poole *et al.*, 2005), long-term numerical simulation (Ennis-King *et al.*, 2005), geomechanical impacts of CO_2 injection (Streit & Hillis, 2004), geophysical monitoring (McKenna *et al.*, 2003), risk assessment (Bowden & Rigg, 2004), CO_2 storage economics (Allinson *et al.*, 2003) and natural CO_2 accumulations as analogues (Watson *et al.*, 2004b).

This PhD is the first detailed study of two conceptual CO_2 storage sites on the North West Shelf of Australia. In the Petrel Sub-basin, the regional tectonic evolution and geological framework has been published in key papers by Gunn (1988), Lee and Gunn (1988), Mory (1988), O'Brien *et al.* (1993), O'Brien *et al.* (1996) and Colwell and Kennard (1996). Most publications relating to the detailed geology have only dealt with the older successions (which are of interest to the petroleum industry) than those studied for this PhD. Only one sequence stratigraphic interpretation has been published in the Petrel Sub-basin over the interval of interest (Messant *et al.*, 1994), however, it was a very different interpretation to that presented here.

The Barrow Sub-basin is a major petroleum province, therefore there are many publications on the regional tectonic evolution and geological framework, key of which include Kirk (1985), Kopsen and McGann (1985), Boote and Kirk (1989), Baillie and Jacobsen (1997) and Romine *et al.* (1997). Detailed sedimentology of the Flag Sandstone has been discussed in Osborne and Howell (1987), de Boer and Collins (1988) and Howell (1988). Despite being an active hydrocarbon production interval, little detail has been published on the Flag Sandstone in the last 15 years or so, especially on the sequence stratigraphy within the chosen study area. This PhD study has therefore been able to provide

a revised sequence stratigraphic framework for the area, incorporating an increased database of sedimentary core, well logs and seismic since previous published interpretations. For both sub-basins, there have been no previous studies on the potential for geological storage of CO_2. The key results from this PhD study have been published in Gibson-Poole *et al.* (2002), Gibson-Poole *et al.* (2004) and Gibson-Poole *et al.* (2005).

1.4 LOCATION AND GEOLOGICAL OVERVIEW OF STUDY AREAS

The study areas for this PhD are located within the Petrel and Barrow sub-basins, on the North West Shelf of Australia. The North West Shelf is the name given to the geographic region bordering the coast of northwest Australia, mostly offshore of Western Australia but also extending into offshore Northern Territory at the northern end (Purcell & Purcell, 1988) (Figure 1.5). It encompasses more than the physiographic continental shelf and extends out from the coastline or the edge of the Proterozoic Australian craton to the approximate continent-ocean boundary. It stretches from North West Cape in the south to Melville Island in the north and covers an area of ~800,000 km^2 (Purcell & Purcell, 1988; AGSO North West Shelf Study Group, 1994; Longley *et al.*, 2002).

NOTE:
This figure is included on page 8 of the print copy of the thesis held in the University of Adelaide Library.

Figure 1.5 Location map of the North West Shelf, Australia (modified after Longley *et al.*, 2002; bathymetric image courtesy of Geoscience Australia).

The Phanerozoic sedimentary basins which underlie the present day continental shelf and slope area of the North West Shelf are, from south to north, the Northern Carnarvon Basin, the Offshore Canning Basin, the Browse Basin and the Bonaparte Basin. Cumulatively, these basins are referred to as the Westralian Superbasin (Yeates *et al.*, 1987). The individual depocentres that make up the Westralian Superbasin all share a common northeast structural grain with predominantly Mesozoic sedimentary fill, in contrast to the northwest-trending onshore basins with thick Palaeozoic sedimentary fill and only a thin drape of younger sediments (Bradshaw *et al.*, 1988). The Petrel Sub-basin and the Barrow Sub-basin, which are the foci of this study, are located within the Bonaparte Basin and the Northern Carnarvon Basin respectively (Figure 1.5).

1.4.1 Regional Geological Evolution of the North West Shelf

The development of the sedimentary basins that make up the North West Shelf is related to successive cycles of rifting and break-up associated with the supercontinent of Gondwana (Purcell & Purcell, 1988). The sedimentary fill of the basins is up to 17 km thick, ranging in age from Palaeozoic to Holocene (Figure 1.6), and comprises several superimposed basin sequences. These can be summarised into three principal phases: Palaeozoic northwest-trending intracratonic basins, Mesozoic northeast-trending rift basins, and Late Cretaceous to Holocene open marine margin (Purcell & Purcell, 1988). The latitude position of the North West Shelf also changed significantly during this 500 million year time span, resulting in different climatic environments at various different times, ranging from glacial to tropical conditions (Bradshaw *et al.*, 1988).

Initial rifting for the basins of the North West Shelf occurred during the Cambrian, with intracratonic rifting creating the southern Bonaparte, Canning and Southern Carnarvon basins (preserved principally in the present-day onshore region) (Purcell & Purcell, 1988; Baillie *et al.*, 1994). A shallow west-northwest trending seaway extended into the Canning Basin from central Australia in the Early Ordovician, persisting intermittently until the mid-Carboniferous (Baillie *et al.*, 1994). The Australian continent occupied low latitudes during the Early Palaeozoic, resulting in a tropical palaeoclimate, and a number of the basins had deposition of evaporites and reef carbonates. By the Late Palaeozoic, however, the Australian continent had moved south to higher latitudes and glacial conditions ensued (Bradshaw *et al.*, 1988; Baillie *et al.*, 1994). The Westralian Superbasin developed along the present-day Western Australia margin by the mid-Carboniferous to Early Permian (Figure 1.7), into which

Figure 1.6 Generalised lithostratigraphy, relative coastal onlap curve and palaeolatitude of the North West Shelf (modified after Bradshaw *et al.*, 1988). The study intervals within the Petrel and Barrow sub-basins are also indicated.

there was widespread deposition of glacial sediments (AGSO North West Shelf Study Group, 1994; Baillie *et al.*, 1994). The glaciation reached its maximum during the Early Permian and the Permian sequence deposited over the North West Shelf region was predominantly clastic, with glacial or glacio-marine facies at the base overlain by shallow marine, deltaic and terrestrial sandstones and mudstones (Bradshaw *et al.*, 1988).

Uplift and rifting recommenced in the Triassic, intensifying through the Early Jurassic, forming the individual northeast-trending depocentres of the Westralian Superbasin (Northern Carnarvon, Offshore Canning, Browse and Bonaparte basins) (Purcell & Purcell, 1988). Triassic climates were temperate to warm as the Australian continent moved back northwards towards lower latitudes. The Triassic sediments are predominantly clastic, with fine-grained marine shales at the base coarsening up to fluvio-deltaic sandstones at the top (Bradshaw *et al.*, 1988). Seafloor spreading commenced in the Argo Abyssal Plain in the Callovian–Oxfordian and the early Indian Ocean was formed as Australia began to separate from India

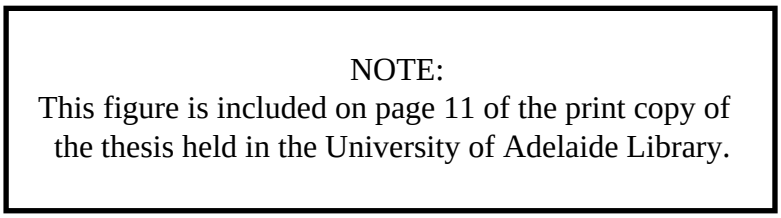

Figure 1.7 Plate tectonic setting of the North West Shelf through time (modified after Doré & Stewart, 2002).

(Figure 1.7) (Bradshaw *et al.*, 1988; Purcell & Purcell, 1988; Baillie *et al.*, 1994). The continental break-up caused rapid deepening of the Jurassic depocentres and resulted in the accumulation of thick marine shales in the troughs and condensed sequences on the platform areas (Bradshaw *et al.*, 1988). India and Australia finally separated in the Early Cretaceous (Valanginian) as Greater India commenced its northwestward rotation away from Australia and Antarctica (Figure 1.7) (Purcell & Purcell, 1988; Baillie *et al.*, 1994). Cretaceous sediments blanketed the entire North West Shelf region, covering the platforms and Jurassic-filled troughs with deltaic sandstones and marine shales (Bradshaw *et al.*, 1988).

From the Late Cretaceous to Holocene, a slowly subsiding open marine margin developed and carbonate sediments accumulated and prograded to build the present day continental shelf (Purcell & Purcell, 1988). The lithological change to dominantly carbonate sedimentation was as a result of the improved oceanic circulation, low relief hinterland and increased climatic warming and aridity as the Australian continent continued to move northwards. A shelf carbonate platform environment was well established by the Middle Eocene and continued northward drift of the Australian continent into tropical latitudes by the Miocene resulted in the development of barrier and patch reef complexes and shelf atolls (Bradshaw *et al.*, 1988). The Indo-Australian Plate collided with Eurasian Plate along the Banda Arc to the north in the Miocene, resulting in extensive folding, faulting and igneous activity plus reactivation of many previous structures within the North West Shelf region (Figure 1.7) (Purcell & Purcell, 1988; Keep *et al.*, 1998).

1.4.2 Petrel Sub-Basin CO_2 Injection and Storage Concept

The Petrel Sub-basin CO_2 storage site is based on the Plover and Sandpiper ESSCIs that were previously identified by Bradshaw *et al.* (2000) during the regional assessment. The Plover and Sandpiper ESSCIs are basin-wide saline formations. The Plover ESSCI comprises the Jurassic Plover and Elang formations as the primary CO_2 injection horizon, sealed by the Frigate Formation (Figure 1.8). The Plover and Elang formations are laterally extensive, fluvial to deltaic sandstones, overlain by lower shoreface to marine shelf siltstones and shales of the Frigate Formation. The Sandpiper ESSCI occurs stratigraphically above the Frigate Formation, comprising the Early Cretaceous Sandpiper Sandstone as the secondary potential injection horizon, sealed by the regionally extensive Bathurst Island Group (Figure 1.8). The Sandpiper Sandstone reservoir is predominantly shoreface sediments, whilst the thick regional seal of the Bathurst Island Group consists of mudstones and limestones deposited in an

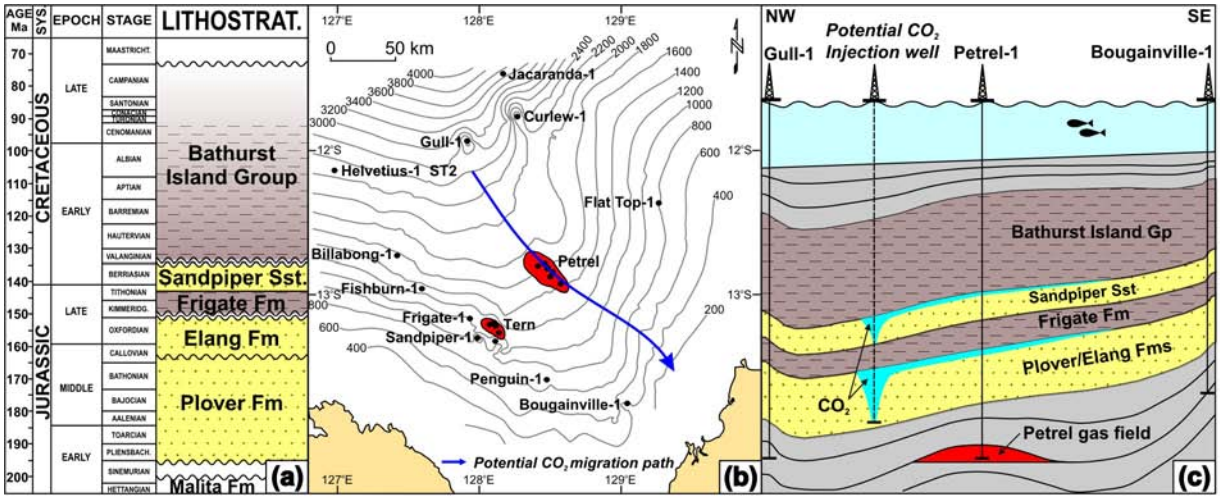

Figure 1.8 Summary of the Petrel Sub-basin CO_2 injection site. (a) Stratigraphic column highlighting the injection horizons (yellow dotted shading) and the seal intervals (brown dashed shading). (b) Depth structure map at the base of the regional seal (Bathurst Island Group), with the predicted primary CO_2 migration pathway highlighted. (c) Simple cross-section (not to scale) of the conceptual injection scenario.

Table 1.1 Summary of key characteristics for the Plover ESSCI of the Petrel Sub-basin case study.

Reservoir	Early–Late Jurassic Plover and Elang formations (primary injection horizon)
Depth to top reservoir (m)	3000–500 m; ~2500 m at potential injection site in between Gull-1 & Petrel-1
Porosity (%)	8–25 %; average 19.1 %
Permeability (mD)	4–1122 mD; average 285 mD
Reservoir thickness (m)	1600–0 m; average 450 m at basin centre
Reservoir areal extent (km^2)	~85,000 km^2
Seal	Late Jurassic Frigate Formation (seal to primary injection horizon)
Seal type	Semi-regional (unproven)
Seal thickness (m)	330–0 m; average 330 m at basin centre
Potential trap mechanism(s)	Hydrodynamic (retention-time); residual; solubility; mineral (Note: no structural closure)
Possible containment risks	Leakage up faults associated with salt diapirs; leakage up old well bores; migration into overlying Sandpiper Sandstone formation due to seal quality of Frigate Formation; loss of CO_2 in the nearshore area due to regional dip and lack of structural closure at injection horizon
Existing resources	Hydrocarbon fields only within deeper Palaeozoic stratigraphy (separated from injection horizons by Early Triassic Mount Goodwin Formation regional seal); limited hydrocarbon prospectivity within injection horizon and above due to low maturity of potential source rocks

Table 1.2 Summary of key characteristics for the Sandpiper ESSCI of the Petrel Sub-basin case study.

Reservoir	Early Cretaceous Sandpiper Sandstone (secondary injection horizon)
Depth to top reservoir (m)	2500–500 m; ~2000 m at potential injection site in between Gull-1 & Petrel-1
Porosity (%)	13–25 %; average 21.5 %
Permeability (mD)	73–3656 mD; average 1673 mD
Reservoir thickness (m)	650–75 m; average 200 m at basin centre
Reservoir areal extent (km^2)	~85,000 km^2
Seal	Cretaceous Bathurst Island Group (seal to secondary injection horizon)
Seal type	Regional (unproven)
Seal thickness (m)	1000–100 m; average 700 m at basin centre
Potential trap mechanism(s)	Hydrodynamic (retention-time); residual; solubility; mineral (Note: no structural closure)
Possible containment risks	Leakage up faults associated with salt diapirs; leakage up old well bores; loss of CO_2 in the nearshore area due to regional dip and lack of structural closure at injection horizon
Existing resources	Hydrocarbon fields only within deeper Palaeozoic stratigraphy (separated from injection horizons by Early Triassic Mount Goodwin Formation regional seal); limited hydrocarbon prospectivity within injection horizon and above due to low maturity of potential source rocks

offshore marine shelf environment. The Jurassic-Cretaceous succession in the Petrel Sub-basin is non-prospective for hydrocarbons; oil and gas accumulations exist only in the underlying Palaeozoic rocks. Figure 1.8, Table 1.1 and Table 1.2 summarise the key characteristics of the Petrel Sub-basin case study.

1.4.3 Barrow Sub-Basin CO_2 Injection and Storage Concept

The Barrow Sub-basin CO_2 storage site is based on the Muderong Shale Subcrop and Flag Sandstone ESSCIs that were previously identified by Bradshaw *et al.* (2000) during the regional assessment. The injection reservoir is the Early Cretaceous Flag Sandstone, a semi-regional hydrocarbon-bearing reservoir of laterally extensive, stacked, amalgamated basin floor fans lobes, which interfinger up-dip with continental slope (Flacourt Formation) and transgressive greensand deposits (Mardie Greensand Member). The seal is provided by the regionally extensive basinal marine shales of the overlying Muderong Shale (Figure 1.9). Injection is envisaged within the water-leg (saline part) of the reservoirs, away from any existing oil and gas fields. Figure 1.9 and Table 1.3 summarise the key characteristics of the Barrow Sub-basin case study.

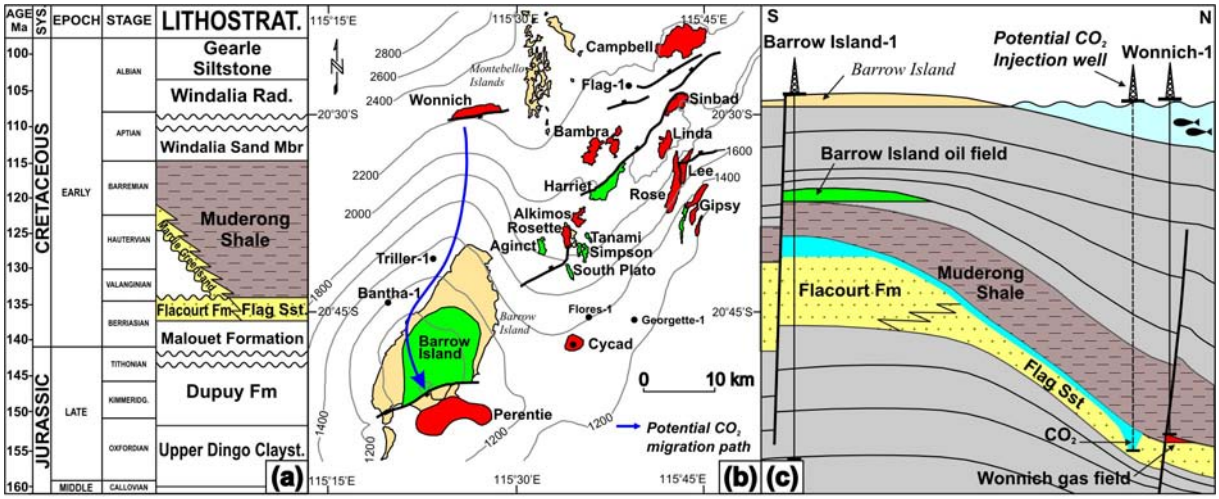

Figure 1.9 Summary of the Barrow Sub-basin CO_2 injection site. (a) Stratigraphic column highlighting the injection horizon (yellow dotted shading) and the seal interval (brown dashed shading). (b) Depth structure map at the base of the regional seal (Muderong Shale), with the predicted primary CO_2 migration pathway highlighted. (c) Simple cross-section (not to scale) of the conceptual injection scenario.

Table 1.3 Summary of key characteristics for the Barrow Sub-basin case study.

Reservoir	Early Cretaceous Flag Sandstone (with up-dip migration into Flacourt Formation and Mardie Greensand Member)
Depth to top reservoir (m)	2900–1300 m; ~2250 m at potential injection site to the south of Wonnich-1
Porosity (%)	3–34 %; average 20.5 %
Permeability (mD)	0.01–7610 mD; average 1096 mD
Reservoir thickness (m)	485–80 m; average 225 m
Reservoir areal extent (km^2)	~2,250 km^2
Seal	Early Cretaceous Muderong Shale
Seal type	Regional; proven hydrocarbon seal
Seal thickness (m)	1025–250 m; average 700 m
Potential trap mechanism(s)	Stratigraphic pinchout/facies change; fault-bound anticline; residual; solubility; mineral
Possible containment risks	Leakage up old well bores; leakage up Barrow Island Fault
Existing resources	Numerous oil and gas fields at multiple stratigraphic intervals (below, within and above selected injected horizon)

CHAPTER 2. GEOLOGICAL STORAGE OF CARBON DIOXIDE

2.1 INTRODUCTION

Geological storage of carbon dioxide is the process whereby CO_2 is captured and separated from a source (such as a high-CO_2 natural gas field, LNG processing plant or coal-fired power station) and is transported and injected into the geological subsurface for long-term storage (Figure 2.1) (Cook *et al.*, 2000; IPCC, 2005). The primary geological constraints for finding the right place to store CO_2 include a porous and permeable reservoir rock (e.g. sandstone) to allow injection and storage of the CO_2, overlain by an impermeable seal rock (e.g. claystone) to retain the injected CO_2 in the geological subsurface (van der Meer, 1992; Bachu *et al.*, 1994; Rochelle *et al.*, 1999).

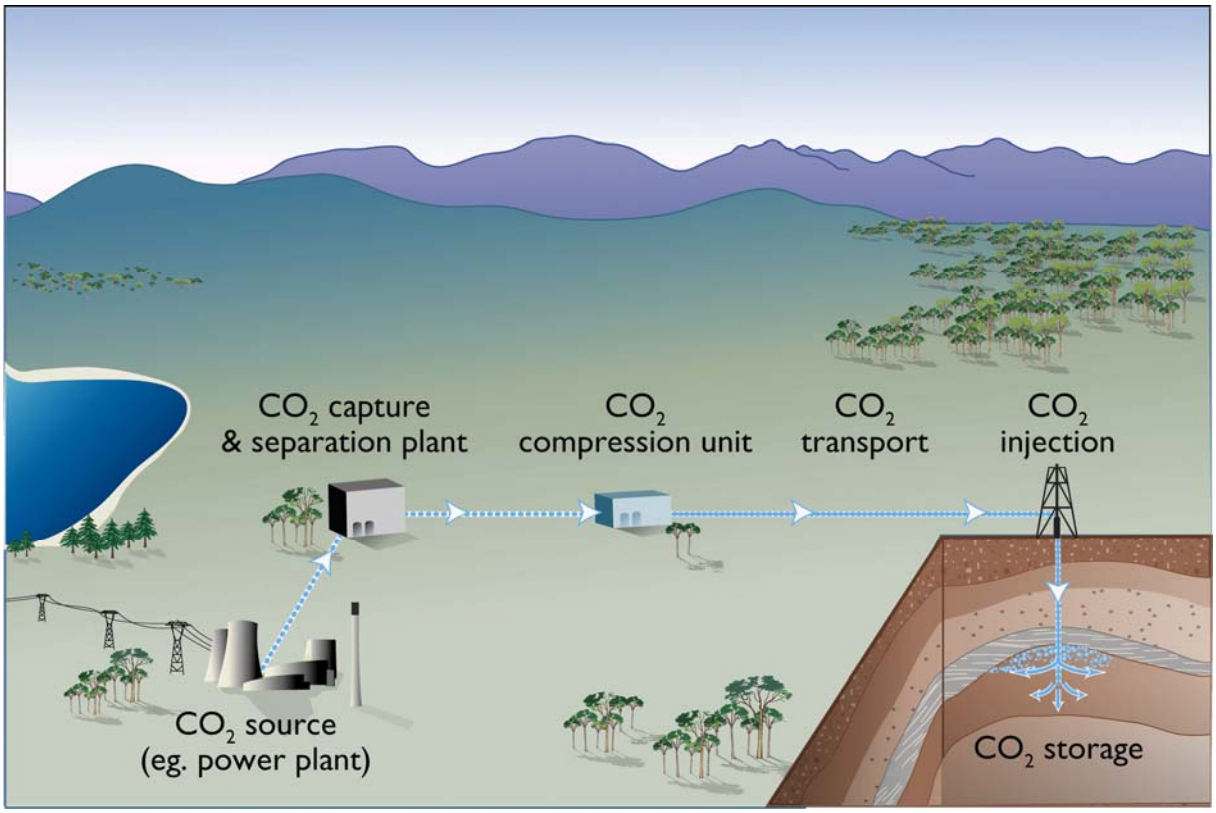

Figure 2.1 A simplified view of the steps involved in CO_2 capture, transport and geological storage (image courtesy of CO2CRC).

2.2 PHYSICAL PROPERTIES OF CO_2

Carbon dioxide will preferentially be injected as a supercritical fluid for geological storage projects, as in this form it is much denser than normal gaseous CO_2 and therefore a

greater volume of CO_2 can be stored in the pore space available (Figure 2.2) (Holloway & van der Straaten, 1995; Cook *et al.*, 2000). Baklid *et al.* (1996) also suggest that the injection of CO_2 as a dense supercritical fluid is preferable due to the complications of hydrate formation in the injection well if the CO_2 is in a gaseous or liquid state.

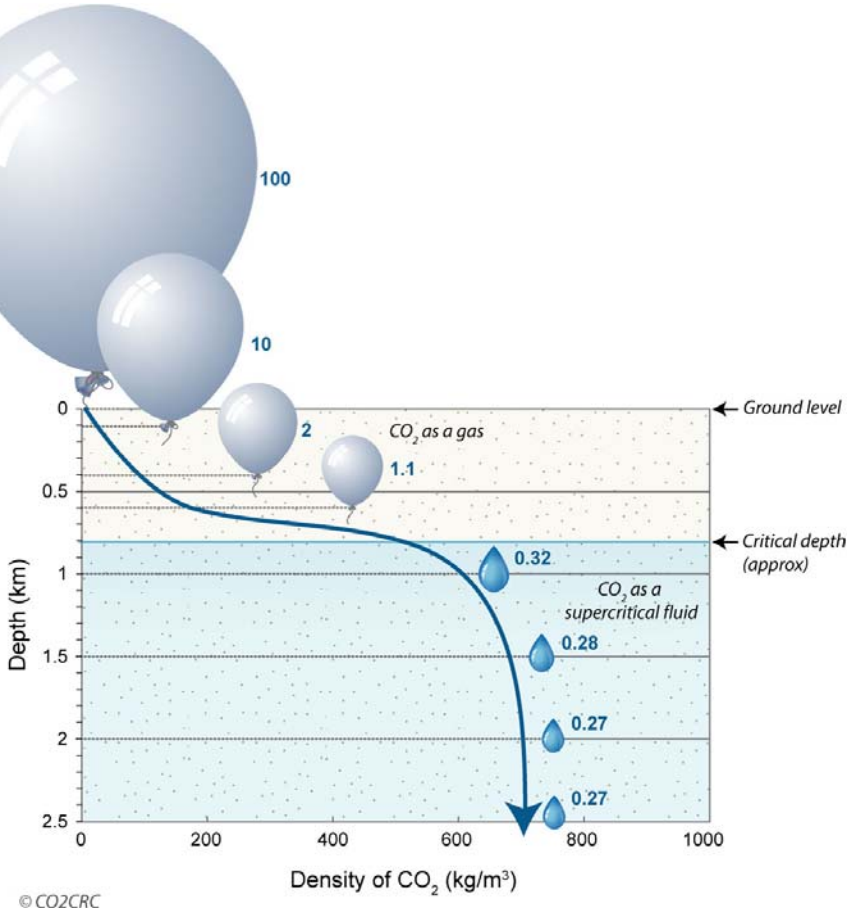

Figure 2.2 Variation of CO_2 density with depth (assuming hydrostatic pressure, geothermal gradient of 25°C/km and surface temperature of 15°C). The size of the balloons/drops represent the relative volume occupied by the CO_2 (image courtesy of CO2CRC).

The critical temperature of CO_2 is 31.1 ºC and the critical pressure is 7.38 MPa (Holloway & Savage, 1993; van der Meer, 1993; Bachu, 2000). At temperatures and pressures above this critical point, CO_2 exists as a supercritical fluid, whereby it has a density similar to a liquid but exhibits gas-type viscosity and behaviour (Holloway & Savage, 1993; van der Meer, 1993; Flett *et al.*, 2003). Figure 2.3 shows the phase relationships of CO_2 as a function of pressure and temperature. The temperature and pressure conditions for each sedimentary basin vary; however, based on average surface temperatures, geothermal and hydrostatic gradients, this equates to an approximate minimum subsurface depth of about 800 m for CO_2 to be in the supercritical phase (van der Meer, 1992; Holloway & Savage, 1993).

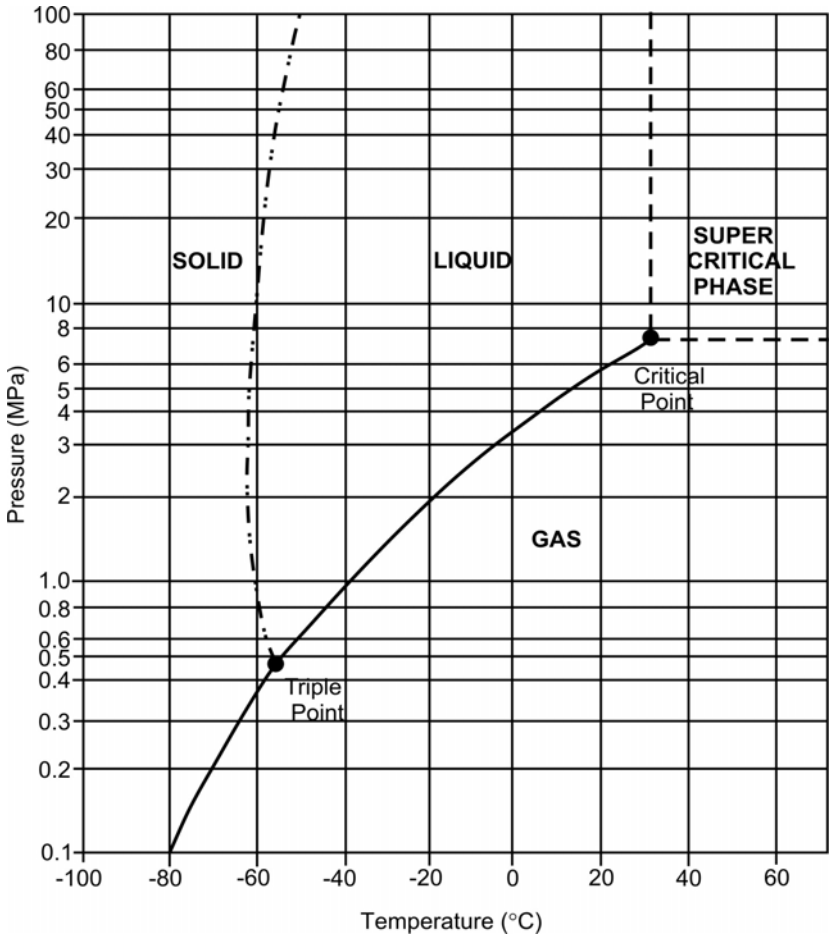

Figure 2.3 Carbon dioxide phase diagram (after Bachu, 2000).

The prevailing temperature and pressure conditions of a sedimentary basin also affect the density and viscosity of CO_2 (Figure 2.4). The density of CO_2 increases sharply at depths between 500–1000 m (under typical sedimentary basin conditions) associated with the phase change of CO_2 to supercritical, and then plateaus to a fairly constant density of around 600–700 kg/m^3 below a depth of about 1000 m (Figure 2.5). These densities are around 30–40% less dense than a typical saline formation water under the same conditions (Ennis-King & Paterson, 2001, 2002). As a result of the significant density difference, the lighter CO_2 will rise upwards by buoyancy through the formation water to accumulate at the highest possible place in the reservoir beneath the seal (van der Meer, 1992; Ennis-King & Paterson, 2001, 2002; Flett *et al.*, 2005). This effect is depth dependent and the intensity of this effect diminishes with increasing depth, although never completely disappearing (van der Meer, 1992; Law & Bachu, 1996).

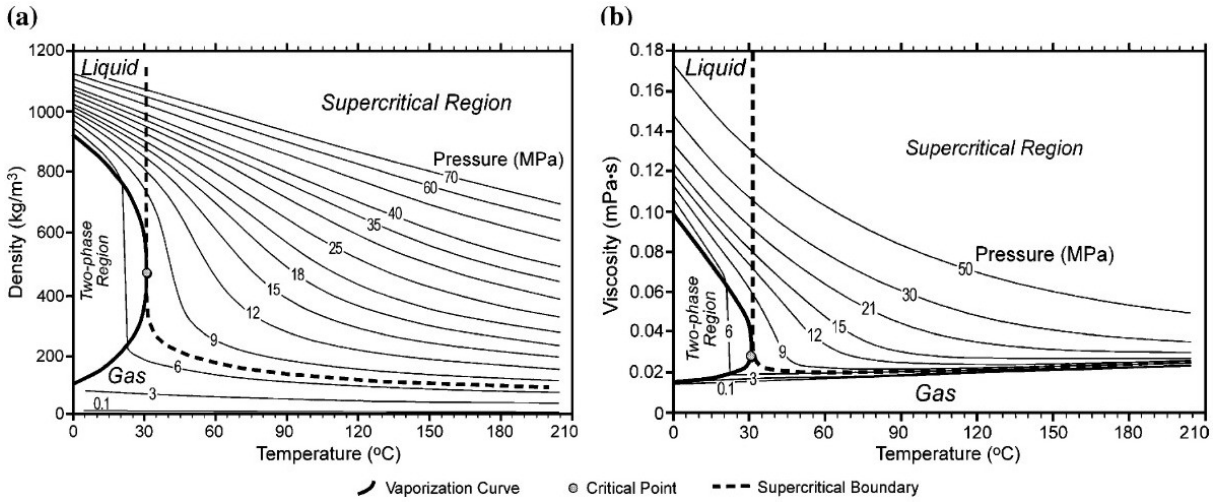

Figure 2.4 Variation of CO_2 (a) density and (b) viscosity as a function of temperature and pressure (after Nordbotten *et al.*, 2005).

NOTE:
This figure is included on page 20 of the print copy of the thesis held in the University of Adelaide Library.

Figure 2.5 CO_2 density and viscosity ratio to brine at typical subsurface conditions (surface temperature 15°C, geothermal gradient 30°C/km, hydrostatic gradient 10 MPa/km, salinity 32000 ppm) (after Ennis-King & Paterson, 2002).

Supercritical CO_2 is significantly less viscous than water or oil by an order of magnitude or more under the same subsurface conditions (IPCC, 2005; Nordbotten *et al.*, 2005). At depths of 1000–3000 m (under typical sedimentary basin conditions) the viscosity ratio of pure CO_2 to a typical saline formation water (e.g. 32000 ppm) varies from 0.05 to 0.2, i.e. it is 20 times less viscous than brine at 1000 m and decreases to 5 times less viscous than brine at 3000 m (Figure 2.5) (Ennis-King & Paterson, 2001, 2002). The difference in mobility between supercritical CO_2 and water means that the CO_2 does not uniformly displace the formation water. This can result in substantial viscous fingering effects, whereby numerous 'fingers' of the displacing fluid (CO_2) develop and penetrate the displaced fluid (water) in an irregular fashion (van der Meer, 1992, 1993; Ennis-King & Paterson, 2001, 2002; Nordbotten

et al., 2005). The mobility ratio between CO_2 and water declines with increasing temperature and pressure, therefore the viscous fingering effect will diminish with increasing depth (van der Meer, 1993; Law & Bachu, 1996; Nordbotten *et al.*, 2005).

2.3 CHEMICAL PROPERTIES OF CO_2

CO_2 is soluble in water, and the level of solubility is variable depending on the specific pressure and temperature conditions, as well as the salinity and chemistry of the *in situ* formation water (Figure 2.6). CO_2 solubility increases with increasing pressure, but decreases with increasing temperature and salinity (Koide *et al.*, 1992; Gunter *et al.*, 1993; Rochelle *et al.*, 1999; Kirste *et al.*, 2004).

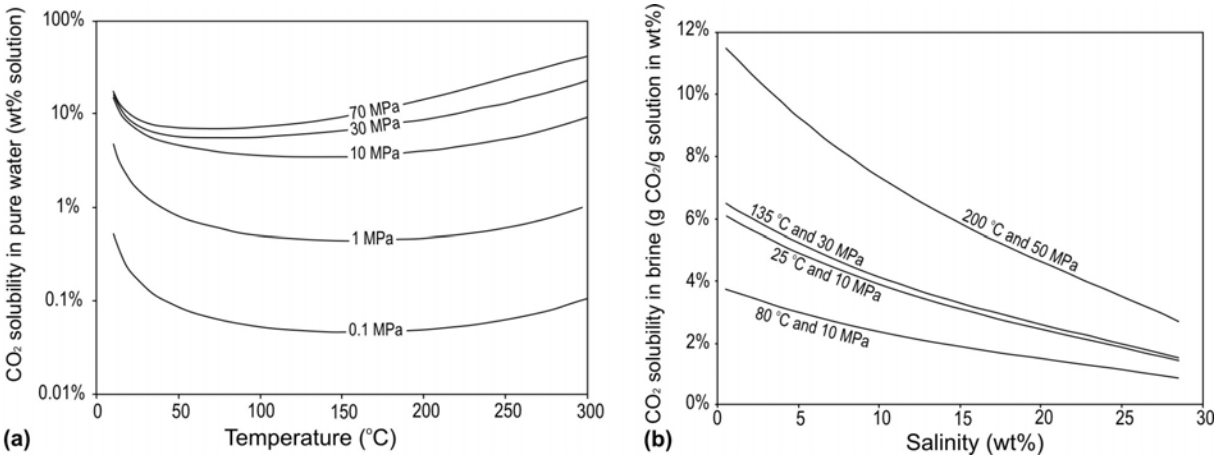

Figure 2.6 Variation of CO_2 solubility in water: (a) with temperature and pressure; and (b) with salinity, for various conditions representative of sedimentary basins (after Bachu & Adams, 2003).

When CO_2 dissolves into water it initially forms carbonic acid, which subsequently dissociates into bicarbonate and carbonate ions, as shown by the following reactions (Eqs. 1–3) (Rochelle *et al.*, 1999; Bachu & Adams, 2003; Kirste *et al.*, 2004):

$$H_2O + CO_2 \leftrightarrow H_2CO_3 \quad [1]$$

water + carbon dioxide ↔ carbonic acid

$$H_2CO_3 \leftrightarrow HCO_3^- + H^+ \quad [2]$$

carbonic acid ↔ bicarbonate + hydrogen

$$HCO_3^- \leftrightarrow CO_3^{=} + H^+ \quad [3]$$

bicarbonate ↔ carbonate + hydrogen

The generation of bicarbonate and carbonate ions release hydrogen ions (H^+), i.e. the pH of the solution is lowered, and the solubility of CO_2 decreases with decreasing pH (Rochelle *et al.*, 1999; Watson *et al.*, 2004a). However, the pH change can be buffered in a system containing mineral phases (e.g. basic aluminosilicate or carbonate minerals present in the host rock) (Rochelle *et al.*, 1999; Kirste *et al.*, 2004). The decrease in pH means that certain mineral phases will no longer be in equilibrium with the formation water, resulting in mineral dissolution and dissociation of cations from the mineral phases. The cations combine with the bicarbonate and hydrogen ions, which buffers the pH change. The consequence of this for the dissolved CO_2 is that it either remains in solution or, if the right conditions exist, it can precipitate out as a new carbonate mineral (Perkins & Gunter, 1995; Bachu *et al.*, 1996; Gunter *et al.*, 1997b; Kirste *et al.*, 2004; Watson *et al.*, 2004a).

The generic reaction for common silicate minerals such as feldspars and clays with CO_2 can be summarised as follows (Eq. 4) (Gunter *et al.*, 1993; Bachu *et al.*, 1996):

$$\text{feldspars} + \text{clays} + CO_2 \leftrightarrow \text{kaolinite} + \text{calcite} + \text{dolomite} + \text{siderite} + \text{quartz} \quad [4]$$

The type of reaction products that occur depend on what cations are released into solution from the reactant mineral phases, as well as the *in situ* pressure, temperature, salinity and pH conditions. For example, sodium (Na^+) or potassium (K^+) cations (e.g. from reaction with feldspars such as albite or orthoclase) combine with the bicarbonate ions and remain in solution (at typical reservoir conditions) (Gunter *et al.*, 1993; Perkins & Gunter, 1995; Gunter *et al.*, 1997b). An example of this is given by the reaction of albite as shown below (Eq. 5) (Watson *et al.*, 2003):

$$2NaAlSi_3O_8 + 3H_2O + 2CO_2 \leftrightarrow Al_2Si_2O_5(OH)_4 + 4SiO_2 + 2NaHCO_{3(aq)} \quad [5]$$

albite + water + carbon dioxide ↔ kaolin + quartz + sodium bicarbonate

If the cations are calcium (Ca^{++}), magnesium (Mg^{++}) or iron (Fe^{++}) (e.g. from reaction with feldspars and clays such as anorthite or chlorite) then the precipitation of new stable carbonate minerals (such as calcite, dolomite and siderite) can occur (Gunter *et al.*, 1993; Perkins & Gunter, 1995; Gunter *et al.*, 1997b; Watson *et al.*, 2004a). An example of this is given by the reaction of magnesium chlorite as shown below (Eq. 6) (Watson *et al.*, 2003):

$$\underset{\text{magnesium chlorite}}{Mg_5Al_2Si_3O_{10}(OH)_8} + 5CaCO_3 + \underset{\text{carbon dioxide}}{5CO_2} \leftrightarrow \underset{\text{dolomite}}{5CaMg(CO_3)_2} + \underset{\text{kaolin}}{Al_2Si_2O_5(OH)_4}$$

$$+ \underset{\text{quartz}}{SiO_2} + \underset{\text{water}}{2H_2O} \qquad [6]$$

2.4 CO_2 Subsurface Flow Behaviour and Storage Mechanisms

The physical and chemical properties of CO_2 influence how it will disperse upon injection into a geological reservoir. The subsurface flow behaviour of the CO_2 is also affected by a number of other variables, such as the rate at which the CO_2 is injected, the natural flow velocity of the existing formation water and the level of heterogeneity within the reservoir rock.

During the injection phase, the migration of the CO_2 away from the injection well involves both gravity override and viscous fingering, as a result of the CO_2 being significantly less dense and less viscous than the saline formation water under typical reservoir conditions (Ennis-King & Paterson, 2001; Nordbotten *et al.*, 2005). Simulations by Holt *et al.* (1995) determined that the rate at which the CO_2 is injected can have an impact on this displacement behaviour. At high injection rates, viscous forces dominate and the CO_2 flows rapidly along the most permeable paths, whereas at lower injection rates gravity forces dominate and buoyancy causes the CO_2 to rise upwards (Figure 2.7). Flow dominated by viscous forces can result in lower storage capacity as pore volume may be bypassed due to preferential flow pathways (Holt *et al.*, 1995). The heterogeneity in the permeability distribution also has a significant impact on the flow behaviour of injected CO_2. If the degree of heterogeneity is large, particularly with respect to the ratio between horizontal and vertical permeability, then channelling of CO_2 along the most permeable paths will be the dominant flow behaviour (van der Meer, 1995; Ennis-King & Paterson, 2001).

Post-injection, the pressure gradient driving the lateral migration relaxes, and CO_2 migration becomes predominantly buoyancy-driven. The CO_2 continues to migrate under the influence of gravity (or buoyancy) and the natural formation water flow (Ennis-King & Paterson, 2001, 2002; Flett *et al.*, 2003; Flett *et al.*, 2005). Stratigraphic heterogeneities, such as intraformational siltstones and shales, play a crucial role in determining the tortuosity of the flow path for migrating CO_2. The intraformational seals act as barriers or baffles to the buoyancy-driven upward flow and induce lateral migration of CO_2 until such time as the CO_2 is able to breach, or migrate beyond, the barrier. This can increase storage capacity as a

greater volume of the pore space may be accessed (Ennis-King & Paterson, 2002; Hovorka *et al.*, 2004; Flett *et al.*, 2005).

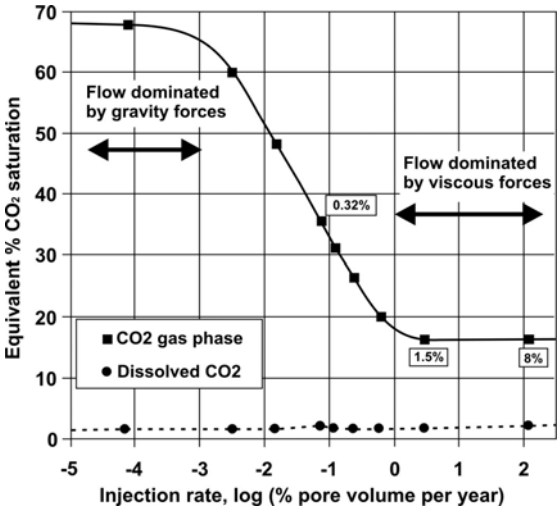

Figure 2.7 Effect of injection rate on dominant flow force and resultant CO_2 storage capacity (after Holt *et al.*, 1995).

Time is also an important factor in the subsurface behaviour of CO_2. With increasing time, more CO_2 dissolves into the formation water (Bachu *et al.*, 1994; Ennis-King & Paterson, 2001). As the CO_2 continues to dissolve into the formation water, it can lead to a phenomenon known as convective mixing. When the CO_2 dissolves into the formation water, the density of the CO_2-saturated water increases to about 1% more than density of the unsaturated water. The dense CO_2-saturated water overlying less dense unsaturated water creates a density instability and plumes of CO_2-rich water flow downward (Figure 2.8) (Lindeberg & Wessel-Berg, 1997; Ennis-King & Paterson, 2002; Lindeberg & Bergmo, 2003; Ennis-King & Paterson, 2005).

NOTE:
This figure is included on page 24 of the print copy of the thesis held in the University of Adelaide Library.

Figure 2.8 Convective mixing of CO_2: example of a numerical simulation showing the high-density plumes of CO_2-saturated brine (grey colours) sinking into the brine column (white colour) below (k_v/k_h = 0.01, after 14400 years) (after Ennis-King & Paterson, 2005).

The subsurface flow behaviour of CO_2, as well as the length of time involved, will influence the ultimate storage mechanism. There are a number of different trapping methods for CO_2 geological storage, which are listed below:

- Structural/stratigraphic trapping
- Hydrodynamic trapping
- Residual trapping
- Solubility trapping
- Mineral trapping
- Adsorption trapping

2.4.1 Structural/Stratigraphic Trapping

Structural/stratigraphic trapping relates to the buoyant free-phase (immiscible) CO_2 that is not dissolved into formation water. When supercritical CO_2 rises upwards by buoyancy it can be physically trapped in a structural or stratigraphic trap (as a result of the CO_2 being the non-wetting phase) in exactly the same manner as a hydrocarbon accumulation. The nature of the physical trap depends on the geometric arrangement of the reservoir and seal units. Common structural traps include anticlinal folds (Figure 2.9a) or tilted fault blocks (Figure 2.9b) and typical stratigraphic traps include those created by a lateral change in facies up-dip, a depositional pinch-out (Figure 2.9c) or an unconformity (Figure 2.9d) (Biddle & Wielchowsky, 1994). As with hydrocarbon accumulations, there are numerous variations of structural and stratigraphic traps, plus combinations of both structural and stratigraphic elements, that can provide physical traps for geological storage of CO_2. In a dipping formation with no defined structural closure, any small bumps in the seal geometry will behave like small anticlinal structural traps and free-phase CO_2 will fill these to the spill point (due to buoyancy) before migration continues (Bergman & Winter, 1995; Lindeberg, 1997; Ennis-King & Paterson, 2002).

2.4.2 Hydrodynamic (Retention-Time) Trapping

Hydrodynamic trapping of CO_2 was defined by Bachu *et al*. (1994) and is not the same concept of hydrodynamic trapping as known from the petroleum industry. Oil and gas can be trapped hydrodynamically when the flow of formation water is opposite to the flow of the migrating hydrocarbons and the hydrodynamic force is sufficient to retain the oil and gas in place (Biddle & Wielchowsky, 1994). Bachu *et al*. (1994) define CO_2 to be

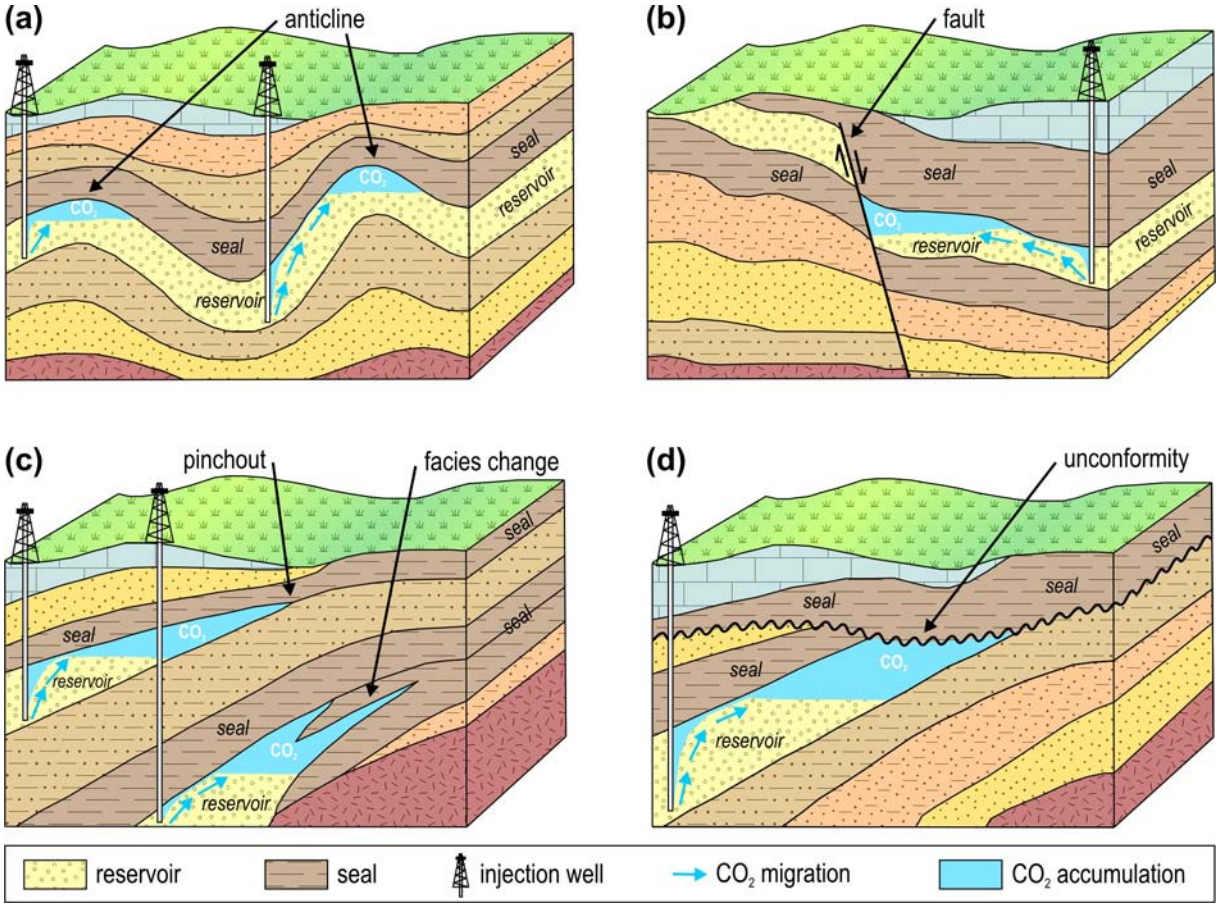

Figure 2.9 Examples of structural and stratigraphic traps for buoyant free-phase CO_2: (a) anticline structural traps; (b) fault structural trap; (c) pinchout and lateral facies change stratigraphic traps; and (d) unconformity stratigraphic trap.

hydrodynamically trapped when the dissolved and immiscible CO_2 travels with the formation water for very long residence (migration) times, of the order of thousands to millions of years (Figure 2.10), i.e. the trapping mechanism is not hydrodynamic *per se* but rather retention time. This trapping concept was developed to allow horizontal or gently dipping reservoirs with no defined structural closures to also be considered as potential storage sites for CO_2. The advantage of this is that the potential pore volume available for storage capacity is vastly increased. Structural and stratigraphic traps are a defined geometric container with storage capacity limited to the physical size and shape of the trap. If a physical structural or stratigraphic trap is not explicitly necessary then a much larger area can be considered for storage, increasing the amount of available pore volume and potential storage capacity.

Ultimately, CO_2 is not trapped by this mechanism, as on long enough time-scales any remaining free-phase CO_2 may escape if it migrates to a point where containment is no longer secure (e.g. the overlying seal rock is no longer present). However, it is the length of time this takes which determines whether hydrodynamic trapping is suitable or not. The disposal

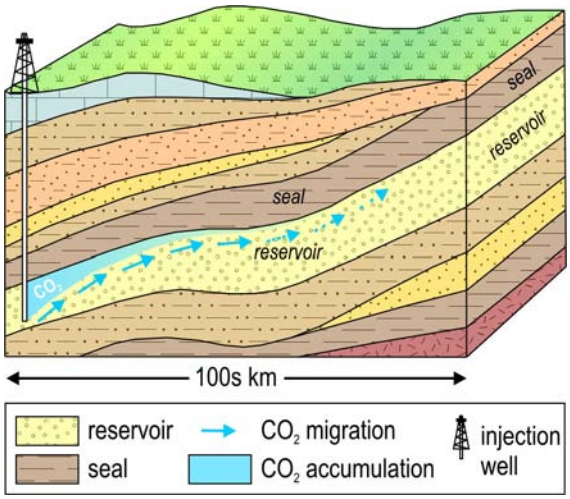

Figure 2.10 Hydrodynamic (retention-time) trapping of CO_2. The CO_2 travels with the *in situ* formation water over large distances beneath a regional seal and is trapped on the basis of long residence time (thousands to millions of years).

of hazardous and non-hazardous industrial waste using this premise is accepted practise in the U.S.A., if the modelling can demonstrate that the injected waste will be retained in the host formation for at least 10,000 years (Bergman & Winter, 1995). The success of hydrodynamic trapping of CO_2 depends on the flow velocity of the *in situ* formation water and the corresponding travel time to reach either the end of the overlying seal or the ~800 m depth limit for the supercritical phase state of CO_2 (Bachu *et al.*, 1994).

Hydrodynamic trapping of CO_2 is perhaps best considered not as a storage mechanism by itself but rather as an aid to trapping CO_2 by other methods. The longer the timeframe and the larger the area that CO_2 travels with the formation water, the more that will become trapped by other storage mechanisms, such as residual trapping and solubility trapping (discussed below).

2.4.3 Residual Trapping

Residual trapping occurs when the CO_2 becomes trapped in the pore space as a residual immobile phase by capillary pressure forces (Figure 2.11) (Ennis-King & Paterson, 2001; Flett *et al.*, 2005). At the tail of the migrating CO_2 plume, imbibition processes are dominant as the formation water (wetting-phase) imbibes behind the migrating CO_2 (non-wetting phase). When the saturation of the CO_2 falls below a certain level it has insufficient buoyancy force to overcome the capillary entry pressures of the pore throats. The CO_2 then becomes trapped in the pores by capillary pressure forces and ceases to flow (Ennis-King & Paterson, 2001; Holtz, 2002; Flett *et al.*, 2003; Flett *et al.*, 2005). Residual CO_2 saturation values vary

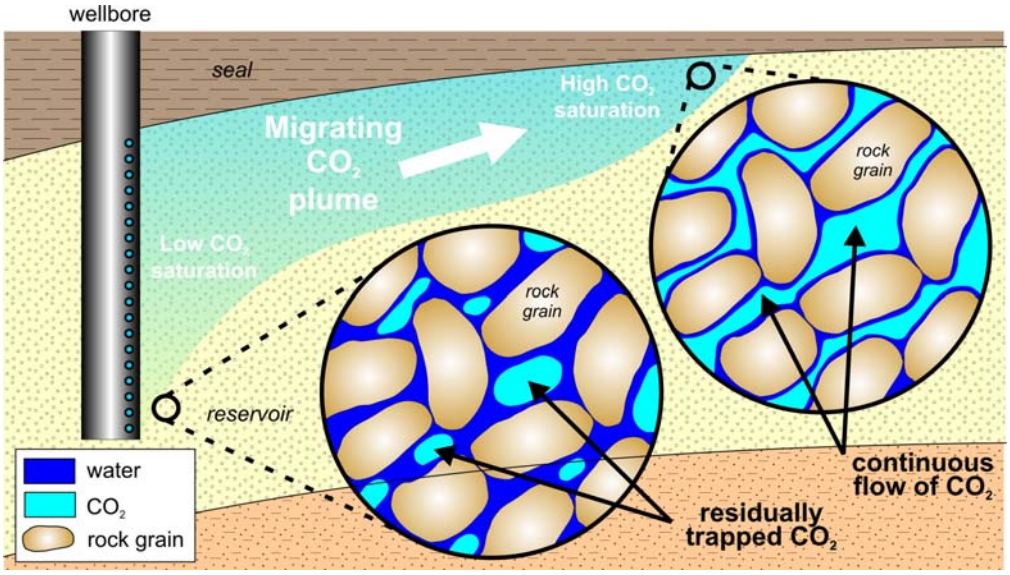

Figure 2.11 Residual trapping of CO_2. At the tail of the migrating plume the CO_2 saturation and buoyancy force is insufficient to overcome the capillary pressure forces of the pore throats and the CO_2 becomes trapped residually in the pore space.

between 5–30% based on typical relative permeability curves (Ennis-King & Paterson, 2001). Over time, the residually trapped CO_2 dissolves into the formation water (Ennis-King & Paterson, 2001; Flett *et al.*, 2005).

2.4.4 Solubility Trapping

Solubility trapping relates to the CO_2 dissolved into the formation water (Figure 2.12) (Koide et al., 1992). The time-scale for complete dissolution is critically dependent on the vertical permeability and the geometry of the top seal, but is predicted to occur on a time-scale of hundreds to thousands of years (Ennis-King & Paterson, 2002). The success of solubility trapping is aided by slow flow velocities of the *in situ* formation water, as this will lead to a greater residence time and allow more time for CO_2 to dissolve into the formation water (Koide et al., 1992; Bachu et al., 1994). Stratigraphic heterogeneities also improve solubility trapping, as they increase the tortuosity of the CO_2 migration path and accordingly the CO_2 is able to contact larger volumes of formation water into which it can dissolve (Lindeberg, 1997; Hovorka et al., 2004; Flett et al., 2005). Convective mixing (resulting from density instability) is also important for solubility trapping of CO_2, as it is orders of magnitude faster than pure diffusion mechanisms, and so accelerates the overall dissolution of the CO_2 into the formation water (Ennis-King & Paterson, 2002, 2005).

NOTE:
This figure is included on page 29 of the print copy of the thesis held in the University of Adelaide Library.

Figure 2.12 Solubility trapping of CO_2. An example of a simulation model showing CO_2 (white to grey colours) dissolving into the *in situ* formation water (black colour) in a homogeneous formation after (a) 930 years and (b) 1330 years (images courtesy of Jonathan Ennis-King, CSIRO).

2.4.5 Mineral Trapping

Mineral trapping of CO_2 results from the precipitation of new carbonate minerals (Figure 2.13) (Gunter *et al.*, 1993). This storage mechanism is the most permanent of the trapping types discussed as it renders the CO_2 immobile (Bachu *et al.*, 1994, 1996). The time-scale for mineral precipitation is typically long, of the order of tens to thousands of years, depending on the initial minerals present (Perkins & Gunter, 1995; Kirste *et al.*, 2004). Siliciclastic reservoirs are favoured over carbonate reservoirs, in particular calcium-, magnesium- or iron-rich siliciclastic reservoirs, as they have the best potential for mineral trapping of CO_2 (Gunter *et al.*, 1993; Bachu *et al.*, 1994; Perkins & Gunter, 1995; Gunter *et al.*, 1997b).

NOTE:
This figure is included on page 29 of the print copy of the thesis held in the University of Adelaide Library.

Figure 2.13 Mineral trapping of CO_2. An example of the precipitation of siderite as a result of CO_2-water-rock interactions, as seen in (a) thin section and (b) scanning electron microscopy, in the Pretty Hill Formation at Garvoc-1, Otway Basin, southeast Australia (after Watson *et al.*, 2004a).

2.4.6 Adsorption Trapping

Adsorption trapping is the mechanism by which CO_2 is stored in coal seams, as opposed to conventional storage in rock pore space like other sedimentary rocks. CO_2 is preferentially adsorbed onto the coal micropore surfaces, displacing the existing methane (CH_4) (Gunter *et al.*, 1997a; Bradshaw & Rigg, 2001; IPCC, 2005). In contrast to porous rock, storage density (i.e. storage capacity) is greatest in coals at depths less than 600 m, when CO_2 is in the gaseous phase, not supercritical (Figure 2.14) (Ennis-King & Paterson, 2001).

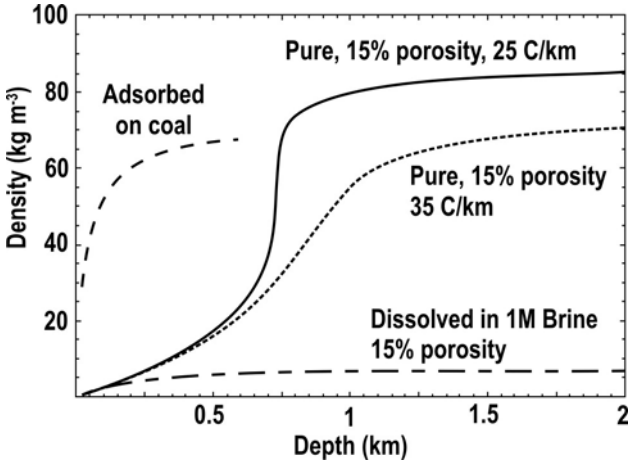

Figure 2.14 Total storage density as a function of depth, highlighting how the storage density of CO_2 adsorbed on coal at subcritical depths is comparable to the storage density of CO_2 captured in pore space at supercritical depths (hydrostatic pressure gradient is 10.5 MPa, mean surface temperature is 15°C and geothermal gradient is 25°C/km unless noted) (after Ennis-King & Paterson, 2001).

The efficiency of adsorption trapping is dependant upon the gas type, temperature and pressure conditions, and the characteristics of the coal, such as rank, moisture content, maceral composition and mineral matter content (White *et al.*, 2005). Coal has a much higher gas adsorption capacity for CO_2 than for CH_4 or nitrogen (N_2): the approximate adsorption ratios are 4:2:1 (i.e. four molecules of CO_2 are adsorbed for two molecules of CH_4 and for every one molecule of N_2, when comparing pure gases under the same temperature and pressure conditions) (Figure 2.15) (Gunter *et al.*, 1997a). This volumetric ratio of CO_2 to CH_4 is variable depending on the maturity of the coal. It can be as low as one for mature coals such as anthracite but up to ten or more for lower rank immature coals such as lignite (although low rank coals commonly contain lower initial total gas contents due to their immaturity and higher moisture content) (IPCC, 2005; White *et al.*, 2005). CO_2 is likely to remain adsorbed onto the coal matrix for geological time as long as the pressure does not drop and the coal is never mined (IPCC, 2005; Bachu *et al.*, 2007).

NOTE:
This figure is included on page 31 of the print copy of the thesis held in the University of Adelaide Library.

Figure 2.15 CO_2, CH_4 and N_2 adsorption (m^3/t) onto coal at varying pressure (temperature 55°C) (after IPCC, 2005).

2.4.7 Storage Security Over Time

In any geological storage site, the injected CO_2 will ultimately be trapped by a number of the mechanisms described above. The type of trapping that occurs, and when, is dependent on the dynamic flow behaviour of the CO_2 and the time-scale involved. With increasing time, the dominant storage mechanism will change and typically the storage security increases also. Figure 2.16 shows how the initial storage mechanism will dominantly be physical structural and stratigraphic trapping of the free-phase (immiscible) CO_2. With increasing time and migration, more CO_2 is trapped residually in the pore space or is dissolved in the formation water, increasing the storage security. Finally, mineral trapping may occur by precipitation of carbonate minerals after geochemical reaction of the dissolved CO_2 with the host rock mineralogy, permanently trapping the CO_2.

NOTE:
This figure is included on page 31 of the print copy of the thesis held in the University of Adelaide Library.

Figure 2.16 Schematic representation of the change of dominant trapping mechanisms and increasing CO_2 storage security with time (after IPCC, 2005).

2.5 GEOLOGICAL STORAGE OPTIONS FOR CO_2

Carbon dioxide can be stored geologically in a variety of different options within the subsurface (Figure 2.17). The three main alternatives in terms of volumetric suitability and technical feasibility are: oil and gas fields, coal seams and saline formations (Bachu & Gunter, 1999; Cook *et al.*, 2000; IPCC, 2005).

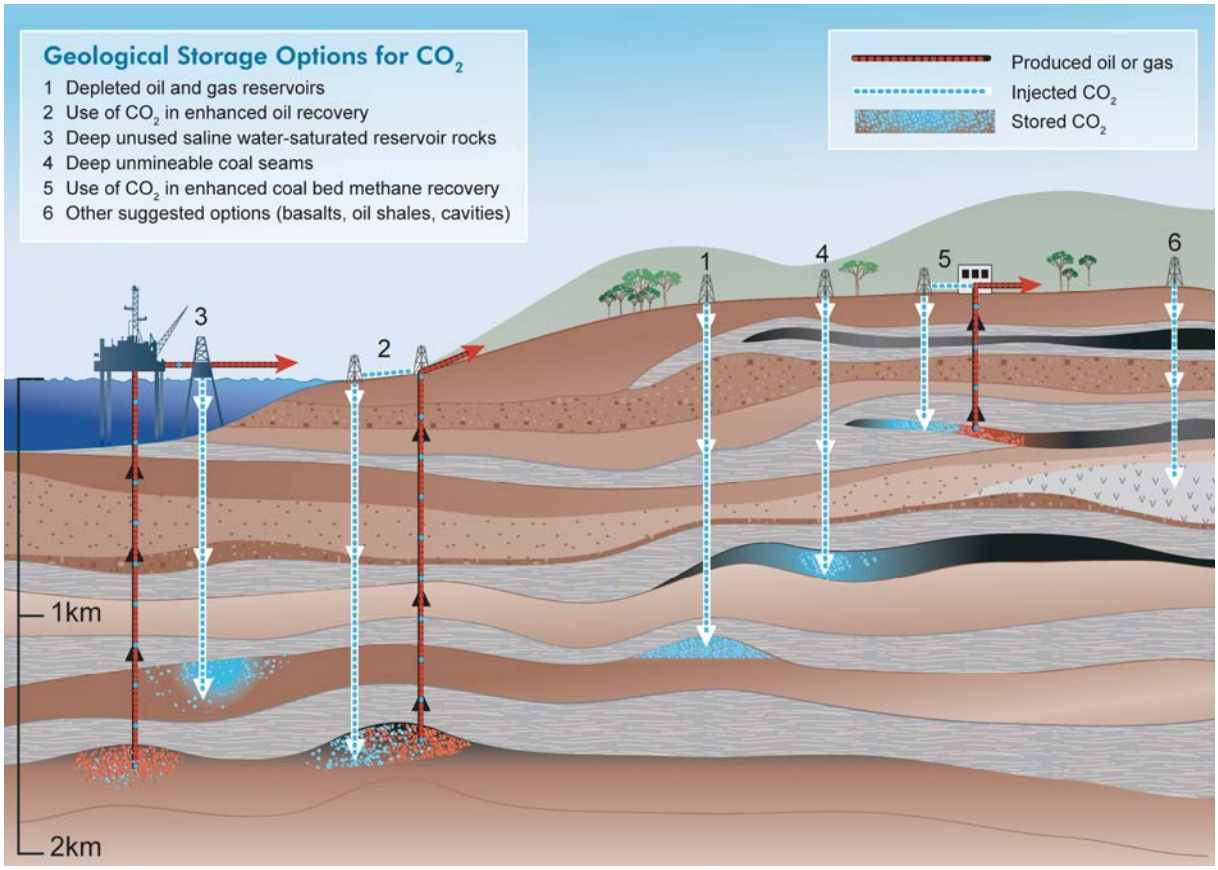

Figure 2.17 Options for the geological storage of carbon dioxide (image courtesy of CO2CRC).

2.5.1 Oil and Gas Fields – Depleted or Enhanced Recovery

CO_2 can be geologically stored in oil and gas fields once they have been depleted and are no longer producing, or can be used to enhance oil or gas recovery (EOR/EGR) in fields that are still producing. The main advantages of storage in depleted oil and gas fields is that the containment potential of the site has been proven by the retention of hydrocarbons for millions of years and there are typically large amounts of geological and engineering data available for detailed site characterisation (Holloway & Savage, 1993; IPCC, 2005). Possible drawbacks, however, may be the physical size of the structural/stratigraphic trap (i.e. potential storage capacity may be limited), the possibility that pore pressure depletion has led to pore

collapse (which will reduce the potential storage capacity), the presence of existing old wells which may provide potential leak points, and the timing of availability and location of depleted fields with respect to the source of CO_2 (Bradshaw & Rigg, 2001; Bradshaw *et al.*, 2002; Celia & Bachu, 2003; Streit & Siggins, 2005).

In EOR or EGR, the CO_2 is used to incrementally increase the amount of hydrocarbons extracted by either immiscible (not mixed) or miscible (mixed) flooding, thus providing an economic benefit whilst also storing CO_2. As with depleted oil and gas fields, the potential storage capacity may be limited due to the physical size of the field but also due to EOR operational issues such as the rate at which the CO_2 is recycled (Islam & Chakma, 1993; Cook *et al.*, 2000; IPCC, 2005).

2.5.2 Coal Seams – Deep Unmineable or Enhanced Recovery

CO_2 can be geologically stored in coal seams that are considered economically unmineable or can be used to enhance coal seam methane recovery (ECSMR). In reality, all CO_2 coal storage projects are likely be in conjunction with an ECSMR program, as the CH_4 that is released from the coal matrix has a higher greenhouse radiative effect (21 times stronger by weight) than CO_2. The CH_4 therefore needs to be captured to ensure a net greenhouse emission mitigation outcome (Bachu *et al.*, 2007). Technical challenges for CO_2 storage in coal seams include the ability to inject the CO_2, due to the typically low permeability characteristics of the coal cleat system (especially with increasing depth and coal maturity), and the economic viability, due to the large number of wells that may need to be drilled to overcome low permeability injectivity issues (Gunter *et al.*, 1997a; Bradshaw & Rigg, 2001; IPCC, 2005). Research into CO_2 storage in coal is still at quite an early stage and further work needs to be conducted to fully understand the processes involved and the most suitable coal characteristics for CO_2 storage (IPCC, 2005).

2.5.3 Saline Formations

Saline formations are deep porous sedimentary rocks saturated with formation waters that are unlikely to be suitable for human consumption or agricultural or industrial use. They have been identified by many studies as one of the best potential options for large volume geological storage of CO_2 (e.g. Bachu, 2000; Bradshaw *et al.*, 2002). Their main advantages are that they are distributed widely over the world and their potential storage capacity is large as the trapping mechanism is not restricted to specific structural/stratigraphic closures like oil

and gas fields (Koide *et al.*, 1992; Hendriks & Blok, 1993; Rigg *et al.*, 2001; IPCC, 2005). Possible drawbacks of saline formations, however, are that the containment potential of the seal rock is usually untested and there are often limited amounts of data available to adequately characterise the site.

2.6 NATURAL CO_2 ACCUMULATIONS

As well as being a by-product of fossil fuel combustion, CO_2 occurs naturally in the subsurface, generated through geological processes and trapped as an accumulation in a similar manner to oil and gas deposits. These natural CO_2 accumulations provide evidence that the long-term storage of CO_2 in subsurface geological reservoirs is a feasible possibility (Holloway & Savage, 1993). For example, the Pisgah Anticline natural CO_2 accumulation in Mississippi, U.S.A., contains CO_2 that was produced by thermal metamorphism of Jurassic carbonates, created when the Jackson Dome igneous intrusion was emplaced (Studlick *et al.*, 1990). This CO_2 migrated into the faulted anticline structure during the Late Cretaceous to Early Tertiary (Studlick *et al.*, 1990), i.e. around 65 million years ago, proving CO_2 can be contained in subsurface reservoirs for considerable time periods if the right geological conditions exist.

Natural CO_2 accumulations can thus be considered analogues for long-term geological storage of CO_2 and so provide vital information on the likely physical and chemical behaviour of CO_2 in subsurface reservoirs over geological time (Pearce *et al.*, 1996). In particular, analysis of equivalent reservoirs with contrasting high and low CO_2 contents can be used to identify the likely post-CO_2 emplacement diagenetic processes (Baines & Worden, 2001). One of the best examples of this is the Ladbroke Grove and Katnook gas fields in the Otway Basin, southeast Australia (Figure 2.18).

The two fields are less than 1 km apart, separated by a major fault, both with methane reservoired within the Early Cretaceous Pretty Hill Formation (Watson *et al.*, 2003; Watson *et al.*, 2004b). The Ladbroke Grove field, however, contains approximately 29–57 mol% CO_2, whilst the Katnook field has less than 1 mol% CO_2. The source for the CO_2 in the Ladbroke Grove field has been determined through helium ($^3He/^4He$) and carbon ($\delta^{13}C$) isotopic studies as mantle-derived, most likely from degassing of the magmas associated with the Pleistocene to Recent Newer Volcanics (Watson *et al.*, 2004a).

Figure 2.18 Location of the Katnook and Ladbroke Grove gas fields, in (a) map view and (b) cross-section (modified after Watson *et al.*, 2003).

The Pretty Hill Formation is a moderate to well sorted, fine- to medium-grained, lithic arenite (Watson *et al.*, 2003; Watson *et al.*, 2004b). Pre-CO_2 influx diagenetic processes that are seen in the Katnook field include extensive albitisation of feldspar, chloritisation of volcanic rock fragments, precipitation of chlorite as grain-rimming clay and precipitation of poikilotopic calcite cement (Watson *et al.*, 2003; Watson *et al.*, 2004b). In the Ladbroke Grove field, the influx of CO_2 into the system has caused both dissolution of existing mineral phases and precipitation of new mineral phases (Figure 2.19). There has been substantial leaching of the plagioclase feldspars (Figure 2.19a), dissolution of the chlorite and partial dissolution of the poikilotopic calcite cement. Kaolinite clay has been precipitated in a grain-rimming habit, replacing the chlorite clay (Figure 2.19b), and there has also been co-genetic precipitation of quartz and kaolinite. In addition, new carbonate minerals have been precipitated, such as siderite, ankerite and ferroan dolomite, generally occurring as microspar replacing feldspar grains (Figure 2.19c) or in more sparry forms filling pore space (Figure 2.19d) (Watson *et al.*, 2003; Watson *et al.*, 2004a; Watson *et al.*, 2004b).

The Ladbroke Grove field when compared to the Katnook field demonstrates the diagenetic processes that can occur when CO_2 enters the system, trapping the CO_2 in solution and as precipitated carbonate minerals. Natural CO_2 accumulations can therefore provide important analogues to the long-term effects of geological storage of CO_2 in the subsurface. It is important to note, however, that CO_2 storage projects are emplaced over injection

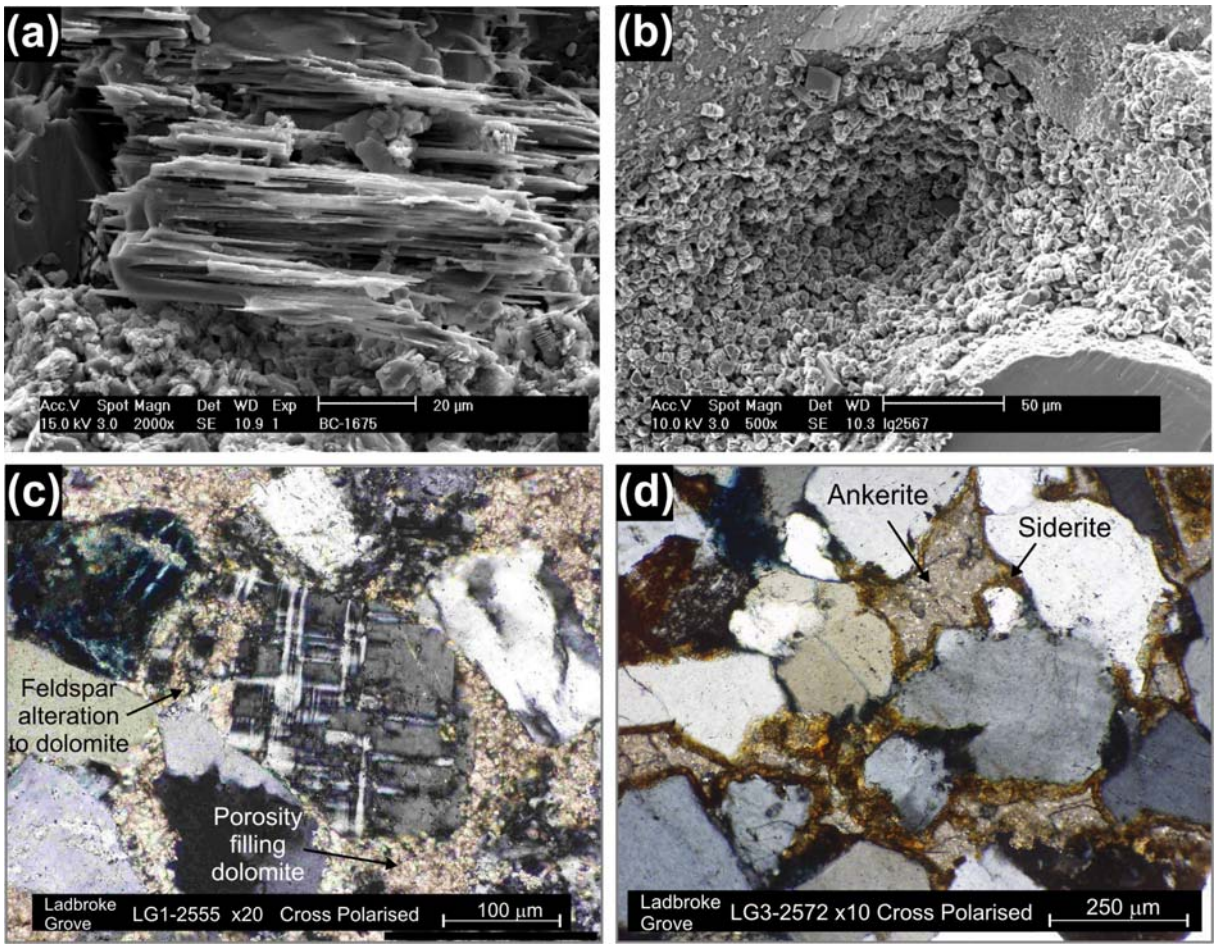

Figure 2.19 Ladbroke Grove Pretty Hill Formation. (a) Scanning Electron Microscope (SEM) image of the skeletal remains of a sodium plagioclase grain. (b) SEM image of kaolin developed as a grain-rimming clay, very similar to the typical growth of chlorite. (c) Thin section of a partly replaced microcline grain with ferroan dolomite replacing the mineral and filling all available pore space. (d) Thin section of multi-phase carbonates. The microspar form of siderite coats the framework gains as replacement cement. Ankerite is the later cement phase precipitating as a sparry pore fill (modified after Watson *et al.*, 2003; Watson *et al.*, 2004a).

time-scales of ~20–40 years, not geological time-scales like natural CO_2 accumulations, thus natural accumulations may not be so analogous to the rapid (geologically-speaking) introduction of CO_2 into the subsurface. However, natural CO_2 accumulations do provide strong evidence that long-term secure containment of CO_2 in the geological subsurface is a feasible possibility.

2.7 OPERATIONAL EXAMPLE: THE SLEIPNER CO_2 STORAGE PROJECT

The Sleipner CO_2 Storage Project is operated by Statoil and is located in the Norwegian sector of the North Sea, about 250 km off the coast of Norway (Figure 2.20). It is the first commercial-scale operational CO_2 injection project for the purposes of geological storage within a saline formation (Baklid *et al.*, 1996; Torp & Gale, 2004; IPCC, 2005). The driver

Figure 2.20 Simplified diagram of the Sleipner CO_2 Storage Project. Inset: location and extent of the Utsira Formation (after IPCC, 2005).

for the project was the Norwegian Government's decision to commit to stabilising the country's anthropogenic CO_2 emissions at the 1989-level by the year 2000. In order to curb increased emissions, the Norwegian Parliament introduced a carbon tax levied at approximately US$50/t of CO_2 (Kaarstad, 1992). The methane of the Sleipner West gas field contains 4–9.5% CO_2, which needs to be reduced to 2.5% by volume for the purpose of the gas sales agreements. This reduction equates to approximately 1 Mt of CO_2 per year or cumulatively 20 Mt over the expected life of the field (Korbøl & Kaddour, 1995; Baklid *et al.*, 1996). It was calculated that the release of this amount of CO_2 to the atmosphere would result in an overall 3% increase in total Norwegian emissions to the atmosphere. Thus, during the early planning of the field development it was recognised that storage of the CO_2 would need to be actioned (Korbøl & Kaddour, 1995; Baklid *et al.*, 1996). Several geological storage options were considered, but the final decision was to pipe the separated CO_2 to the platform above the Sleipner East gas field and to reinject the CO_2 into the Utsira Formation, a shallower saline formation above the methane production interval (Figure 2.20) (Korbøl & Kaddour, 1995; Baklid *et al.*, 1996).

The Utsira Formation is a basinally-restricted, elongate, mostly unconsolidated sandstone deposit of Miocene–Pliocene age. It extends for more than 400 km from north to south and 50–100 km from east to west. Mounded seismic reflections and blocky wireline log character have led to the interpretation that the sediments are stacked lowstand fans, deposited by mass flows in a marine environment in water depths of 100 m or more (Gregersen *et al.*, 1997; Chadwick *et al.*, 2004). At the Sleipner Field location, the Utsira Formation is around 300 m thick, with the top of the formation at about 800 m below sea level (Chadwick *et al.*, 2004). Pre-injection simulation studies determined that the CO_2 should be injected at the bottom of the formation to minimise the lateral distribution and maximise the amount of CO_2 dissolved in the formation water (Korbøl & Kaddour, 1995; Baklid *et al.*, 1996). The CO_2 is therefore injected at a depth of 1012 m below sea level, near the base of the Utsira Formation (Arts *et al.*, 2004; Chadwick *et al.*, 2004). The temperature in the reservoir is 37°C and the pressure is hydrostatic (8–11 MPa), therefore the CO_2 will be supercritical (Baklid *et al.*, 1996). The injectivity potential is good, as the Utsira Formation has excellent reservoir quality, with porosities of 35–40% and permeabilities of 1–3 D (Baklid *et al.*, 1996; Chadwick *et al.*, 2004). Containment is provided by an overlying, similarly basinally-restricted lower seal unit of 50–100 m thick shale, which is in turn overlain by a middle seal unit of Pliocene prograding sediment wedges (dominantly shaly in the basin centre) and upper seal unit of Quaternary glacial deposits (Chadwick *et al.*, 2004).

Injection commenced in October 1996 at a rate of 2700 t/day, and by 2008 approximately 10 Mt of CO_2 had been injected (IPCC, 2005; Hermanrud *et al.*, 2009). The migration and distribution of the CO_2 plume has been monitored by time-lapse seismic surveys (Arts *et al.*, 2004). The injected CO_2 has had a significant impact on the seismic signal, causing large increases in the seismic reflectivity, clearly demonstrating the position of the injected CO_2 within the Utsira Formation (Figure 2.21) (Arts *et al.*, 2004). The CO_2 is present at several stratigraphic intervals, accumulating beneath the thin intraformational shales in between individual sand lobes (Arts *et al.*, 2004; Chadwick *et al.*, 2004; Arts *et al.*, 2005). The time-lapse seismic surveys demonstrate that the CO_2 is still successfully contained within the Utsira Formation (Arts *et al.*, 2005). By 2008, about one third of the injected CO_2 was stored within the structural closure in the upper two layers (above structural spill point) and the remaining two thirds was below the structural spill point within the deeper layers of the Utsira Formation. It is estimated that about 40% of the CO_2 that has entered the pore systems will remain as residually trapped CO_2, whilst an unknown fraction of the remaining CO_2 will migrate towards the top of the reservoir (Hermanrud *et al.*, 2009).

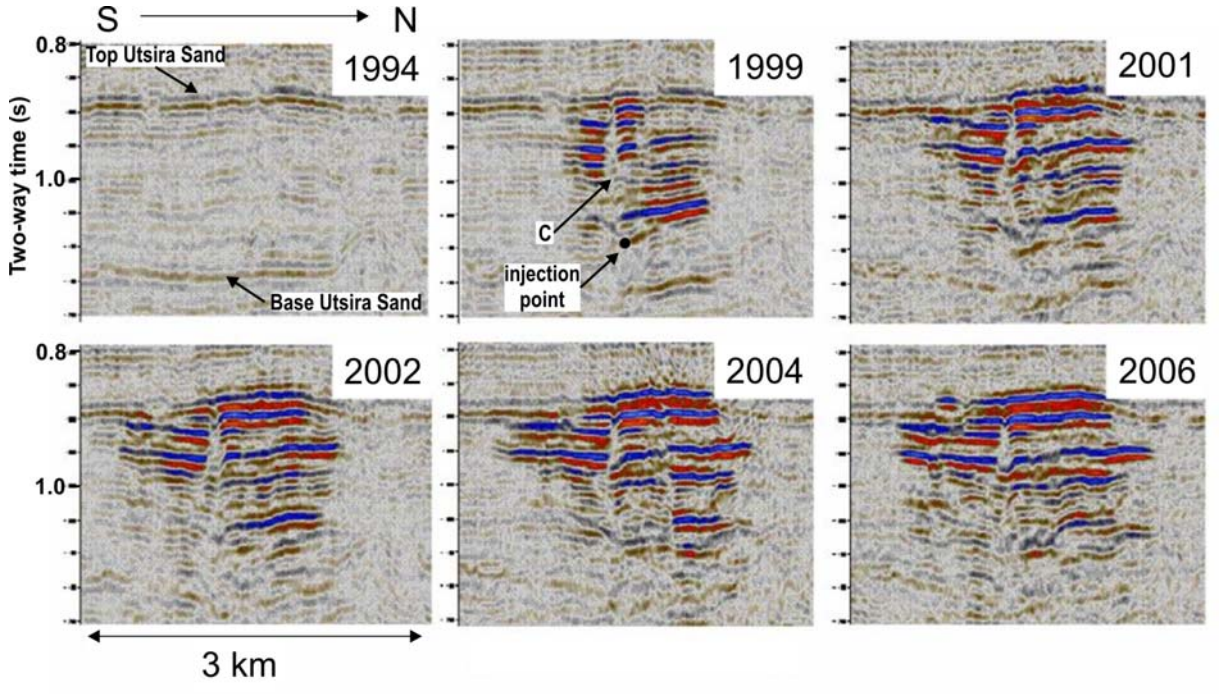

Figure 2.21 Vertical seismic sections through the CO_2 plume in the Utsira Formation at the Sleipner gas field, North Sea, showing its development over time. Note the chimney of high CO_2 saturation (C) above the injection point (black dot). The bright amplitude layers correspond to the presence of injected CO_2 in porous sandstone beneath thin low-permeability shale layers within the reservoir (modified after Hermanrud *et al.*, 2009).

CHAPTER 3. DATABASE AND METHODOLOGIES

3.1 INTRODUCTION

Numerous data types and methodologies have been integrated to interpret the suitability of the Petrel and Barrow sub-basins for geological storage of CO_2. The data types and analysis techniques employed are those commonly used in the petroleum industry for the exploration of oil and gas. The data types include 2D and 3D seismic surveys, wireline logs, sedimentary core, biostratigraphic reports and various other well-derived data extracted from well completion reports (such as pressure, temperature, salinity and velocity data). Interpretation methodologies include sequence stratigraphy, seismic interpretation, wireline log well correlation, sedimentology, mercury injection capillary pressure analysis, computer mapping and 3D geological modelling.

3.2 DATABASE: PETREL SUB-BASIN

3.2.1 Seismic

Sixteen 2D seismic surveys of varying vintage across the Petrel Sub-basin were used for the study (~ 6000 km in total). The vintage of the seismic data ranges from 1967 to 1997. Geoscience Australia's regional deep seismic lines (surveys 100 and 118) were used for the main regional interpretation, with a selection of other commercially-derived seismic to complete the detail. A very detailed 2D seismic survey over the Petrel Field (B89WA) was also interpreted. Table 3.1 lists the details of the 2D seismic surveys used in this study and Figure 3.1 displays the seismic data coverage in the Petrel Sub-basin. The seismic data available provided reasonable regional coverage across the sub-basin, with only the northeastern edge rather sparsely covered. Due to the differing vintages, the surveys were of variable quality, but most surveys were of satisfactory quality for regional interpretation. Salt diapirism in the sub-basin has affected the quality of the seismic directly overhead, which sometimes made interpretation over these areas very difficult (the wells Gull-1, Curlew-1, Sandpiper-1 and Bougainville-1 are all located over salt diapers).

Table 3.1. Details of the Petrel Sub-basin seismic surveys (or parts of) that were used for this PhD study.

Survey Name	Line Prefix	Survey Type	Km Shot	Date
67H	67H	2D	N/A	1967 (?)
80HD	80HD	2D	N/A	1980 (?)
AGSO Survey 100; Petrel Sub-basin M.S.S.	100	2D	N/A	01-Apr-1991
AGSO Survey 118; Malita Graben M.S.S.	118	2D	N/A	01-May-1993
BP 1990 Bonaparte Gulf M.S.S.	90BG	2D	N/A	13-May-1990
BP 1991 Bonaparte Gulf M.S.S.	BG91	2D	1501	17-Nov-1991
EP97	EP97	2D	N/A	1997 (?)
Gale Bank M.S.S.	GB	2D	1346	21-Sep-1971
HCB91A M.S.S.	HCB91A	2D	2257	27-Aug-1991
Pago M.S.S.	P	2D	4359	25-May-1972
Peron Island M.S.S.	PI	2D	1645	23-Aug-1972
Pompano M.S.S.	MB85	2D	328	10-Sep-1985
SPA 2SL/1989-90	B89WA	2D	1190	16-Sep-1989
T83 M.S.S.	T83	2D	93	18-Jun-1983
T84 M.S.S.	T84	2D	180	07-Apr-1984
Van Cloon M.S.S.	VC	2D	1298	10-Mar-1976

The seismic surveys were loaded into and interpreted within the IESX™ module of GeoFrame™ (versions 3.8 and 4.0.2, Schlumberger). Velocity survey data were collated from available well completion reports. These were loaded into the GeoFrame™ project to provide the time/depth relationships and enable intersecting well logs and markers to be displayed on the seismic sections.

3.2.2 Wells

Over 40 wells have been drilled in the offshore region of the Petrel Sub-basin, of which 23 open-file wells penetrate some or all of the Sandpiper Sandstone and Plover Formation and were selected for use in this PhD study (the Jurassic-Cretaceous stratigraphy is absent in the other wells in the sub-basin, with Tertiary sediments directly overlying the Triassic, Permian or Carboniferous successions). The vintage of the study wells varies from 1969 to 1998, and the spacing varies from a few kilometres (e.g. the Petrel Field wells) to ~100 km (e.g. Petrel-1 to Gull-1). Table 3.2 lists the details of the wells used in this study and Figure 3.2 displays the location of the study wells in the Petrel Sub-basin. Appendix A lists the datasets available for each well.

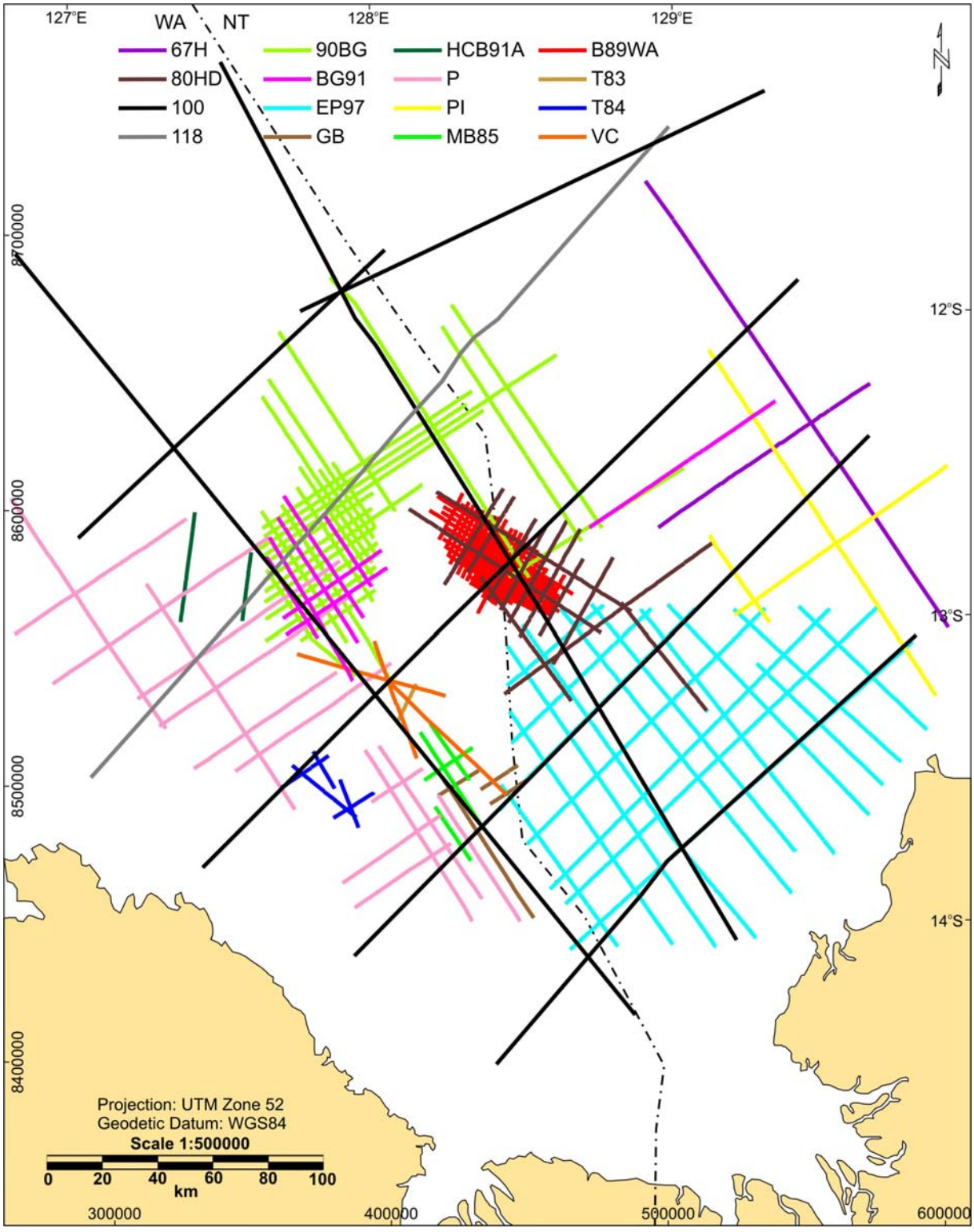

Figure 3.1 Location map of seismic lines in the Petrel Sub-basin available for this PhD study.

Table 3.2 Details of the key wells in the Petrel Sub-basin that were used for this PhD study (locations referenced to WGS84 geodetic datum, UTM Projection Zone 52).

Well Name	Longitude	Latitude	Easting (m)	Northing (m)	KB (m)	Spud Date
Billabong-1	127.4121370	-12.73776200	327610.92	8591337.11	30.7	29/10/1992
Bougainville-1	129.0430400	-13.77218200	504652.47	8477468.58	12.8	08/02/1972
Curlew-1	128.2651197	-11.76916126	419932.15	8698867.11	25.0	06/11/1974
Fishburn-1	127.5855940	-12.96655700	346585.27	8566137.65	30.4	23/09/1992
Flat Top-1	129.2667540	-12.37507200	528997.93	8631956.61	12.2	04/01/1970
Frigate-1	127.9248510	-13.17860466	383487.15	8542863.67	21.3	04/01/1978
Gull-1	127.9115120	-11.93999600	381475.48	8679848.53	13.1	05/06/1970
Helvetius-1 ST2	126.9737335	-12.13943704	279494.31	8657207.41	22.0	06/09/1994
Jacaranda-1	128.1652042	-11.46955580	408948.10	8731968.85	27.0	25/06/1984
Penguin-1	128.4695720	-13.60637900	442621.78	8495743.04	34.4	22/06/1972
Petrel-1	128.4754010	-12.82499200	443071.45	8582159.77	34.4	12/05/1969
Petrel-1A	128.4734565	-12.82971373	442861.49	8581637.17	34.4	06/02/1970
Petrel-2	128.5151230	-12.85249127	447387.83	8579127.10	34.4	18/12/1970
Petrel-3	128.5706371	-12.93386897	453426.61	8570138.38	30.5	28/10/1981
Petrel-4	128.4959566	-12.88704408	445315.59	8575301.95	25.0	20/04/1988
Petrel-5	128.4094238	-12.81234345	435908.31	8583543.11	22.3	27/07/1994
Petrel-6	128.4570005	-12.79949430	441068.68	8584975.41	22.3	18/11/1995
Sandpiper-1	127.9776290	-13.31332600	389268.14	8527986.80	11.9	07/08/1971
Tern-1	128.0659613	-13.21943725	398797.26	8538408.68	11.9	26/01/1971
Tern-2	128.1340278	-13.27720628	406194.90	8532045.94	10.0	16/11/1981
Tern-3	128.1053561	-13.33420355	403111.51	8525731.02	9.7	23/09/1982
Tern-4	128.1072030	-13.22843400	403269.66	8537429.93	22.5	23/10/1994
Tern-5	128.0987577	-13.20475233	402345.16	8540045.86	21.0	30/11/1997

Basic wireline log suites for the wells were provided digitally by Wiltshire Geological Services and were loaded into the GeoFrame™ project. Deviation survey data were collated for non-vertical wells from all available well completion reports and also loaded into the GeoFrame™ project to allow conversion back to true vertical depth. Formation tops for the Petrel Sub-basin were obtained from the lithostratigraphic picks of Grech (1998). The formation tops were loaded into the GeoFrame™ project so that they could be posted onto the wireline logs for reference to help constrain the intervals of interest for the sequence stratigraphic study.

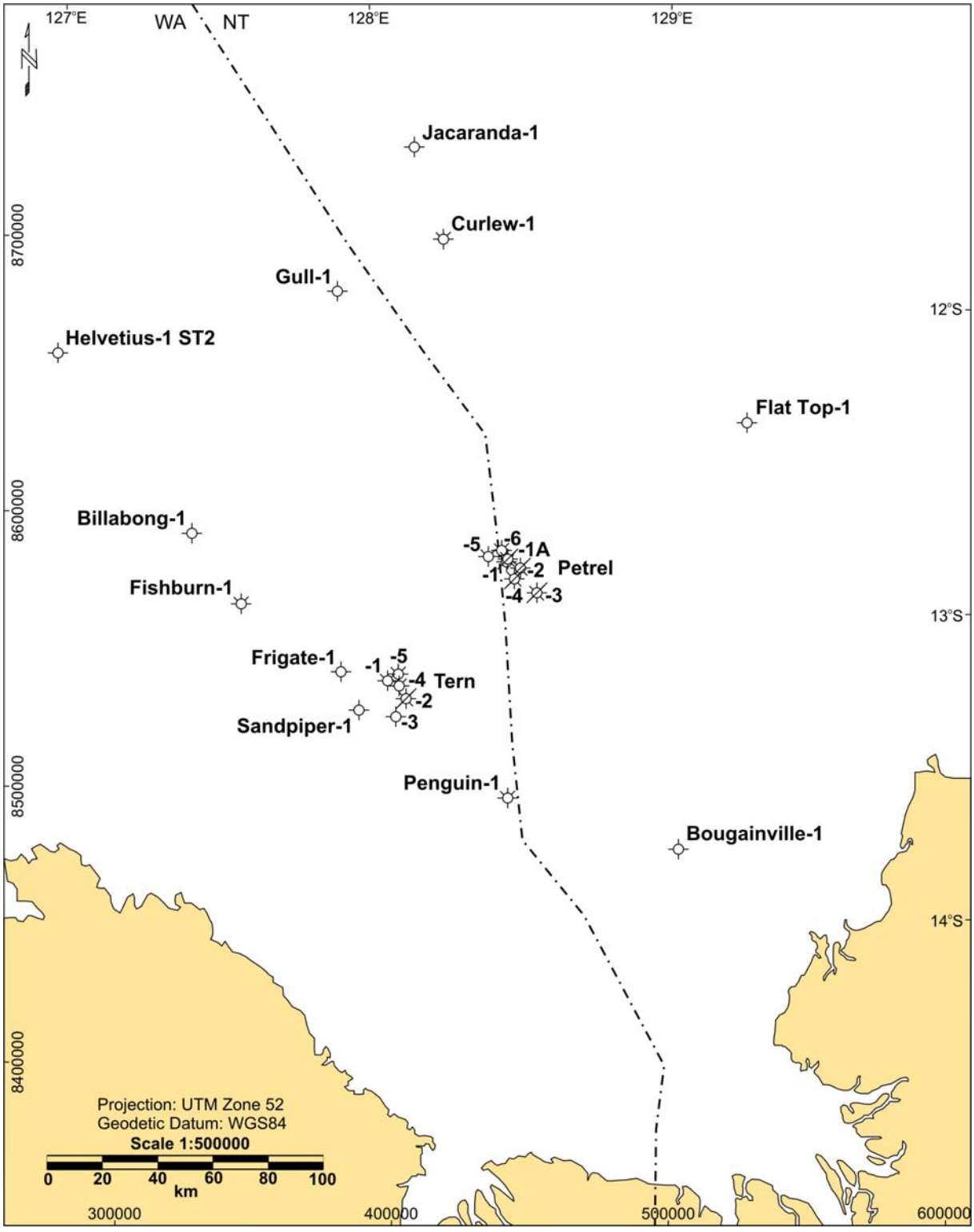

Figure 3.2 Location map of wells in the Petrel Sub-basin used for this PhD study.

3.2.3 Pressure, Temperature and Salinity Data

Pressure, temperature and salinity data were obtained where available from well completion reports. Pressure data were collated from various formation pressure tests, such as repeat formation tests (RFT), formation integrity tests (FIT) and drill stem tests (DST). The pressure data collated for the Petrel Sub-basin are provided in Appendix B. Geothermal gradients were calculated for each well from bottom hole depth temperature data. The temperature data and gradients calculated are provided in Appendix C. Salinity data were collated where available over the intervals of interest and mean averages were calculated.

3.2.4 Core

Core data is very limited in the Petrel Sub-basin over the Jurassic–Cretaceous stratigraphic section, with only two wells, Gull-1 and Petrel-1, with any core through the intervals of interest (representing less than 3% of the formations). The cores from these wells were viewed at Geoscience Australia's core store. Table 3.3 lists the core depths and the host formation. As both wells were drilled in the late 1960s and early 1970s, the core is not in a particularly good condition and is often fractured into many pieces (due to the core recovery process and length of time stored). In addition, all the cores are positioned from the top recovery depth, with all the non-recovery attributed to the base of the cored interval, which is not necessarily the case. However, the quality of the core and the absence of a core gamma ray log meant that more precise depth matching was not possible.

3.2.5 Conventional Core Analyses

Conventional core analyses of porosity and permeability derived from core plug samples were collated where available. As only a limited amount of core has been drilled through the Jurassic–Cretaceous stratigraphic section, the database of porosity and permeability values from conventional core analyses is similarly very limited (48 data points in total). The available data points from Gull-1 and Petrel-1 in the Petrel Sub-basin were obtained from Geoscience Australia's PORPERM digital database. The collated core plug porosity and permeability data is provided in Appendix D.

Table 3.3 Details of core intervals in the Petrel Sub-basin that were viewed for this PhD study.

Well Name	Core No.	Depth From: (m MD)	Depth To: (m MD)	Recovery		Quality	Formation Name
				m	%		
Gull-1	2	1531.6	1537.7	5.56	91.5	poor	Bathurst Island Gp
	3	1828.8	1834.9	5.64	92.5	very poor	Bathurst Island Gp
	4	2208.0	2214.1	4.11	67.5	moderate	Sandpiper Sst
	5	2437.8	2444.2	4.88	76.0	moderate	Elang Fm
	6	2690.8	2696.9	2.13	35.0	moderate	Plover Fm
	7	2852.9	2859.0	4.72	78.0	moderate	Plover Fm
	8	3041.9	3045.4	3.51	100.0	moderate	Plover Fm
Petrel-1	1	755.9	762.0	5.79	95.0	very poor	Bathurst Island Gp
	2	1062.2	1064.4	2.13	100.0	very poor	Bathurst Island Gp
	3	1373.4	1379.8	2.44	38.0	very poor	Sandpiper Sst
	4	1585.0	1591.4	6.40	100.0	moderate	Frigate Fm
	5	1967.2	1972.1	4.65	89.0	moderate	Plover Fm

3.2.6 Biostratigraphic Data

Biostratigraphic data are crucial to sequence stratigraphic interpretation to constrain the chronostratigraphic framework. Biostratigraphic data for wells from the Petrel Sub-basin were provided by Geoscience Australia from their digital STRATDAT database. Each individual biostratigraphic data point has been cross-checked by Geoscience Australia for its reliability and comes supplied with its own reference, confidence code and remarks. Additional biostratigraphic data were used if necessary from palynological data sheets of Morgan Palaeo Associates (donated to the Australian School of Petroleum by Roger Morgan) and well completion reports; however, these were used more cautiously as they have not been cross-checked to the same degree as Geoscience Australia's STRATDAT database. The biostratigraphic data are referenced to the biozonation scheme of Helby *et al*. (1987). The biostratigraphic data were loaded into the GeoFrame™ project so that they could be posted onto the wireline logs for reference during the wireline log correlation (discussed in section 3.4.4 below).

3.2.7 Mercury Injection Capillary Pressure Analyses

Mercury injection capillary pressure (MICP) analyses were undertaken on 18 core samples collected from the cores of Gull-1 and Petrel-1. The samples were processed by the Australian School of Petroleum using a *Micromeritics Autopore 9410 Mercury Injection*

Porosimeter. The samples were chosen to represent different facies within the Bathurst Island Group regional seal, as well as intraformational seals, stylolites and reservoir units of the Plover, Elang and Frigate formations and the Sandpiper Sandstone. Table 3.4 lists the details of the collected core samples in the Petrel Sub-basin that were selected for MICP analysis. The MICP data for each of the core samples analysed is provided in Appendix E.

Table 3.4 Details of MICP core samples from the Petrel Sub-basin.

Well Name	Sample No.	Depth (m MD)	Formation	MICP Sample Type	Facies
Gull-1	000-268	1535.60	Bathurst Island Gp	Regional top seal	Argillaceous siltstone
	000-269	1536.28	Bathurst Island Gp	Regional top seal	Silty claystone
	000-270	1830.55	Bathurst Island Gp	Regional top seal	Claystone
	000-272	2209.00	Sandpiper Sandstone	Intraformational seal	Micaceous siltstone
	000-271	2209.05	Sandpiper Sandstone	Reservoir	Fine-grained sandstone
	000-273	2441.85	Elang Formation	Stylolite	Medium- to fine-grained sandstone
	000-274	2691.22	Plover Formation	Reservoir	Cross-bedded, medium-grained sandstone
	000-275	2853.89	Plover Formation	Reservoir	Medium-grained sandstone
	000-276	3044.69	Plover Formation	Stylolite	Medium-grained sandstone
Petrel-1	000-277	758.26	Bathurst Island Gp	Regional top seal	Claystone
	000-278	761.31	Bathurst Island Gp	Regional top seal	Claystone
	000-279	1062.61	Bathurst Island Gp	Regional top seal	Claystone
	000-280	1063.89	Bathurst Island Gp	Regional top seal	Micritic limestone
	000-282	1064.13	Bathurst Island Gp	Regional top seal	Claystone
	000-281	1373.75	Sandpiper Sandstone	Reservoir	Fine-grained sandstone
	000-285	1588.00	Frigate Formation	Local top seal	Very fine-grained, bioturbated, silty sandstone
	000-283	1967.50	Plover Formation	Reservoir	Fine-grained sandstone
	000-284	1970.86	Plover Formation	Reservoir	Very fine-grained sandstone

3.3 DATABASE: BARROW SUB-BASIN

3.3.1 Seismic

Two open-file 3D seismic surveys were available for use in the study, the North West Barrow and Cash 3D seismic surveys, plus a selection of 2D seismic surveys of varying

vintages (1982 to 1995). Table 3.5 lists the details of the seismic surveys used in this study and Figure 3.3 displays the seismic data coverage. The Cash 3D seismic survey provided excellent coverage across the eastern part of the sub-basin; however, seismic coverage was very sparse in the middle of the study area (in between the Montebello Islands and Barrow Island) and totally absent over Barrow Island. Due to the lack of data in the middle of the study area, correlations could not be confirmed between the eastern and western parts of the study area. The North West Barrow 3D survey was of limited use for regional mapping as only two shallow wells (Triller-1 and Bantha-1) intersected the survey area.

Table 3.5. Details of the **s**eismic surveys (or parts of) that were used for this PhD study.

Survey Name	**Line Prefix**	**Survey Type**	**Km Shot**	**Date**
A95T M.S.S.	A95T	2D	150	06-Jun-1995
B85T M.S.S.	B85T	2D	210	17-Feb-1986
Cash 3D M.S.S.		3D	33019	11-Jun-1997
Elliot M.S.S.	PW93	2D	1487	19-Dec-1993
Felicity M.S.S.	A95F	2D	192	31-Aug-1995
H90 M.S.S.	H90	2D	558	26-Aug-1990
H92T M.S.S.	H92T	2D	151	15-Apr-1993
Leanne M.S.S.	A95L	2D	114	21-May-1995
Maritsa Extension Shallow M.S.S.	A94M	2D	85	01-May-1995
North West Barrow 3D M.S.S.	NWBN97	3D	18858	12-Mar-1997
O82 M.S.S.	82	2D	6127	19-Jun-1982
O83 M.S.S.	83	2D	1269	12-May-1983

The seismic surveys were loaded into and interpreted within the IESX™ module of GeoFrame™ (versions 3.8 and 4.0.2, Schlumberger). Velocity survey data were collated from the Western Australian Department of Industry and Resources WAPIMS database (provided digitally in Haworth & Arden, 1999) or well completion reports. These were loaded into the GeoFrame™ project to provide the time/depth relationships and enable intersecting well logs and markers to be displayed on the seismic sections.

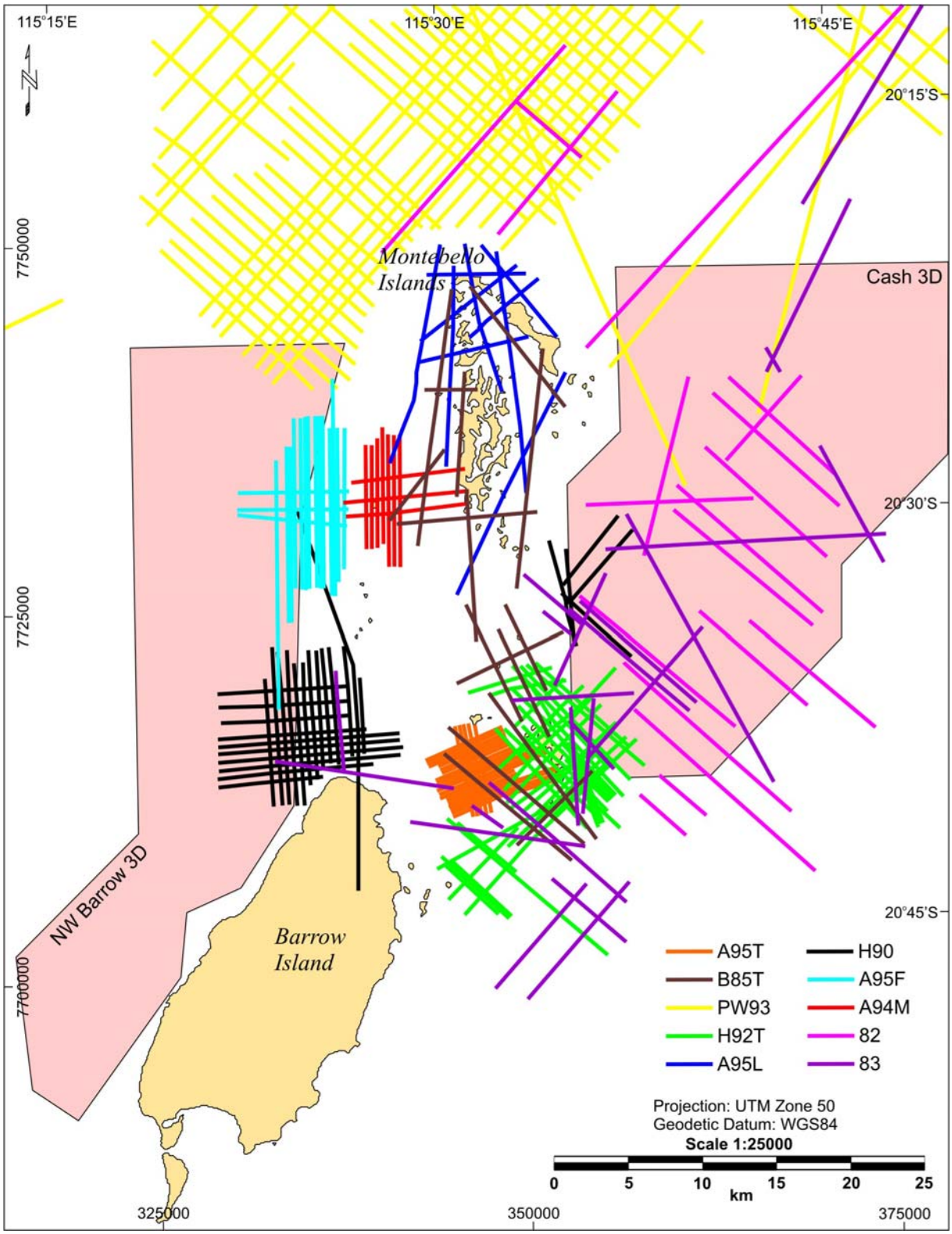

Figure 3.3 Location map of seismic data in the Barrow Sub-basin available for this PhD study.

3.3.2 Wells

About 150 wells have been drilled in the study area of the Barrow Sub-basin, of which 42 were selected as key wells for the purposes of this PhD study. The vintage of the study wells varies from 1964 to 2000. Despite being a much smaller study area than the Petrel Sub-basin, the well density is much greater in the Barrow Sub-basin as it is a much more significant hydrocarbon discovery area. Table 3.6 lists the details of the key wells selected for use in this study and Figure 3.4 displays the location of the study wells in the Barrow Sub-basin. Appendix A lists the datasets available for each well.

Table 3.6 Details of the key wells in the Barrow Sub-basin that were used for this PhD study (locations referenced to WGS84 geodetic datum, UTM Projection Zone 50).

Well Name	Longitude	Latitude	Easting (m)	Northing (m)	KB (m)	Spud Date
Agincourt-1 ST1	115.5142982	-20.66879037	345241.61	7713799.20	29.5	25/05/1996
Alkimos-1	115.5796245	-20.65354633	352032.65	7715547.56	15.3	14/08/1994
Austin-1	115.4604721	-20.29239532	339241.98	7755412.53	28.7	12/05/1995
Bambra-1	115.6336155	-20.52492438	357538.55	7729833.16	31.8	21/11/1982
Bambra-2	115.6021185	-20.54429974	354272.49	7727660.68	26.0	03/05/1983
Bantha-1	115.3246546	-20.73643808	325560.77	7706117.86	25.8	18/06/2000
Barrow-1	115.3952410	-20.81703605	333000.47	7697269.98	55.0	07/05/1964
Barrow-25	115.4393514	-20.67031549	337434.96	7713557.09	19.0	1966
Barrow Deep-1	115.3835931	-20.83401125	331806.95	7695378.65	47.0	16/09/1972
Belinda-1	115.6512760	-20.48865069	359347.00	7733863.58	33.5	14/09/1994
Campbell-1	115.7180948	-20.41029025	366248.37	7742593.05	21.2	20/03/1979
Campbell-2	115.7302380	-20.41408604	367518.77	7742182.76	34.0	31/01/1986
Cycad-1	115.5733474	-20.79214007	351513.84	7700200.19	32.4	13/03/1995
Doric-1	115.7052624	-20.52829777	365012.52	7729520.60	24.8	06/05/1996
Dorrigo-1	115.7131831	-20.66268571	365955.97	7714651.91	35.0	09/10/1982
Dylan-1	115.6775464	-20.55988612	362150.83	7726000.96	29.3	11/10/2000
Emma-1	115.7798765	-20.51720070	372783.43	7730808.78	38.0	05/04/1983
Flag-1	115.6513482	-20.46397665	359332.05	7736594.80	23.3	02/09/1969
Flores-1	115.5950566	-20.75750389	353740.31	7704054.06	31.5	02/10/1983
Forrest-1A ST1	115.5389086	-20.22419383	347367.07	7763036.22	22.0	21/05/1992
Georgette-1	115.6558952	-20.76066454	360077.65	7703758.07	25.4	10/09/1983
Gipsy-1	115.7211556	-20.64044790	366767.17	7717119.95	33.0	21/02/1998
Harriet-A1	115.6142445	-20.60221778	355591.30	7721260.41	34.7	20/10/1983
Harriet-B1	115.6375993	-20.57519966	358000.42	7724271.62	26.9	30/08/1984

Well Name	Longitude	Latitude	Easting (m)	Northing (m)	KB (m)	Spud Date
Harriet-C1	115.6272026	-20.58899688	356929.51	7722735.29	27.9	20/09/1985
Marra-1	115.6456195	-20.60119336	358860.39	7721401.32	30.7	29/11/1992
Menzies-1	115.6863284	-20.70536714	363196.49	7709905.06	30.8	11/04/1995
Nyanda-1	115.6263140	-20.61546955	356861.61	7719804.21	26.9	02/06/1985
Orpheus-1	115.6721084	-20.48469440	361516.28	7734319.27	31.0	03/03/1986
Plato-1	115.5669539	-20.69324887	350751.30	7711141.11	30.0	30/03/1986
Rose-1	115.7173440	-20.59506547	366330.41	7722140.15	30.9	08/07/1998
Rosette-1	115.5752518	-20.65523015	351578.69	7715357.18	12.0	08/07/1987
Sinbad-1	115.7123577	-20.48337908	365713.21	7734498.39	33.4	21/02/1990
Sinbad-2	115.7210427	-20.48336418	366619.07	7734507.15	38.7	18/06/1992
Tanami-1	115.5812001	-20.65351169	352196.78	7715552.83	16.4	08/06/1991
Tanami-2	115.6004798	-20.68133408	354232.10	7712490.51	28.4	29/09/1991
Triller-1	115.3869028	-20.68148255	331982.87	7712267.44	26.0	28/06/2000
Trimouille-1	115.5726479	-20.40338523	351063.79	7743232.21	9.1	12/02/1967
Ulidia-1	115.7222042	-20.51944227	366771.41	7730514.71	26.2	12/11/1992
West Harriet-1	115.5968275	-20.60168472	353775.50	7721303.86	33.0	12/05/1998
Whitlock-1	115.4168911	-20.72842533	335157.78	7707101.62	48.3	07/07/1976
Wonnich-1	115.4290258	-20.49957690	336176.94	7732447.29	29.5	05/07/1995

Basic wireline log suites for the wells were provided digitally by Wiltshire Geological Services and were loaded into the GeoFrame™ project. Deviation survey data were collated for non-vertical wells from all available well completion reports and also loaded into the GeoFrame™ project to allow conversion back to true vertical depth. Formation tops for the Barrow Sub-basin were obtained from the Western Australian Department of Industry and Resources WAPIMS database (provided digitally in Haworth & Arden, 1999) or well completion reports. The formation tops were loaded into the GeoFrame™ project so that they could be posted onto the wireline logs for reference to help constrain the intervals of interest for the sequence stratigraphic study.

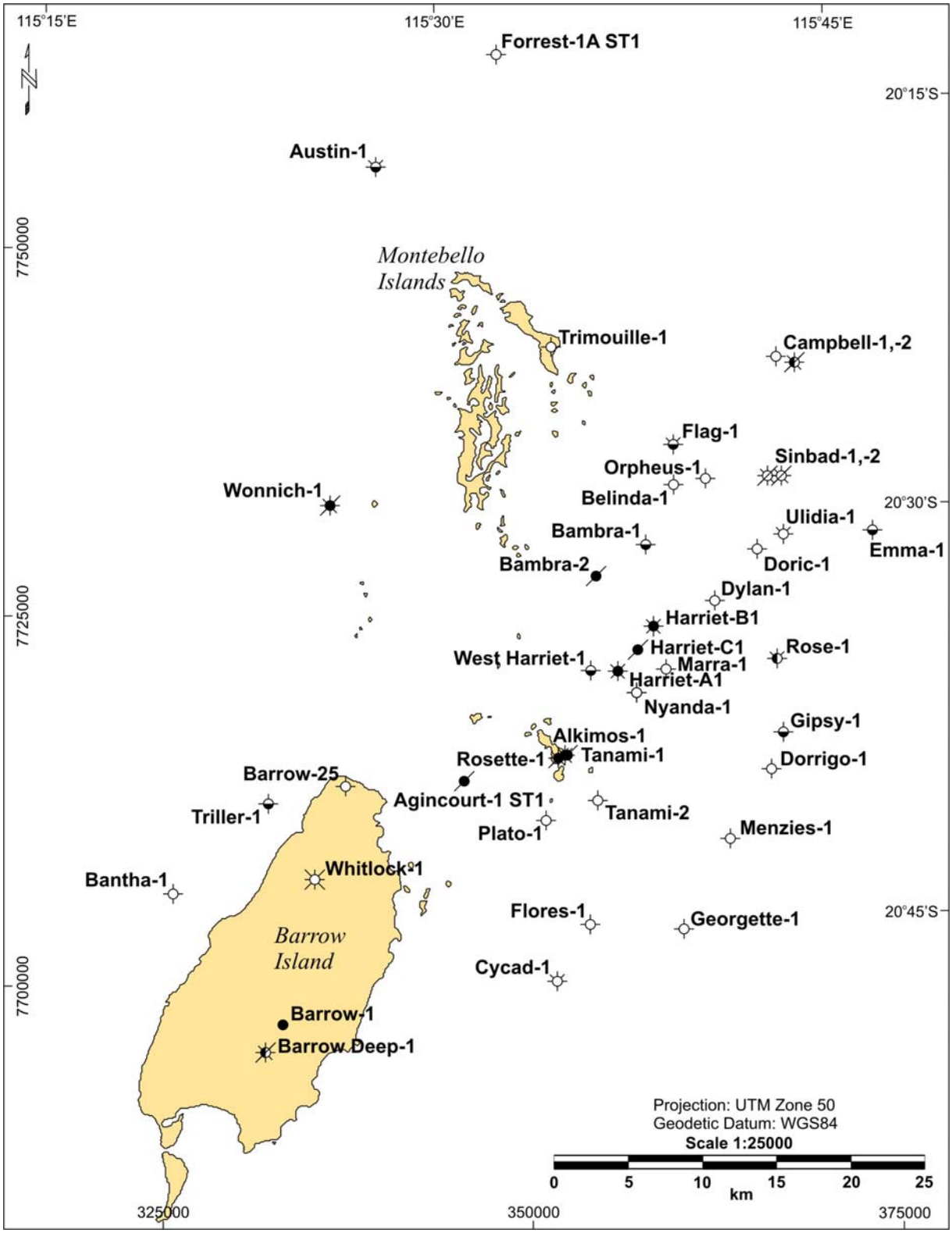

Figure 3.4 Location map of wells in the Barrow Sub-basin used for this PhD study.

3.3.3 Pressure, Temperature and Salinity Data

Pressure, temperature and salinity data were obtained where available from well completion reports. Pressure data were collated from various formation pressure tests, such as repeat formation tests (RFT), sequential formation tests (SFT), modular formation dynamic tests (MDT) and drill stem tests (DST). The pressure data collated for the Barrow Sub-basin are provided in Appendix B. Geothermal gradients were calculated for each well from bottom hole depth temperature data. The temperature data and gradients calculated are provided in Appendix C. Salinity data were collated where available over the interval of interest and a mean average was calculated.

3.3.4 Core

Core data is much more abundant in the Barrow Sub-basin than the Petrel Sub-basin, as the Flag Sandstone is a major hydrocarbon-producing interval; therefore numerous wells had cores drilled through the interval of interest. The cores from 19 wells, amounting to approximately 430 m in total (representing up to 40% of the reservoir formation and up to 5% of the seal), were viewed at Geoscience Australia's core store and the core storage facilities of the Western Australian Department of Industry and Resources. Table 3.7 lists the details of the core intervals viewed. The quality of the cores are variable, ranging from excellent (e.g. Sinbad-2, Tanami-1, Ulidia-1) to very poor (e.g. Trimouille-1, which had fractured into many pieces due to the core recovery process and length of time stored; and Harriet-B1, which had disintegrated due to the friable nature of the sandstones so that only bags of loose sand remained). The core from Wonnich-1 was particularly useful for the sedimentary study, as it consists of five consecutive cores of 100% recovery over the Flag Sandstone. Hence, 90 m of good quality continuous sedimentary core was available for viewing, providing an excellent opportunity to assess the heterogeneity within a reservoir-scale interval.

Table 3.7 Details of core intervals in the Barrow Sub-basin that were viewed for this PhD study.

Well Name	Core No.	Depth From: (m MD)	Depth To: (m MD)	Recovery		Quality	Formation Name
				m	%		
Alkimos-1	1	2385.0	2403.0	17.60	97.8	good	Flag Sandstone
Austin-1	1	2875.5	2886.9	11.40	100.0	excellent	Upper Barrow Gp
	2	2934.0	2952.5	18.10	97.8	good	Lower Barrow Gp
Bambra-2	1	2025.0	2034.0	1.74	19.3	moderate	Flag Sandstone
	2	2039.8	2048.8	6.90	76.4	moderate	Flag Sandstone
Campbell-2	1	2195.0	2197.2	0.52	23.6	moderate	Flag Sandstone
	2	2201.8	2205.8	4.00	100.0	moderate	Flag Sandstone
	3	2205.8	2220.8	10.20	68.0	moderate	Flag Sandstone
Dorrigo-1	1	975.0	985.0	9.10	91.0	poor	Muderong Shale
	2	985.0	1001.0	16.00	100.0	moderate	Muderong Shale
Emma-1	1	1707.0	1716.2	8.50	92.4	good	Mardie Greensand
	2	1726.0	1735.0	8.20	91.1	moderate	Barrow Gp
Flag-1	1	1291.1	1299.7	8.53	100.0	moderate	Muderong Shale
	2	2210.4	2218.0	7.62	100.0	moderate	Barrow Gp
Flores-1	1	1702.0	1711.4	2.22	23.6	moderate	Flag Sandstone
Harriet-A5	1	2243.2	2261.7	18.50	100.0	moderate	Flag Sandstone
	2	2262.3	2280.8	18.20	98.4	moderate	Flag Sandstone
	3	2280.8	2299.3	18.50	100.0	moderate	Flag Sandstone
Harriet-B1	1	1946.0	1964.7	18.70	100.0	very poor	Flag Sandstone
	2	1965.0	1982.4	17.40	100.0	very poor	Flag Sandstone
Marra-1	1	1997.6	2003.0	5.20	96.3	good	Flag Sandstone
Nyanda-1	1	1949.7	1950.0	0.27	90.0	good	Muderong Shale
	2	1950.0	1953.0	2.62	87.3	good	Muderong Shale
Orpheus-1	1	2087.0	2105.0	9.94	55.2	moderate	Flag Sandstone
Plato-1	1	2175.5	2188.9	10.90	81.3	good	Flag Sandstone
Sinbad-2	1	2277.0	2299.5	22.50	100.0	excellent	Flag Sandstone
Tanami-1	1	2184.4	2202.2	17.80	100.0	excellent	Flag Sandstone
	2	2202.2	2220.7	18.50	100.0	excellent	Flag Sandstone
Trimouille-1	4	2432.3	2435.4	3.00	100.0	very poor	Muderong Shale
Ulidia-1	2	2055.0	2080.5	25.10	98.4	excellent	Flag Sandstone
Wonnich-1	1	2254.5	2272.7	18.20	100.0	excellent	Flag Sandstone
	2	2272.7	2290.7	18.00	100.0	excellent	Flag Sandstone
	3	2290.7	2308.7	18.00	100.0	excellent	Flag Sandstone
	4	2308.7	2326.9	18.20	100.0	excellent	Flag Sandstone
	5	2326.9	2345.2	18.30	100.0	excellent	Flag Sandstone

3.3.5 Conventional Core Analyses

Conventional core analyses of porosity and permeability derived from core plug samples were collated where available. As the study interval is also a hydrocarbon-producing interval, many core plug samples had been collected and analysed for porosity and permeability. The core plug porosity and permeability data from wells within the study area (over 1600 data points in total) were collated from both Geoscience Australia's PORPERM database and the Western Australian Department of Industry and Resources WAPIMS database (provided digitally in Haworth & Arden, 1999). The collated core plug porosity and permeability data is provided in Appendix D.

3.3.6 Biostratigraphic Data

Biostratigraphic data are crucial to sequence stratigraphic interpretation to constrain the chronostratigraphic framework. Biostratigraphic data for wells from the Barrow Sub-basin were provided by Geoscience Australia from their digital STRATDAT database. Each individual biostratigraphic data point has been cross-checked by Geoscience Australia for its reliability and comes supplied with its own reference, confidence code and remarks. Additional biostratigraphic data were used if necessary from palynological data sheets of Morgan Palaeo Associates (donated to the Australian School of Petroleum by Roger Morgan) and well completion reports; however, these were used more cautiously as they have not been cross-checked to the same degree as Geoscience Australia's STRATDAT database. The biostratigraphic data are referenced to the biozonation scheme of Helby *et al*. (1987). The biostratigraphic data were loaded into the GeoFrame™ project so that they could be posted onto the wireline logs for reference during the wireline log correlation (discussed in section 3.4.4 below).

3.3.7 Mercury Injection Capillary Pressure Analyses

Mercury injection capillary pressure (MICP) analyses were undertaken on 29 core samples collected from the cores of 15 wells in the Barrow Sub-basin. The samples were processed by the Australian School of Petroleum using a *Micromeritics Autopore 9410 Mercury Injection Porosimeter*. The samples were chosen to represent different facies within the Muderong Shale regional seal, as well as intraformational seals and reservoir units of the Flag Sandstone and Barrow Group. Table 3.8 lists the details of the collected core samples in

the Barrow Sub-basin that were selected for MICP analysis. The MICP data for each of the core samples analysed is provided in Appendix E.

Table 3.8 Details of MICP core samples from the Barrow Sub-basin.

Well Name	Sample No.	Depth (m MD)	Formation	MICP Sample Type	Facies
Alkimos-1	000-665	2388.77	Flag Sandstone	Intraformational seal	Claystone
	000-709	2391.19	Flag Sandstone	Reservoir	Medium-grained sandstone
Austin-1	000-621	2877.62	Upper Barrow Gp	Intraformational seal	Claystone
Bambra-2	000-710	2041.95	Flag Sandstone	Reservoir	Medium-grained sandstone
Campbell-2	000-680	2210.27	Flag Sandstone	Intraformational seal	Laminated siltstone
Dorrigo-1	000-627	981.90	Muderong Shale	Regional top seal	Glauconitic claystone
	000-628	992.42	Muderong Shale	Regional top seal	Glauconitic siltstone
	000-624	994.47	Muderong Shale	Regional top seal	Very fine-grained, glauconitic sandstone
Flag-1	000-618	1294.89	Muderong Shale	Regional top seal	Very fine-grained, bioturbated, glauconitic sandstone
	000-664	1296.90	Muderong Shale	Regional top seal	Very fine-grained, bioturbated, glauconitic, siderite-cemented sandstone
	000-620	2217.88	Barrow Group	Intraformational seal	Silty claystone
Harriet-A5	000-629	2261.68	Flag Sandstone	Intraformational seal	Claystone
Harriet-B1	000-630	1943.72	Flag Sandstone	Intraformational seal	Claystone
Marra-1	000-626	1999.71	Flag Sandstone	Intraformational seal	Claystone
Nyanda-1	000-611	1949.88	Muderong Shale	Regional top seal	Claystone
	000-612	1951.17	Muderong Shale	Regional top seal	Claystone
	000-613	1952.14	Muderong Shale	Regional top seal	Claystone
	000-686	1952.77	Muderong Shale	Regional top seal	Claystone
Orpheus-1	000-625	2095.78	Flag Sandstone	Intraformational seal	Claystone
Sinbad-2	000-616	2282.68	Flag Sandstone	Intraformational seal	Claystone
	000-711	2291.23	Flag Sandstone	Reservoir	Medium-grained sandstone
Trimouille-1	000-632	2433.32	Muderong Shale	Regional top seal	Claystone
	000-631	2434.95	Muderong Shale	Regional top seal	Claystone

Well Name	Sample No.	Depth (m MD)	Formation	MICP Sample Type	Facies
Ulidia-1	000-615	2059.76	Flag Sandstone	Intraformational seal	Siltstone
Wonnich-1	000-707	2257.54	Flag Sandstone	Reservoir	Fine-grained, argillaceous sandstone
	000-623	2278.85	Flag Sandstone	Intraformational seal	Argillaceous siltstone
Wonnich-1	000-718	2282.43	Flag Sandstone	Reservoir	Fine-grained, laminated (horizontal) sandstone
	000-708	2301.95	Flag Sandstone	Reservoir	Fine-grained, siderite-cemented sandstone
	000-705	2320.98	Flag Sandstone	Reservoir	Medium-grained sandstone

3.4 INTERPRETATION TECHNIQUES

3.4.1 Sequence Stratigraphy: Theory

Sequence stratigraphy is the foundation methodology for all the seismic interpretation, well correlation and geological modelling. Sequence stratigraphy is the study of rock relationships within a chronostratigraphic framework (Van Wagoner *et al.*, 1988). It differs from lithostratigraphy in that it is a correlation of time-significant geological surfaces, whereas lithostratigraphy correlates rocks of a similar lithology (Emery & Myers, 1996) (Figure 3.5). Sequence stratigraphy provides a powerful tool to help analyse, understand and predict the spatial and temporal distributions of reservoir and seal lithologies within a basin and the geometry, continuity, heterogeneity and interconnectivity of those units (Kennard *et al.*, 1999; Posamentier & Allen, 1999).

Sequence stratigraphy as a methodology has been in existence for many years. The basic concepts were first defined from seismic stratigraphy, detailed in the ground-breaking AAPG Memoir 26 publication (Payton, 1977), and later developed into sequence stratigraphy in the landmark SEPM Special Publication 42 (Wilgus et al., 1988). However, many different authors have varied the manner of its application over the years, particularly with reference to the bounding surfaces of a depositional sequence and the influence of eustasy or tectonics as a controlling mechanism for the development of sequences. The approach to sequence stratigraphic analysis therefore followed for this PhD study is that outlined by Posamentier and Allen (1999), where sequences are defined as relatively conformable successions bounded by unconformities or their correlative conformities, and systems tracts are identified by key stratigraphic surfaces and stacking patterns.

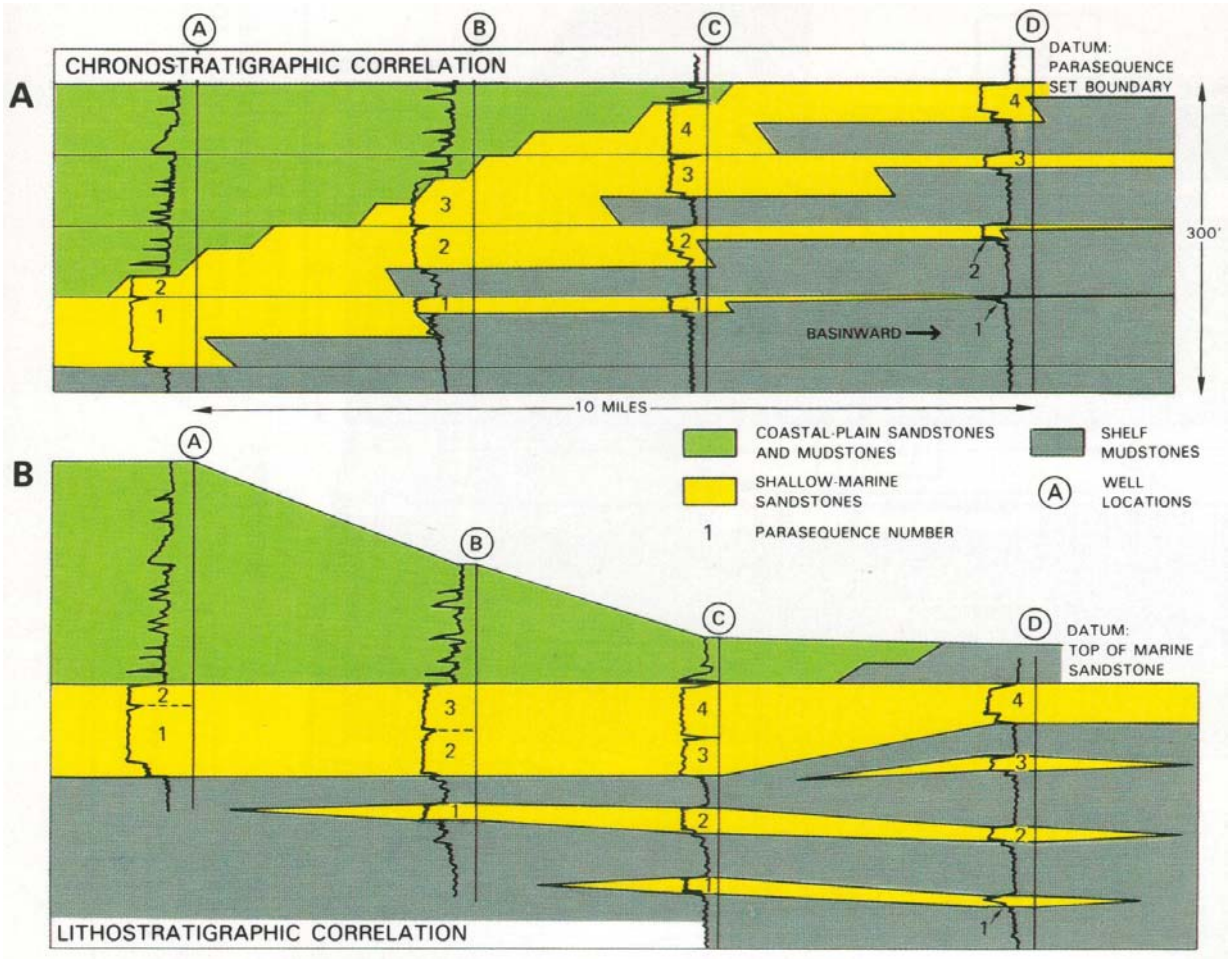

Figure 3.5 Comparison of (A) chronostratigraphic correlation (sequence stratigraphy), which has a geological time significance, and (B) lithostratigraphic correlation, which correlates rocks of similar type (after Van Wagoner *et al.*, 1990).

The application of sequence stratigraphy requires an analysis of the cyclic sedimentation patterns that are present in stratigraphic successions, which develop as a result of the interaction between sediment supply and the space available for that sediment to fill (Posamentier & Allen, 1999). The available space is called accommodation (Jervey, 1988) and is a function of several factors, including eustasy, tectonics, sediment compaction and physiographic setting. For all practical purposes, relative sea level is a proxy for accommodation, as sedimentary patterns respond to changes in accommodation irrespective of whether eustasy or tectonics was the predominant factor in creating the accommodation space (Posamentier & Allen, 1999). How the accommodation space changes with time determines the sedimentary patterns that result (Figure 3.6). When the sedimentation rate is less than the rate at which accommodation space is created, relative sea level rises (i.e. water depth increases) and there is a transgression of the sea and the shoreline backsteps landward (retrogrades). However, if the rate of relative sea level rise and creation of accommodation

Figure 3.6 Sedimentary stacking patterns as a function of accommodation volume and sediment supply (after Posamentier & Allen, 1999).

space is less than the rate of sediment accumulation, the water depth decreases as sediments gradually fill the available space, and a regression of the sea occurs with sediments prograding out into the basin (Posamentier & Allen, 1999) (Figure 3.6).

Two types of regression can occur: normal regression and forced regression (Figure 3.7). In a normal regression, the shoreline progrades seaward out into the basin as a result of the sediment filling the available accommodation space (i.e. relative sea level is rising but at a rate less than the rate of sediment accumulation). In a forced regression, relative sea level falls and progressively exposes the shelf (forming an unconformity) and forces the shoreline to migrate seaward out into the basin (Posamentier & Allen, 1999) (Figure 3.7).

The sedimentary fill of a basin can be subdivided into sequences on the basis of the cyclic sedimentary patterns created through changes in accommodation space, relative sea level and sediment supply. A sequence is defined as "a relatively conformable succession of genetically related strata and bounded at its top and base by unconformities or their

NOTE:
This figure is included on page 61 of the print copy of the thesis held in the University of Adelaide Library.

Figure 3.7 Stratal architecture of A) "normal" regression, contrasted with that of B) "forced" regression. Note that "normal" regression is associated with aggradation as well as progradation, whereas "forced" regression is associated with downstepping and progradation (after Posamentier & Allen, 1999).

correlative conformities" (Mitchum *et al.*, 1977b). A complete depositional sequence deposited during a cycle of accommodation change consists of a regressive-transgressive-regressive facies succession (Posamentier *et al.*, 1988). A sequence can therefore be subdivided into systems tracts, which are a linkage of contemporaneous depositional systems (Brown & Fisher, 1977), that represent the different phases of regression and transgression within a depositional sequence (Figure 3.8).

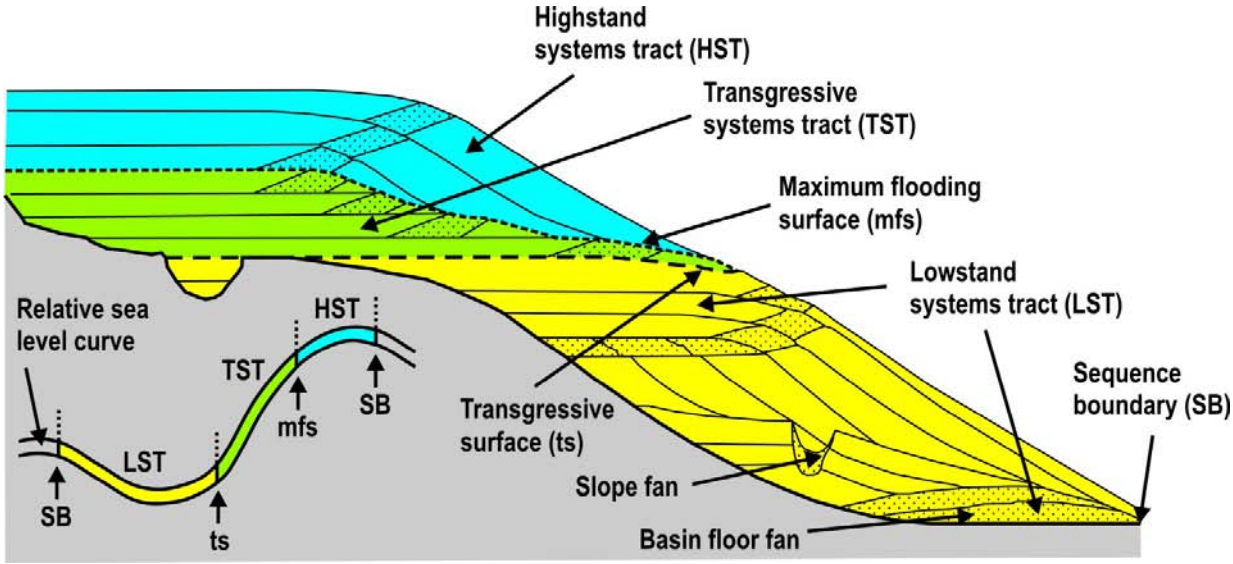

Figure 3.8 Stratal geometries, key surfaces and systems tracts within a depositional sequence (modified after Emery & Myers, 1996).

At the base of the sequence is the lowstand systems tract (Figure 3.8), overlying the sequence boundary (which consists of a stratigraphic unconformity on the exposed shelf and a correlative conformity seaward of the lowstand shoreline). The lowstand systems tract forms a regressive (progradational to aggradational) succession deposited during falling relative sea level, subsequent stillstand and initial rise of relative sea level (whilst shoreline regression is still maintained) (Van Wagoner *et al.*, 1988; Emery & Myers, 1996; Posamentier & Allen, 1999). When continued relative sea level rise outpaces sediment supply (i.e. accommodation increases) transgression is initiated, forming the transgressive surface that separates the lowstand systems tract from the overlying transgressive systems tract (Figure 3.8). The transgressive systems tract comprises a transgressive (retrogradational) succession deposited during the time when relative sea level rise is greater than sediment supply (Van Wagoner *et al.*, 1988; Emery & Myers, 1996; Posamentier & Allen, 1999). The peak of maximum transgression of the sea forms the maximum flooding surface, which represents the upper limit of the transgressive systems tract (Figure 3.8). Above the maximum flooding surface is the highstand systems tract, which constitutes a regressive (aggradational to progradational) succession deposited as sediment accumulation rates exceed the rate of relative sea level rise. The sequence is bounded at the top by another unconformity or its correlative conformity (Figure 3.8) (Van Wagoner *et al.*, 1988; Emery & Myers, 1996; Posamentier & Allen, 1999).

3.4.2 Sequence Stratigraphy: Methodology

The procedure for sequence stratigraphic interpretation is summarised by Posamentier and Allen (1999) as follows:

1. Establish the palaeogeographic setting;
2. Interpret depositional systems and facies using all available data;
3. Subdivide the stratigraphic succession through the identification of maximum flooding surfaces and sequence boundaries; and
4. Analyse facies stacking patterns and identify systems tracts.

For this PhD study, the general regional palaeogeographic setting was determined from interpretation of regional seismic lines and regional well correlations, calibrated by sedimentary core and biostratigraphic data. The depositional systems were interpreted predominantly from sedimentological assessment of the core data, and assisted by analysis of the log motifs observed in the wireline logs. Maximum flooding surfaces were identified

from condensed sections on wireline logs (e.g. maximum shale peaks on the gamma ray log) and from regional reflectors below progradational seismic facies (downlap surface) on seismic data. Sequence boundaries were identified through biostratigraphy (missing section), wireline log motifs (e.g. sharp-based sandy intervals) and seismic characteristics such as truncated reflectors, downlap surfaces and down-stepping progrades (forced regression). Facies stacking patterns were analysed in sedimentary core, wireline logs and seismic data in terms of aggradational, progradational and retrogradational packages and used in conjunction with the interpreted depositional environments to identify systems tracts. Thus, the integration of seismic stratigraphic interpretations with well correlations, core lithofacies and biostratigraphy enabled sedimentary depositional models and sequence stratigraphic frameworks to be developed for both case studies.

3.4.3 Seismic Interpretation

The seismic data were interpreted across the study areas based on the seismic stratigraphy interpretation principles defined by Mitchum *et al*. (1977a). Reflector termination patterns (such as downlap, onlap and truncation) were identified (Figure 3.9) and distinct seismic facies were distinguished on the basis of reflector continuity, amplitude strength and configuration (geometry) (Figure 3.10). The analysis of seismic reflector terminations and facies helped to identify key seismic stratigraphic packages and allowed significant seismic horizons to be interpreted across the study areas.

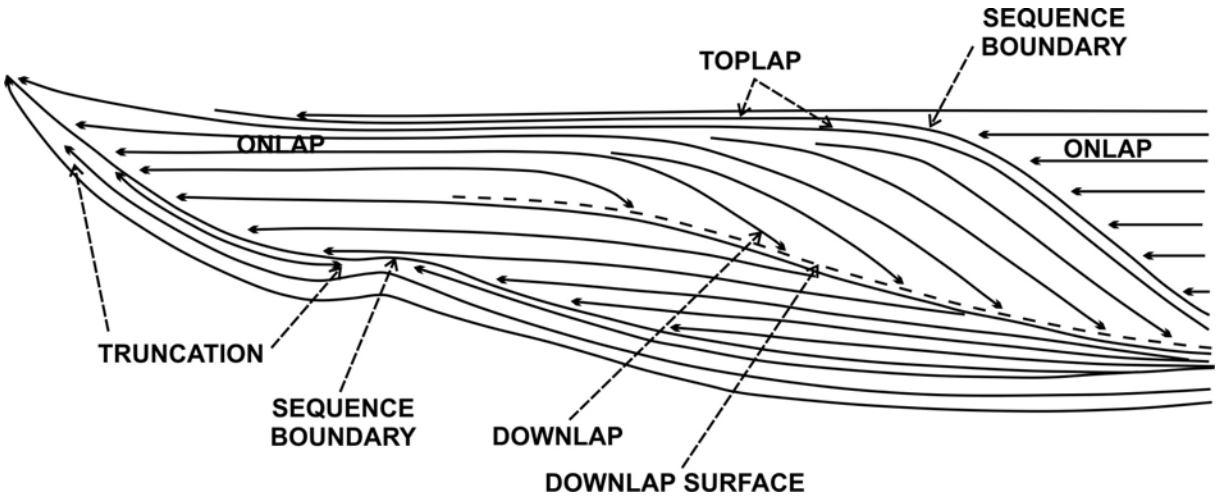

Figure 3.9 Diagram showing reflection termination patterns and types of discontinuity in the process of defining a sequence (in the sense of Mitchum *et al.*, 1977a) (after Van Wagoner *et al.*, 1987).

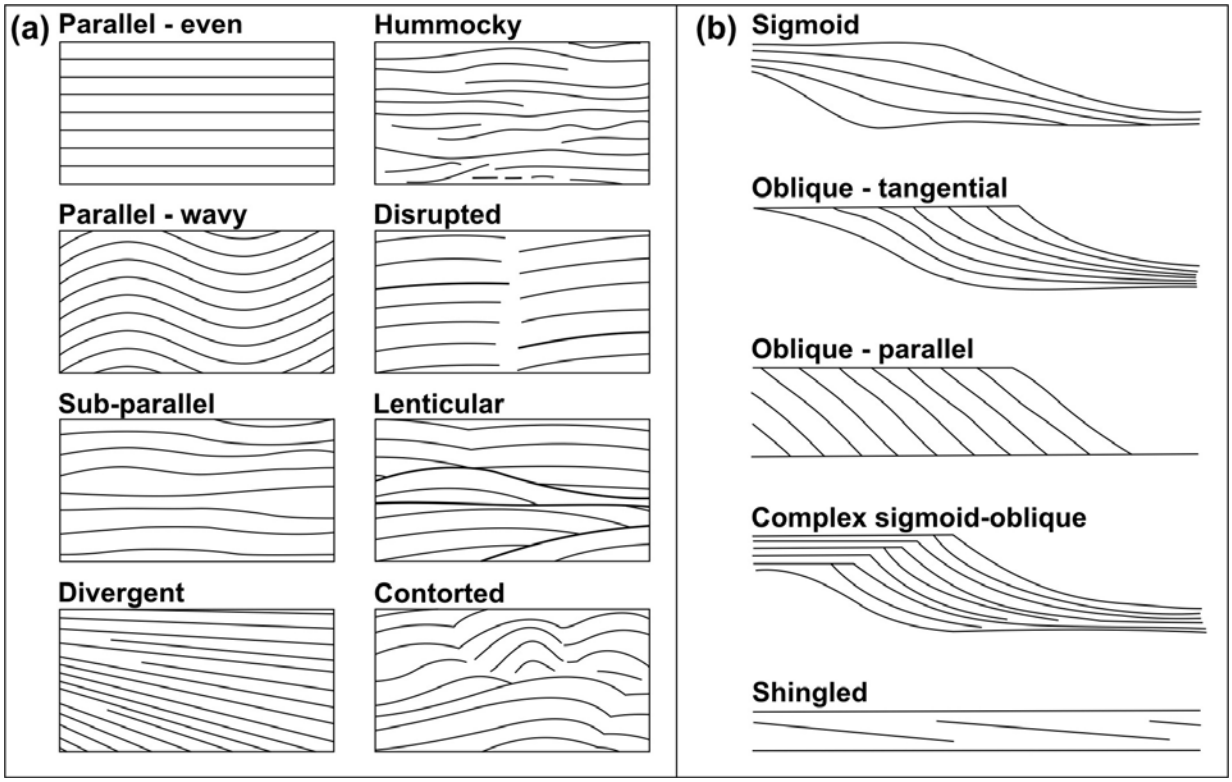

Figure 3.10 Examples of (a) seismic reflection configurations and (b) prograding clinoform seismic reflection patterns (modified after Mitchum *et al.*, 1977a).

3.4.4 Wireline Log Well Correlation

The wells were interpreted within the WellPix™ module of GeoFrame™ (versions 3.8 and 4.0.2, Schlumberger) using a sequence stratigraphic approach (Van Wagoner *et al.*, 1990; Rider, 1996; Posamentier & Allen, 1999). The log motifs of wireline logs such as the gamma ray (GR) and sonic (DT) were analysed for coarsening upward (progradational), fining upward (retrogradational) and blocky (aggradational) sedimentary stacking patterns (Figure 3.11). Key stratigraphic surfaces, such as maximum flooding surfaces and sequence boundaries, were identified in the wells from log characteristics such as maximum shale peaks or sharp-based sandy intervals on the gamma ray log (Figure 3.11). The wells were correlated across the study areas using a combination of the biozonation information, the key stratigraphic surfaces and stacking pattern log motifs, the depositional environments interpreted from the sedimentology and the regional seismic interpretation.

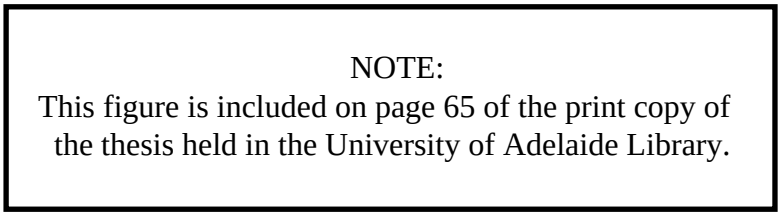

Figure 3.11 Example of sequence stratigraphic surfaces and sedimentary stacking patterns interpreted from wireline log motifs (modified after Posamentier & Allen, 1999).

3.4.5 Sedimentology

Graphical core log descriptions were drawn up for each of the sedimentary cores viewed in the Petrel and Barrow sub-basins and photographs taken where possible (Appendix F). The graphic core logs depict the lithology, grainsize and sedimentary structures observed along the length of the core. Lithofacies were identified within the cored intervals, based on variations in characteristics such as colour, bedding, composition, texture, fossils and sedimentary structures. The lithofacies were then grouped together into various facies associations and an interpretation was made as to their possible environment of deposition.

3.4.6 Core Plug Porosity and Permeability Data Analysis

Conventional core analyses of porosity and permeability derived from core plug samples were used to provide insights into the potential reservoir quality (and also to enable the petrophysicists to groundtruth the porosity and permeability values derived during the petrophysical interpretation of the wireline logs). The core plug porosity and permeability

data were plotted on graphs of porosity versus permeability by formation to identify the reservoir quality characteristics of the different reservoir intervals.

The dataset for the Barrow Sub-basin was considerably larger than that of the Petrel Sub-basin, which allowed further analysis of the core plug data within the Flag Sandstone to be undertaken. Each core plug data point that had been viewed as part of the core description work was assigned a specific lithofacies based on variations in grainsize, composition and sedimentary structures (987 data points in total; Appendix D). These were plotted by facies association on a graph of porosity versus permeability, to evaluate the different reservoir quality characteristics of the various facies associations. The dataset was statistically analysed to assess the average porosities, permeabilities and abundances of various facies associations within the Flag Sandstone.

3.4.7 Pressure and Temperature Gradients

The pressure data were plotted on graphs of pressure versus depth and linear gradients through the datasets were calculated. The pressure data collated and gradients calculated for both sub-basins is provided in Appendix B. Geothermal gradients were calculated for each well from bottom hole depth temperature data, using the formula (Rider, 1996):

$$G = \frac{T^{\circ}_{formation} - T^{\circ}_{surface}}{Depth} \qquad [7]$$

where G is the geothermal gradient, $T^{o}_{formation}$ is the formation temperature and $T^{o}_{surface}$ is the average mean surface temperature. The average mean surface temperature for all calculations was assumed to be 20ºC. The temperature data and gradients calculated for wells in both sub-basins are provided in Appendix C.

3.4.8 Seal Capacity

Seal capacity is the maximum height of a CO_2 column beneath a caprock or intraformational seal that the rock is capable of retaining. The potential seal capacity of the regional top seals and intraformational seals in the Petrel and Barrow sub-basins were assessed by Mercury Injection Capillary Pressure (MICP) analysis. MICP tests are a measurement of the pressures required to move mercury through the pore network system of a core sample. The theory of mercury porosimetry is that a non-wetting fluid (i.e. mercury) will

not displace the wetting phase that initially saturates the pores of the rock (i.e. air) until sufficient pressure is exerted (Purcell, 1949). This is analogous to the CO_2/water system at reservoir conditions, where the seal rock will not fail until the buoyancy pressure (defined by the density differences between CO_2 and water and the height of the CO_2 column) is sufficient for the CO_2 to enter the pores and displace the formation water (Berg, 1975; Schowalter, 1979; Vavra *et al.*, 1992). The smaller the pore throat size, the greater the amount of buoyancy pressure required for the non-wetting fluid to penetrate the pores, and thus the greater the retention capacity of the seal.

The MICP data are plotted on graphs of increasing pressure versus mercury saturation (Figure 3.12). As the pressure initially begins to increase, mercury is able to fill any surface voids and fractures that may exist, which is termed conformance. Entry pressure (P_e) is defined as the pressure at which mercury first begins to enter the pores of the rock. When the pressure is sufficient for a continuous filament of mercury to extend through the sample, the threshold pressure (P_{th}) has been reached, which is the point at which the seal rock is considered to have failed. The methodology for determining the threshold pressure adopted for this PhD study is that of Dewhurst *et al*. (2002), whereby the threshold pressure was picked where the large gradient increase occurred on the first derivative (incremental pore volume) of the capillary pressure curve (cumulative pore volume) (Figure 3.12).

The mercury/air threshold capillary pressures were converted to equivalent CO_2/water threshold capillary pressures at reservoir conditions using the following equation (Purcell, 1949; Schowalter, 1979):

$$Pc_{CO2/w} = \frac{\gamma_{CO2/w} COS\,\theta_{CO2/w}}{\gamma_{m/a} COS\,\theta_{m/a}} \times Pc_{m/a} \quad [8]$$

where: $Pc_{CO2/w}$ is the capillary pressure in the CO_2/water system (psi), $\gamma_{CO2/w}$ is the interfacial tension of CO_2 and water (dynes/cm), $\theta_{CO2/w}$ is the contact angle of CO_2 and water (i.e. wettability), $\gamma_{m/a}$ is the interfacial tension of mercury and air (dynes/cm), $\theta_{m/a}$ is the contact angle of mercury and air against the rock and $Pc_{m/a}$ is the capillary pressure in the mercury/air system (psi). The values of the parameters for the mercury/air system are: $\gamma_{m/a}$ is 480 dynes/cm and $\theta_{m/a}$ is 40º (Schowalter, 1979), therefore $\gamma_{m/a}\ COS\ \theta_{m/a}$ = 367.7. The values of interfacial tension for the CO_2/water system were determined from the sample-specific pressure, temperature and salinity conditions of each of the core samples, which were input into the proprietary GEODISC™ website calculator (created by Jonathan Ennis-King, CSIRO

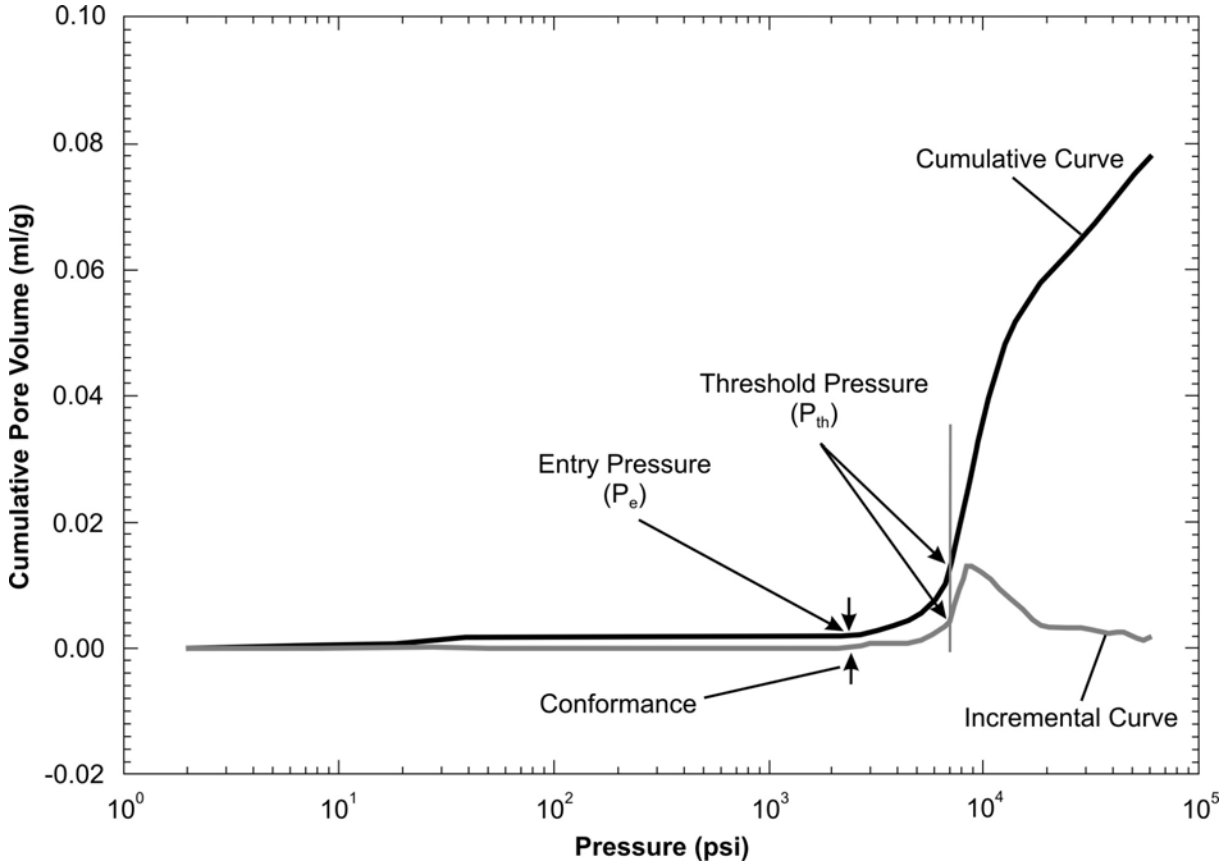

Figure 3.12 Mercury intrusion capillary pressure curves displaying terminology and method of determination of threshold pressure used in this PhD study (after Dewhurst *et al.*, 2002).

Petroleum) to obtain the interfacial tension between CO_2 and water. The contact angle for the CO_2/water system was assumed to be 0º, reflecting the initial water-wet state of the reservoir prior to and during migration (Vavra *et al.*, 1992).

The converted threshold capillary pressures for both the seal and the reservoir samples were then used to calculate the maximum CO_2 column height (seal capacity), using the following equation (Smith, 1966):

$$h_{CO2}\,\max \;=\; \frac{P_{dB} - P_{dR}}{(\rho_w - \rho_{CO2}) \times 0.433} \qquad [9]$$

where: h_{CO2}max is the maximum vertical CO_2 column that can be sealed (ft), P_{dB} is the CO_2/water threshold pressure of the boundary bed (i.e. seal) (psi), P_{dR} is CO_2/water threshold pressure of the reservoir rock (psi), ρ_w is the subsurface density of water (g/cm^3), ρ_{CO2} is the subsurface density of CO_2 (g/cm^3) and 0.433 is the gravity constant. The densities of the CO_2 and water at reservoir conditions were obtained using the proprietary GEODISC™ website

calculator (created by Jonathan Ennis-King, CSIRO Petroleum) using sample-specific pressure, temperature and salinity values for each of the core samples. The MICP data and interpretation for each of the core samples analysed is provided in Appendix E.

3.4.9 Computer Mapping of Geological Surfaces and Depth Conversion

The two-way-time, velocity and depth surfaces of significant seismic and stratigraphic horizons for each of the case studies were created within the CPS-3™ mapping software of GeoFrame™ (versions 3.8 and 4.0.2, Schlumberger). Two sets of geological surfaces were produced for the Petrel Sub-basin: a regional set covering the full extent of the sub-basin (~350 km x 450 km) and a smaller set over the greater Petrel gas field area (~40 km x 80 km). The two-way-time surfaces were gridded from the 2D seismic interpretation using CPS-3's convergent gridding algorithm and the grid parameters specified in Table 3.9.

Table 3.9 Grid parameters used in creating two-way time, velocity and depth surface maps in CPS-3™.

Basin			Petrel Sub-Basin		Barrow Sub-Basin
Model Name			Regional Model	Small Model	Barrow Anticline Model †
Mapping Grid Parameters	**Origin X (Easting m)**		259608	470000	306102
	Origin Y (Northing m)		8341439	8539500	7677565
	Rotation About Origin		0º	58º	0º
	X-Axis	**Range (m)**	357000	40000	72000
		Increment (m)	3000	500	500
		Column Count	120	81	145
	Y-Axis	**Range (m)**	447000	80000	89000
		Increment (m)	3000	500	500
		Column Count	150	161	179

† The map grid extents of the Barrow Anticline Model reflect the dimensions of the original maps of Campbell *et al.* (1984). The resulting depth surface structure maps were reduced in size to over the area of interest (~30 km x 50 km) using a limiting polygon.

A simple average velocity technique was employed to convert the surfaces in time to depth. The two-way time values where the time surface intersected the well bores were extracted from the time surface grid. The well depth markers for that particular time surface were divided by the extracted two-way time values to create an average velocity value at the well location. The average velocity datasets were then gridded across the study area using the convergent gridding algorithm and the previous grid parameters. Multiplying the two-way

time grids by the relevant average velocity grids then created the depth structure surfaces. Depth structure surfaces were created for the following horizons in both Petrel models: Malita (SB1), Plover 1 (SB2), Plover 2 (ts2), Elang (SB3), Frigate 1 (SB4), Frigate 2 (mfs4), Frigate 3 (SB5), Sandpiper 1 (mfs6) and Sandpiper 2 (SB8). An additional depth horizon was created in the Petrel Small Model equivalent to SB7 (top sand depth) by creating an isopach of the depth difference between the SB8 and SB7 well markers and subtracting it from the SB8 depth surface.

In the Barrow Sub-basin, the lack of seismic data over Barrow Island meant that depth structure maps had to be created in a different manner. A publication by Campbell *et al.* (1984) provided a generalised structure map of the near top Muderong Shale and a generalised isopach of the Muderong Shale, covering the greater Barrow Island area. These two contour maps were digitised within Petrosys mapping software, then exported as xyz ASCII data and loaded into the CPS-3™ mapping module of GeoFrame™, to form the basis of the depth structure maps created for the Barrow Anticline geological model. The depth structure surfaces were created using CPS-3's conformable modelling option, using the digitised contour maps of Campbell *et al.* (1984) to provide the structural template and constrained by the sequence stratigraphic well markers of the various surfaces interpreted during the well correlation. The gridding algorithm used was the convergent gridding algorithm and the grid specifications were as shown in Table 3.9. Depth structure surfaces were created for the following horizons: SB4 (base Flag Sandstone), ts4, SB5, ts5, SB6, ts6 (top Flag Sandstone), SB7 (Intra-Muderong Hiatus) and SB8 (top Muderong Shale).

3.4.10 Migration Pathway Mapping

The structural geometry at the top of the reservoir (base regional seal) will influence the migration direction of the buoyancy-driven CO_2. Depth structure maps of the base Bathurst Island Group in the Petrel Sub-basin and base Muderong Shale in the Barrow Sub-basin were exported as xyz ASCII data from the CPS-3™ module of GeoFrame™ and loaded into Petrosys mapping software to create orthocontour maps. The orthocontours are vectors that are tangential to the structural contours (90°) and flow towards the maximum up-dip direction of the slope of the surface. Orthocontours (flow vectors) were created across each of the base regional seal maps to indicate the possible migration directions for CO_2 flow once the base of the regional seal is reached.

3.4.11 3D Geological Model Construction

The complexity of interrelated variables that affect the subsurface behaviour of CO_2 necessitates 3D geological model construction and subsequent numerical flow simulation to develop a predictive appreciation of the feasibility of CO_2 injection and storage scenarios. Geological model construction for CO_2 storage differs from traditional petroleum reservoir modelling because of the long-term storage objective, behaviour of CO_2 at reservoir conditions and the need to assess larger areas (Root *et al.*, 2004; Root, 2007). Three 3D geological models were created for the potential CO_2 storage sites investigated in this PhD study: a regional-scale model of the Petrel Sub-basin (~350 km x 450 km), a smaller scale model over the greater Petrel gas field area (~40 km x 80 km) and a semi regional-scale model of the Barrow Island anticline (~30 km x 50 km) in the Barrow Sub-basin (Figure 3.13). The 3D modelling software package used was GEOCard (Geo Visual Systems Ltd.).

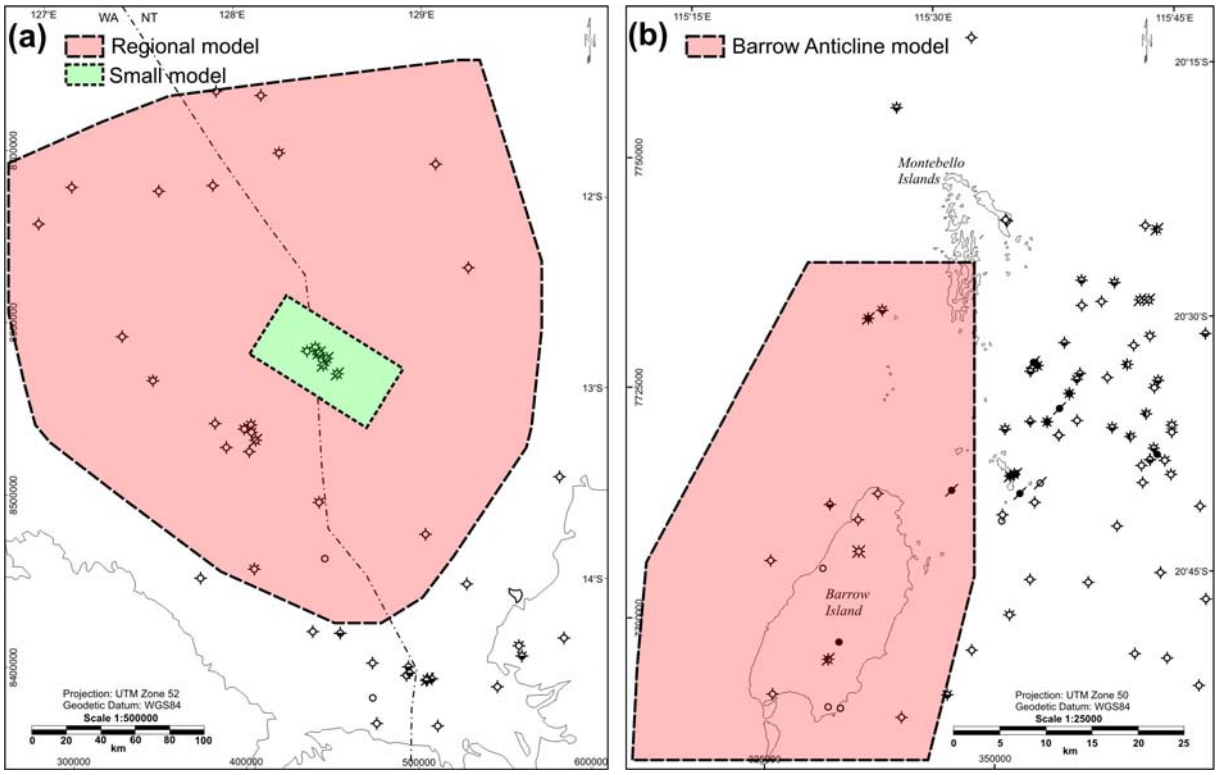

Figure 3.13 Areas covered by the 3D geological models in: (a) Petrel Sub-basin; and (b) Barrow Sub-basin.

The depth structure surfaces created from the significant seismic and stratigraphic horizons in the each of the sub-basins were exported as xyz ASCII data from GeoFrame™ and imported into GEOCard 3D modelling software. The depth structure surfaces provided

the structural framework for the 3D geological models and were the bounding surfaces for the zones of the 3D geological models (Table 3.10). The reservoir heterogeneity in potential CO_2 storage sites can be represented in 3D geological models through the zone geometry and layering style, to reflect the interpreted stratigraphic architecture of the geological units and stratal relationships such as downlap, onlap and truncation. In the Petrel Sub-basin, the zones of the 3D geological model comprise the interpreted seismic packages, whereas in the Barrow Sub-basin, the zones broadly encapsulate the three reservoir units and their intervening intraformational seals. The geometry of the layers within the zones were defined using the functions parallel to top, parallel to base or proportional, to reflect the internal geometries of the various seismic packages seen on the seismic sections. The thicknesses of the layers within each zone were chosen as the thickness required to accurately capture the vertical heterogeneity. Table 3.10 details the parameters used for the construction of the zones and layers in each of the 3D geological models.

Table 3.10 Details of the zones and layers created in the GEOCard 3D geological model grid construction.

GEOCard Model	Top Surface	Base Surface	Zone	Layer Geometry	Number or Thickness of Layers
Petrel Regional Model and Petrel Small Model	Bathurst	Sandpiper 2	Bathurst (seal)	Proportional	4 layers
	Sandpiper 2	Sandpiper 1	Sandpiper Upper	Proportional	6 layers
	Sandpiper 1	Frigate 3	Sandpiper Lower	Parallel to Top	15 m
	Frigate 3	Frigate 2	Frigate Upper	Parallel to Top	20 m
	Frigate 2	Frigate 1	Frigate Mid	Parallel to Top	10 m
	Frigate 1	Elang	Frigate Lower	Parallel to Base	15 m
	Elang	Plover 2	Elang	Parallel to Top	10 m
	Plover 2	Plover 1	Plover Upper	Proportional	10 layers
	Plover 1	Malita	Plover Lower	Proportional	10 layers
Barrow Anticline Model	SB8 (top Mud. Sh.)	ts6 (top Flag Sst)	Sq6-7_tst-hst (seal)	Proportional	4 layers
	ts6 (top Flag Sst)	SB6	Sq6_lst	Parallel to Top	10 m
	SB6	ts5	Sq5_tst-hst	Parallel to Top	15 m
	ts5	SB5	Sq5_lst	Proportional	5 layers
	SB5	ts4	Sq4_tst-hst	Parallel to Top	5 m
	ts4	SB4 (base Flag)	Sq4_lst	Proportional	10 layers

A cellular 3D grid was generated within the structural framework of the 3D geological models, defined horizontally by a specified grid cell size and vertically by the thickness of the

layers. The grid cell size selected had to adequately represent the reservoir heterogeneity without creating an unnecessarily large model. When producing 3D models at petroleum field-scale it would normally be appropriate to use a horizontal grid cell size such as 50 m by 50 m. However, the semi-regional to regional nature of the models produced for CO_2 storage would have far too many cells for the numerical flow simulations to process if a 50 m by 50 m cell size were used. The horizontal grid cell size used in the Petrel Regional Model was 5 km by 5 km and in the Petrel Small Model was 1 km by 1 km. In the Barrow Sub-basin, the horizontal grid cell size used for the Barrow Anticline Model was 500 m by 500 m. The lesser vertical dimensions of the Barrow Anticline Model meant that a smaller horizontal grid cell size could be selected, without creating too many grid cells in total. All the 3D geological models created had less than one million grid cells in total (which was a requirement of the reservoir engineers for the GEODISC™ project).

The 3D cellular grids were populated with reservoir parameters derived from the petrophysical assessment (e.g. volume of shale, porosity, permeability). Firstly, the attributes from the petrophysical wireline logs were averaged at the wells for each cell intersected along the location of the well bore. The attributes were then propagated through the entire grid using stochastic conditional simulations. Deterministic methodologies (such as kriging or moving average) were not used because the data density was mostly not sufficient to allow interpolation between many of the well locations and the data points also exhibited clustering with respect to the volumes being populated. Therefore, sequential Gaussian simulation was used in conjunction with simple variogram models to describe the spatial variability of the parameters. For each attribute, multiple realisations were generated, with each realisation being equally likely to occur. Other physical parameters important to the behaviour of CO_2 (e.g. pressure, temperature) were also be populated in the 3D geological models. The attributes created in each of the 3D geological models are detailed in Table 3.11.

3.4.12 CO_2 Storage Capacity Calculations

CO_2 storage capacity is a very hard parameter to determine, although it is the question that most often needs to be answered. The buoyant nature of CO_2 and the dynamic manner in which it migrates thorough a reservoir rock means that not all the rock pore space available for storage will be filled. Therefore, an accurate assessment of how much of the available interconnected pore volume is actually utilised (sweep efficiency) cannot be answered until the dynamic numerical flow simulation stage of a potential site assessment. At the static

Table 3.11 Grid attributes created in the 3D geological models.

Attribute Name	Unit	Description
ZoneNo		Zones in 3D model, numbered from top to bottom
Layer		Layers in 3D model, numbered from top to bottom
VshAtWells	%	Vshale at the wells, sampled from the log-derived Vshale curve
PhiAtWells	%	Porosity at the wells, sampled from the log-derived porosity curve
KAtWells	mD	Permeability at the wells, sampled from the log-derived permeability curve
VshSGS	%	Vshale populated to each grid cell in the 3D model, using sequential Gaussian simulation
PhiSGS	%	Porosity populated to each grid cell in the 3D model, using sequential Gaussian simulation
KcoSGS	mD	Permeability populated to each grid cell in the 3D model, using co-located sequential Gaussian simulation with PhiSGS attribute
Depth	m	Depth at the centre of each grid cell
Temperature	^{o}C	Temperature of each grid cell, calculated using the average temperature gradient of the Petrel Sub-basin for the Petrel Sub-basin models and the Wonnich-1 temperature gradient for the Barrow Sub-basin model, applied to the Depth attribute
Pressure	MPa	Pressure of each grid cell, calculated using the average hydrostatic pressure gradients, applied to the Depth attribute
Volume	m^3	Volume of each grid cell
PoreVolume	m^3	Pore volume of each grid cell, calculated by multiplying the Volume attribute by the PhiSGS attribute
CO2ExpansionFactor †	m^3/m^3	CO_2 Expansion Factor ($1/b_g$) of each grid cell, calculated from cubic fit equation (Jonathan Ennis-King, CSIRO Petroleum, pers. comm., 2003)
CO2Volume †	m^3	CO_2 volume of each grid cell, calculated by multiplying PoreVolume attribute by CO2ExpansionFactor attribute

† Attributes created only in Barrow Anticline Model.

geological model stage, all that can be determined accurately in terms of CO_2 storage capacity is the likely pore volume that is available for storage. The calculation methodology used for this PhD study is therefore a simple volumetric assessment of the available pore volume at the prospective site, multiplied by a storage efficiency factor to account for the proportion of the injection horizon that may actually be filled by CO_2. This gives an estimate of the possible CO_2 storage capacity, although numerical flow simulation is required to give a more certain answer. CO_2 storage capacity was calculated using the following equation (DOE, 2007):

$$G_{CO2} = A \times h_g \times \phi_{tot} \times \rho \times E \quad [10]$$

where: G_{CO2} is the mass estimate of CO_2 storage capacity, A is area, h_g is the gross thickness, ϕ_{tot} is the average porosity, ρ is the density of CO_2 at reservoir conditions and E is the CO_2 storage efficiency factor that reflects a fraction of the total pore volume that is filled by CO_2. The storage efficiency factors used were those of DOE (2007), which have been derived by Monte Carlo statistical simulations. They account for factors such as net to total area, net to gross thickness, effective to total porosity, areal displacement efficiency, vertical displacement efficiency, gravity, and microscopic displacement efficiency.

In the Petrel Sub-basin, the pore volume (A x h_g x ϕ_{tot}) was calculated from the 3D geological model (PoreVolume attribute of Table 3.11). As the density of CO_2 changes with increasing temperature and pressure, it should therefore actually be a variable number dependent on the depth. However, for the purposes of this calculation a static number of 0.6 g/cm^3 was chosen to represent the density. This number was derived from a CO_2 density curve, which was generated using the average pressure and temperature gradients of the Petrel Sub-basin and the proprietary GEODISC™ website calculator (created by Jonathan Ennis-King, CSIRO Petroleum). The point at which the curve plateaued, 0.6 g/cm^3, was selected as a representative density for the CO_2. Therefore, the shallower areas of the basin, which would have a lower CO_2 density, are probably overestimated, and vice versa for the deeper areas of the basin. The DOE (2007) storage efficiency factors for saline formations of 1–4 % were used to complete the calculation.

In the Barrow Sub-basin, the pore volume was calculated within the 3D geological model in exactly the same way as the Petrel Sub-basin. However, rather than using a static CO_2 density, the pore volume was converted directly to an equivalent CO_2 volume by multiplying by a CO_2 expansion factor ($1/b_g$) (Jonathan Ennis-King, CSIRO Petroleum, pers. comm., 2003), which takes into consideration the CO_2 density and compressibility at reservoir temperatures and pressures (CO2ExpansionFactor and CO2Volume attributes of Table 3.11). The DOE (2007) storage efficiency factors for saline formations of 1–4 % were used to complete the calculation.

CHAPTER 4. SITE CHARACTERISATION

4.1 INTRODUCTION

Site characterisation is the description of the features and attributes of an area or site to evaluate its potential suitability for CO_2 storage. The geological setting of a site needs to be characterised to determine if a proposed reservoir rock is sufficiently porous and permeable to allow injection of supercritical CO_2, that the overlying seal rock provides effective containment, and that its size is large enough to provide sufficient capacity for the anticipated source of CO_2. This requires the integration and interpretation of all available data, via a broad spectrum of disciplines, to develop robust predictive models of the subsurface behaviour of injected CO_2. Careful site characterisation and selection is vital to the success of geological storage of CO_2. Site characterisation needs to be able to demonstrate, to both project proponents and regulatory authorities, that CO_2 injection and storage is technically and economically feasible, that any risks to integrity can be adequately managed, and that it is secure enough to provide safe long-term containment (IPCC, 2005; Cook, 2006; Birkholzer & Tsang, 2008).

4.2 SITE CHARACTERISATION WORKFLOW FOR GEOLOGICAL STORAGE OF CO_2

The selection of a suitable site for the geological storage of CO_2 comprises mainly geoscientific evaluation on increasingly detailed scales. The different levels of site characterisation that can be undertaken range from an initial regional screening to very detailed site-specific characterisation, and incorporates aspects such as geology, geophysics, geochemistry, geomechanics, hydrogeology, engineering, economics and risk assessment. The workflow shown in Figure 4.1 summarises the different scales of site characterisation and encapsulates all the necessary elements to allow comprehensive evaluation of potential sites for geological storage of CO_2.

There are two broad levels of characterisation: regional characterisation and, following the selection of a preferred site, detailed site characterisation (comprising geoscience characterisation, engineering characterisation and socio-economic characterisation). Regional characterisation reviews the overall suitability of a basin or area for CO_2 storage, and identifies and prioritises potential sites for CO_2 geological storage. Once a site has been

selected, it can proceed to detailed site-specific characterisation, where many aspects need to be researched under a broad spectrum of different disciplines (Figure 4.1).

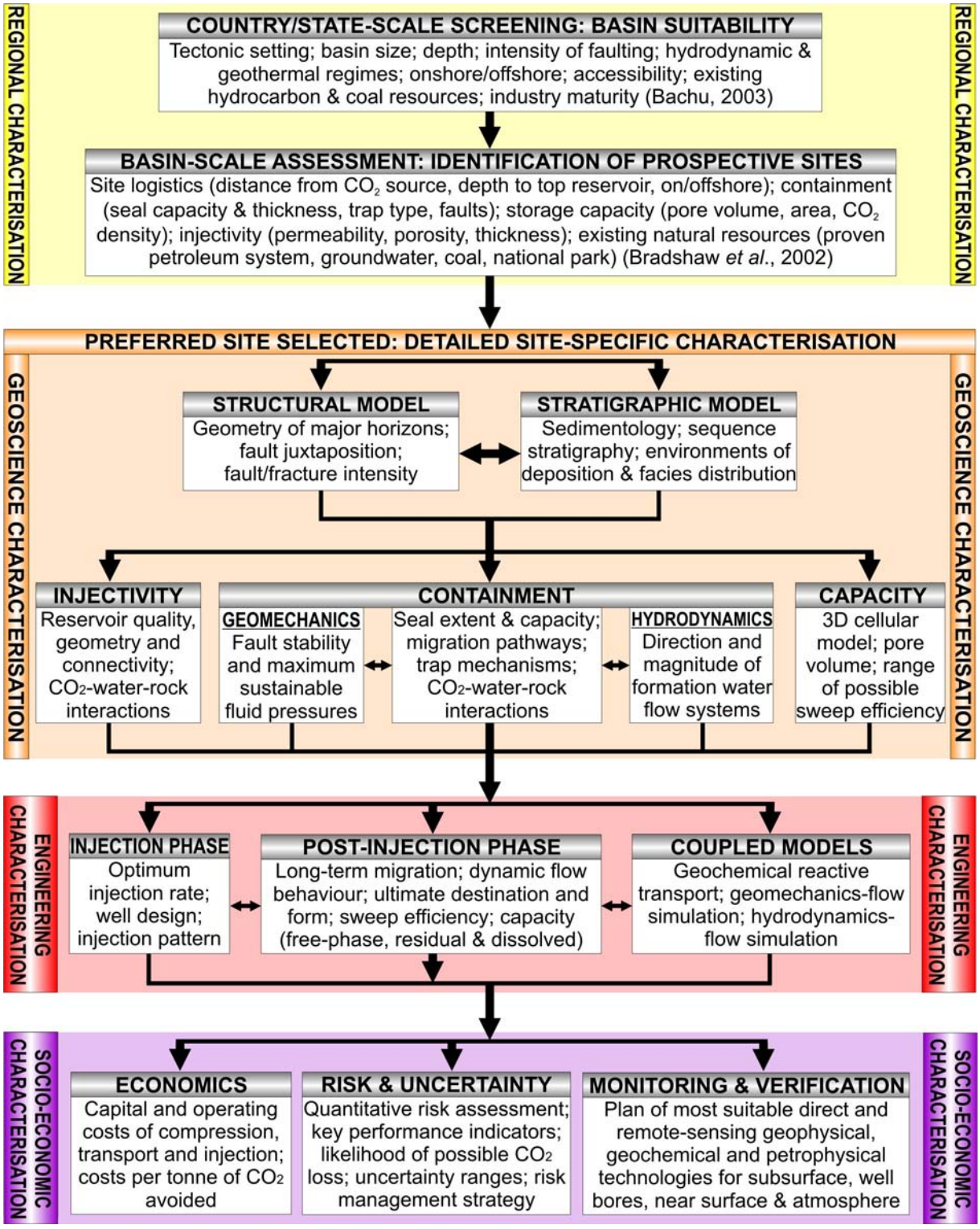

Figure 4.1 Site characterisation workflow for geological storage of CO_2.

4.3 REGIONAL CHARACTERISATION

A regional characterisation process is used to establish the potential of an area for geological storage of CO_2 before an actual site location can be selected. Regional characterisation methodologies have been developed by workers such as Bachu (2003) and Bradshaw *et al*. (2002).

4.3.1 Country/State-Scale Screening: Basin Suitability

Country/state-scale screening represents the coarsest scale of assessment with the least site-specific detail. This level of screening focuses on large geographic areas and evaluates the overall suitability of sedimentary basins for CO_2 storage within a country or state before specific sites are identified and selected for further investigation. The methodology for country/state-scale screening is as follows:

1. **Identify sedimentary basins.** Within sedimentary basins there is potential for CO_2 storage via filling of pore space (e.g. in sandstones and limestones) and/or adsorption onto coals. Areas of crystalline rocks or meta-sediments can generally be disregarded for CO_2 storage due to their low storage capacity and injectivity potential.
2. **Review characteristics of sedimentary basins.** The geological, geographical and industrial characteristics of sedimentary basins can be used as screening criteria. An example is the basin-scale criteria for CO_2 storage developed by Bachu (2003), which includes factors such as tectonic setting, basin size and depth, intensity of faulting, hydrodynamic and geothermal regimes, existing resources and industry maturity. The screening criteria are discussed in more detail below.
3. **Qualitatively or quantitatively rank sedimentary basins in order of suitability.** Once data have been compiled on the characteristics of the sedimentary basins, they can be compared, contrasted and ranked for their suitability for CO_2 storage. This can be done either qualitatively or quantitatively if scores are given for each criterion (e.g. as per Bachu, 2003).

Table 4.1 is a modified version of the basin-scale criteria for CO_2 storage developed by Bachu (2003) and documents the screening criteria that can be used to assess the suitability of sedimentary basins for geological storage of CO_2. For each criterion, the classes are arranged from least favourable (red) to most favourable (green) left-to-right across the table. The

criteria relate to either the containment security, the volume of storage capacity achievable, or consider the economic or technological feasibility.

Table 4.1 Criteria for assessing sedimentary basins for CO_2 geological storage (modified after Bachu, 2003).

Criterion		Classes				
		1	**2**	**3**	**4**	**5**
1	Tectonic stability	Very unstable (e.g. subduction)	Unstable (e.g. synrift, intermontane, strike-slip)	Intermediate (e.g. foreland)	Mostly stable (e.g. passive margin)	Stable (e.g. cratonic)
2	Size	Very small (<1000 km^2)	Small (1000–5000 km^2)	Medium (5000–25000 km^2)	Large (25000–50000 km^2)	Very large (>50000 km^2)
3	Depth	Very shallow (<300 m)	Shallow (300–800 m)		Deep (>3500 m)	Intermediate (800–3500 m)
4	Reservoir–seal pairs	Poor		Intermediate		Excellent
5	Faulting intensity	Extensive		Moderate		Limited
6	Geothermal	Warm basin (>40°C/km)		Moderate (30–40°C/km)		Warm basin (<30°C/km)
7	Hydrocarbon potential	None	Small	Medium	Large	Giant
8	Maturity	Unexplored	Exploration	Developing	Mature	Over mature
9	Coal	None	Very shallow (<300 m)		Deep (>800 m)	Shallow (300–800 m)
10	Coal rank	Anthracite	Lignite		Sub-bituminous	Bituminous
11	Salt	None		Domes		Beds
12	Onshore/ Offshore	Deep offshore (>200 m)		Shallow offshore		Onshore
13	Climate	Arctic	Sub-arctic	Desert	Tropical	Temperate
14	Accessibility	Inaccessible	Difficult		Acceptable	Easy
15	Infrastructure	None	Minor		Moderate	Extensive

The present-day tectonic setting of a basin gives an indication as to the likely tectonic stability of the region, which is an important consideration for containment risk (i.e. tectonically-active areas, such as subduction zones, are the least favourable due to their increased susceptibility to natural earthquake risk and attendant fault seal failure). The basin size and depth reflects the possible storage capacity achievable, as the larger and deeper the

basin is, the greater the likelihood of having laterally extensive reservoir and seal pairings, possibly in more than one stratigraphic interval. The depth of the sedimentary fill of the basin is also relevant to the phase state of the CO_2 (i.e. depths greater than ~800 m result in dense supercritical CO_2 and hence significantly increased storage capacity) and also impacts on the likely economic feasibility, as the greater the depth to the injection target the larger the associated costs of drilling.

The stratigraphy of each area is reviewed to identify possible rock combinations that may provide reservoir and seal pairs. The reservoir–seal pairs criteria is a qualitative assumption about the likely abundance, lateral extent, thickness and depth of possible reservoir–seal horizons. Faulting intensity is both a containment and a capacity issue. The more extensively fractured that an area is, the greater the risk for containment breaches, and the lower the likely storage volume achievable due to the need to inject within individual fault blocks. The geothermal conditions of the basin impact the storage capacity, as within colder basins, more CO_2 can be contained within the same unit volume of rock due to the increased density of the CO_2.

The hydrocarbon potential of a region gives an indication of the suitability of the area for CO_2 storage, on the assumption that if the rocks are suitable for containing and storing oil and gas, then it is likely that they are also suitable for storing CO_2. Maturity of the extractive industries in the region reflects the likely database available, that is the more developed an area is the greater amounts of data available for CO_2 storage assessment.

Coals are potential reservoirs and so their presence in sedimentary basins provides another possibility for CO_2 storage. Shallower coals are likely to have better permeability characteristics (and hence easier injection and less cost) than deeper coals, as well as increased storage efficiency at depths of 300–600 m (in comparison to saline formations/hydrocarbon reservoirs at the same depths). With respect to coal rank, bituminous coals are considered to be the best targets for CO_2 storage; although lignites have a better adsorption capacity, their higher moisture content means that the CO_2 is likely to dissolve into the water rather than adsorb onto the coal's surface.

Evaporites or salt generally provide the best caprock seals, and hence the presence of salt, particularly in beds, is likely to be beneficial to CO_2 containment. Whether a basin is onshore or offshore provides an important economic consideration, as it is likely to be cheaper and easier to implement a CO_2 injection site onshore rather than offshore. The climate of the region affects the likely surface temperatures (and hence the geothermal conditions) and also

the ease of development. Likewise, accessibility and infrastructure reflect the technological feasibility and ease of future developments.

By compiling data on the criteria above, different basins can be compared, contrasted and ranked for their suitability for CO_2 storage. This can be a simple qualitative assessment or, if scores are given for each criterion, the ranking can be performed semi-quantitatively (e.g. Gibson-Poole *et al.*, 2008a) or quantitatively (as per Bachu, 2003). This allows the sedimentary basins within a country or state to be ranked in order of their suitability for geological storage of CO_2.

4.3.2 Basin-Scale Assessment: Identification of Prospective Sites

Once a sedimentary basin has been identified as potentially suitable for CO_2 storage, a basin-scale assessment can be undertaken to locate possible injection and storage sites. This is an intermediate scale of assessment for CO_2 storage evaluation (Figure 4.1). Potential sites can then be scored and ranked in order to identify those that have the highest prospect of successful CO_2 storage and that warrant further detailed site characterisation. The geology of a sedimentary basin is appraised in three basic steps to identify possible CO_2 injection and storage sites:

1. **Review basin stratigraphy.** The stratigraphy of the entire sedimentary basin fill is reviewed to identify suitable rock combinations that may provide reservoir–seal pairs and potentially injectable coal seams.
2. **Determine reservoir–seal pair and coals seam distributions.** The distribution of reservoir–seal pairs and coal seams within the basin are then determined and mapped. It is also useful to establish the minimum and maximum depth distributions of these media where CO_2 storage is likely to be suitable:
    a. For saline formations and hydrocarbon reservoirs, the minimum depth is considered to be the depth where the top of the target reservoir (or base of the overlying seal) is deep enough for injected CO_2 to be in the dense supercritical phase (i.e. ~800 m below surface). The maximum depth may be established based on either permeability or economic constraints, such as the depth at which the permeability of the reservoir is no longer sufficient to allow viable injection rates (e.g. ~3500–4000 m) or the maximum depth for economic drilling of injection wells. The depth

window will vary from basin to basin based on factors such as geothermal gradient, pressure, fluid composition and mineralogy.

b. For coal seams, the minimum depth may be the limit at where the overburden pressure is still sufficient to retain the CO_2 adsorbed to the coal, generally assumed to be 300 m or greater (Bradshaw *et al.*, 2001), or it could be the current (or future) economic depth limit for underground coal mining. The maximum depth may again be determined by the permeability characteristics which control the potential injectivity. Coal seams deeper than 1300–1500 m are commonly expected to be too impermeable to allow sufficient CO_2 injection rates (Bachu *et al.*, 2007).

3. **Assess CO_2 migration pathways and possible traps.** The subsurface geometry of the reservoir and seal units can then be assessed for the likely CO_2 migration pathways and for physical traps, such as structural closures and stratigraphic pinch-outs, to identify possible injection and storage sites. Structural or stratigraphic traps containing existing hydrocarbon accumulations need not be discounted if it can be assumed that these sites will eventually be available but at a later date post-depletion, or can be evaluated as possible candidates for enhanced recovery. A physical structural or stratigraphic trap may not always be necessary if the expected migration pathway is sufficiently long enough to allow residual trapping or dissolution of the injected CO_2 into the formation water before it reaches the edge of the overlying seal, subcritical depths or surface (i.e. hydrodynamic (or retention-time) trap of Bachu *et al.*, 1994).

Once prospective sites have been identified, the relative merits of one potential site over another site can be compared and contrasted by utilising a ranking scheme, such as that devised by the GEODISC™ Program (Bradshaw & Rigg, 2001; Rigg *et al.*, 2001; Bradshaw *et al.*, 2002). Data are compiled for each potential site to assess five key factors fundamental to any potential CO_2 storage site: storage capacity, injectivity potential, site logistics, containment and existing natural resources (Table 4.2).

Table 4.2 Ranking factors for saline formations/hydrocarbon reservoirs as potential CO_2 storage sites (modified after Bradshaw & Rigg, 2001; Rigg *et al.*, 2001; Bradshaw *et al.*, 2002).

Factor	Chance being assessed	Considerations
Storage capacity	Will meet the volume requirements of neighbouring, currently identified CO_2 sources	Temperature, pressure, area, pore volume
Injectivity potential	Reservoir conditions viable for injection	Porosity, permeability, thickness
Site logistics	Site is economically and technically viable	Distance from CO_2 source, water depth, reservoir depth, overpressure
Containment	Seal and trap will work for CO_2	Seal capacity and thickness, trap, faults
Existing natural resources	No viable natural resources in the site that may be compromised	Proven or potential petroleum system, groundwater, coal or other natural resource (e.g. National Park)

1. **Storage capacity.** This evaluates the pore volume available for CO_2 storage at a particular site, and compares it to the likely CO_2 source volume that the site will need to accommodate. This is controlled by parameters such as the size of the injection site area, the thickness of the reservoir, the pore volume available and the density of the CO_2.
2. **Injectivity potential.** This considers the reservoir characteristics, such as porosity and permeability, which will impact on how easily the CO_2 can be injected into the reservoir.
3. **Site logistics.** These are a reflection of the likely economic and technological feasibility, such as how deep an injection well needs to be drilled (depth to reservoir) or how far a pipeline might need to extend (distance from CO_2 source).
4. **Containment.** This considers the seal and trap characteristics, such as the likely effectiveness of the seal based on its thickness, extent and lithology, or the faulting size and intensity and the possibility for leakage via faults.
5. **Existing natural resources.** This assesses the likely presence of another resource that could potentially be compromised by CO_2 storage, such as oil and gas, mineable coal, potable water, or proximity to population centres or national parks, which could limit surface operations.

The storage potential of coal seams can be assessed in a similar manner to saline formations and hydrocarbon reservoirs, focussing on the same five key parameters of storage capacity, injectivity potential, site logistics, containment and existing natural resources. However, the differences in the CO_2 trapping mechanism in coals in comparison to saline

formations/ hydrocarbon reservoirs means that the characteristics under consideration for each factor are different (Table 4.3).

Table 4.3 Ranking factors for coal seams as potential CO_2 storage sites (modified after Bradshaw *et al.*, 2001).

Factor	Chance being assessed	Considerations
Storage capacity	Will meet the volume requirements of neighbouring, currently identified CO_2 sources	Temperature, pressure, rank, ash content, lithotype, seam thickness, continuity, aerial extent
Injectivity potential	Reservoir conditions viable for injection	Permeability, stress regime, mineralisation, structure, rank, lithotype
Site logistics	Site is economically and technically viable	Distance from CO_2 source, coal seam depth, infrastructure, CSM potential
Containment	Seal and trap will work for CO_2	Seal type and thickness, hydrology, trap, fault breaches
Existing natural resources	No viable natural resources in the site that may be compromised	Proven or potential coal resource, groundwater, coal or other natural resource (e.g. National Park)

1. **Storage capacity.** This is the ability of the site to accommodate the necessary source volume of CO_2. In coal seams, this is controlled by parameters such as size of the injection site area (continuity of coal seams), the thickness of the coal seams, the ash and moisture content (low ash and low moisture contents are favourable) and the rank of the coal. Higher ranked coals have greater storage capacity potential due to having greater adsorptive capabilities and methane contents (methane contents can be considered indicative of the CO_2 storage potential, as the adsorptive capability of CO_2 is at least double that of methane).
2. **Injectivity potential.** This is one of the most crucial factors in coal seams, due to the typically low permeabilities (in comparison to saline formations and hydrocarbon reservoirs). Injectivity tends to be more favourable in higher ranked and vitrinite-rich coals, as lower ranked coals have lower permeability due to higher moisture contents and reduced cleat formation.
3. **Site logistics.** These are a reflection of the likely economic and technological feasibility, such as infrastructure (e.g. road access) or how far a pipeline might need to extend (distance from CO_2 source). Coal seam methane potential can also be another important economic indicator; especially if net greenhouse gas

emissions are to be decreased because the methane released through CO_2 storage must be captured (due to its greater greenhouse radiative effect).

4. **Containment.** This considers the possibilities for leakage out of the storage coal seam(s). The CO_2 is most likely to be well-contained where coal seams are at depths greater than 300 m (for sufficient overburden pressure), have limited faulting and are overlain by a suitable seal lithology.
5. **Existing natural resources.** This assesses the likely presence of another resource that could potentially be compromised by CO_2 storage, such as oil and gas, mineable coal, potable water, or proximity to population centres or national parks, which could limit surface operations.

By compiling data on the factors listed above, different sites can be compared, contrasted and ranked for their suitability for CO_2 storage. Following the ranking scheme of GEODISC™ Program (Bradshaw & Rigg, 2001; Rigg *et al.*, 2001; Bradshaw *et al.*, 2002), the sites are qualitatively scored between 0 and 1 for each of the five factors (0 = worst, 1 = best). The factors are then multiplied together to obtain a Chance Factor. The higher the value of the Chance Factor, the more favourable the site characteristics and the greater will be the likelihood of technical and commercial success. This ranking allows each site under analysis to be ranked relative to one another to determine a seriatim of sites within a particular basin in order of preference for further consideration.

4.4 DETAILED SITE CHARACTERISATION

Once potential storage sites have been identified and ranked during the basin-scale assessment stage of investigation, a prospective site has to be further evaluated through a process of detailed site-specific characterisation (Figure 4.1). The subsurface behaviour of CO_2 is influenced by many variables, including reservoir and seal structure, stratigraphic architecture, reservoir heterogeneity, relative permeability, faults/fractures, pressure/temperature conditions, mineralogical composition of the rock framework, and hydrodynamics and chemistry of the *in situ* formation fluids. Therefore, accurate appraisal of a potential CO_2 storage site requires detailed reservoir and seal characterisation, 3D modelling and numerical flow simulation to develop a predictive understanding of CO_2 behaviour in the subsurface (Root *et al.*, 2004; Root, 2007).

The first step in a detailed site evaluation is the geoscience characterisation (Figure 4.1), and in particular, the establishment of a structural and stratigraphic subsurface framework. The structural model determines the shape of the 'container' and the stratigraphic model defines the sedimentary fill. The integration of seismic structural and stratigraphic interpretations with wireline log well correlations, detailed sedimentological core descriptions and biostratigraphy, enable structural and stratigraphic models for the potential sites to be developed. A sequence stratigraphic approach is recommended because it focuses on key surfaces that naturally subdivide the sediment succession into chronostratigraphic units. This is vital to understanding the likely distribution and connectivity of the reservoirs and seals. Three key factors that require further detailed geological characterisation, from the five suggested by Bradshaw *et al*. (2002) in the basin-scale regional characterisation, are: injectivity, containment and capacity. These three factors form the basic requirements for CO_2 storage in geological media and are described in more detail below.

4.4.1 Injectivity

Injectivity is the rate at which CO_2 can be injected into a given reservoir interval (a volume of CO_2 per unit of time) and the ability of the subsequent CO_2 plume to migrate away from the injection well. Upon injection into a reservoir rock, the flow behaviour and migration of CO_2 will depend primarily on parameters such as the injection rate, viscosity ratio and relative permeability, but is also influenced by the stratigraphic architecture, reservoir heterogeneity and structural configuration of the rocks. Injectivity issues that can be assessed through the geological characterisation therefore include the geometry and connectivity of individual flow units, the nature of the heterogeneity within those units (i.e. the likely distribution and impact of baffles such as interbedded siltstones and shales) and the physical quality of the reservoir in terms of porosity and permeability characteristics (Figure 4.1).

The sedimentary depositional models derived from the sequence stratigraphic interpretation will provide information about the reservoir distribution and the likely lateral and vertical connectivity, as the geometry and spatial distribution of individual flow units is a function of their environment of deposition. The quality of the reservoir can be assessed via detailed analysis of core plug porosity and permeability characteristics, petrography and wireline log petrophysical interpretation. In addition, evaluation of injectivity for a site should also incorporate examination of the mineralogical composition of the reservoir, as CO_2

dissolution into the formation water may result in CO_2-water-rock interactions, which can alter the mineralogy and pore system of the rock (Watson *et al.*, 2004a). This can have important implications for injectivity, as mineral dissolution may lead to increased porosity and permeability, but may also result in mobilisation of fine clay minerals and sand grains, or precipitation of new minerals, either of which can block or occlude the porosity and permeability of the reservoir rock and thereby decrease injectivity.

4.4.2 Containment

Containment is the ability of a storage site to securely retain the injected CO_2 in the subsurface. Containment is important in CO_2 storage because injected supercritical CO_2 is less dense than water and, once pressures have relaxed after injection ceases, it will be driven upward towards the surface by buoyancy forces. Consequently, loss of containment could occur through vertical fluid migration via a stratigraphic loss in top seal, faults/fractures and existing well penetrations. Containment issues that need to be assessed therefore include: the distribution and continuity of the seal; the seal capacity (maximum CO_2 column height retention); CO_2-water-rock interactions (potential for mineral trapping); potential migration pathways (structural orientation and dip, and distribution and extent of intraformational baffles); hydraulic gradient (formation water flow direction and rate); integrity of the reservoir and seal (rock strength, fault/fracture stability and maximum sustainable pore fluid pressures) and the completion quality of existing wellbore penetrations (Figure 4.1).

The distribution and continuity of the seal can be assessed from the sequence stratigraphic framework and sedimentary depositional model in the same way as the reservoir units. The potential seal capacity of the regional top seals and localised intraformational seals is a function of their capillary pressure properties and the CO_2-water displacement pressure. This can be assessed by analysis of the fluid properties (e.g. density, wettability and interfacial tension) and by mercury injection capillary pressure (MICP) analysis, using techniques as reviewed by Schowalter (1979), Vavra *et al.* (1992) and Dewhurst *et al.* (2002).

CO_2 introduced into the reservoir system can also chemically interact with the host rock. Detailed petrology, water chemistry and pressure–temperature conditions provide information necessary for modelling potential mineral reactions associated with CO_2, including dissolution, alteration and precipitation. Whereas for injectivity mineral precipitation could be detrimental, for containment purposes mineral precipitation can result in mineral trapping of CO_2 and therefore increased containment security as the CO_2 is permanently trapped

(Bachu *et al.*, 1996; Perkins & Gunter, 1996; Watson *et al.*, 2004a; Watson & Gibson-Poole, 2005).

With regards to potential migration pathways, the buoyancy of the free-phase (immiscible) CO_2 due to its density will cause it to migrate vertically to the top of the reservoir. Stratigraphic heterogeneities, such as intraformational siltstones and shales, have the potential to reduce the effective vertical permeability and create a more tortuous migration pathway for the injected CO_2. Once the CO_2 plume has reached the top of the reservoir, the structural dip and geometry at the base of the overlying seal will have a strong influence on the subsequent migration direction and rate. Trapping mechanisms that can be identified through the geoscience characterisation include physical structural and stratigraphic traps, and potential hydrodynamic or retention-time traps (as defined by Bachu *et al*. (1994) on the basis of long residence time). Other mechanisms such as residual and solubility trapping can be identified through the dynamic numerical flow simulations (as part of the engineering characterisation).

CO_2 injection into the geological subsurface increases the formation pressure, which can then potentially reactivate pre-existing faults or generate new fractures. Opening of fractures or causing slip movement on faults could lead to a loss of containment (Holloway & Savage, 1993; Bergman & Winter, 1995; Streit & Hillis, 2004). Thus, an understanding of the pressure regime and geomechanical modelling needs to be undertaken to estimate maximum sustainable fluid pressures for CO_2 injection that will not induce fracturing and faulting. This requires the determination of prevailing stresses, fault geometries and rock strengths. Details on geomechanical modelling techniques are described in Streit and Hillis (2004).

The rate and direction of flow of the existing formation water flow system within a geological reservoir may influence CO_2 migration pathways and the effectiveness of hydrodynamic, residual and solubility trapping along the migration pathway. Hydrodynamic modelling can be used to assess the formation water flow systems operating within a basin by evaluating the degree of vertical and lateral hydraulic communication and by estimating the direction and magnitude of flow (Bachu *et al.*, 1994; Hennig *et al.*, 2003; Underschultz *et al.*, 2003). An assessment of the hydrodynamic regime is used to provide an understanding of the long-term (hundreds to thousands of years) influence of the formation water flow systems on the injected CO_2. In areas where there has been prior fluid removal from the subsurface (e.g. water extraction or oil production), it may be necessary to interpret both the virgin (pre-production) hydrodynamic regime and the present-day (post-production) hydrodynamic regime, as the existing formation water flow system may have been affected by hydrocarbon

or water production-induced pressure decline. The present-day (post-production) hydrodynamic regime can be used to evaluate the potential short-term (tens to hundreds of years) influence on the predicted migration pathway of CO_2 immediately after injection (Underschultz & Johnson, 2005). The past and present formation water flow systems can be characterised from pressure-elevation plots and hydraulic head distribution maps using standard hydrodynamic analysis techniques as presented by Dahlberg (1995), Bachu (1995), Otto *et al.* (2001) and Bachu and Michael (2002).

4.4.3 Capacity

Capacity is an estimate of the amount of CO_2 that can be stored in the subsurface at a defined storage site location. The amount of CO_2 storage capacity at a specific site is a function of the size of the containment area, the thickness of the reservoir, the effective pore volume of the reservoir rock, the compressibility and/or displacement properties of existing formation fluids and the density of the CO_2 at subsurface reservoir conditions. Due to the flow behaviour of CO_2 in the subsurface, not all potentially available pore volume will become occupied during injection and migration. After initial accumulation around the injection well, the CO_2 will preferentially flow upward due to buoyancy forces or laterally below low permeability zones (i.e. spreading out in thin layers beneath intraformational seals or the regional top seal) rather than filling the entire pore volume. This can make CO_2 storage capacity volumes difficult to calculate, particularly in the reservoir rocks without defined structural or stratigraphic closures, where much of the available rock pore volume can be bypassed in favour of higher permeability zones.

For the geoscience characterisation, potential CO_2 storage capacity can be assessed in terms of available interconnected pore volume; however, the efficiency of that storage capacity will be dependent on the injection rate, rate of CO_2 migration, the dip of the reservoir, the heterogeneity of the reservoir and the potential for fill-to-spill structural closures encountered along the migration path, as well as the long-term prospects of residual trapping, dissolution into the formation water or precipitation of new carbonate minerals. The dynamic numerical flow simulations undertaken as part of the engineering characterisation will give a more accurate assessment of how much of the available pore volume is actually used (sweep efficiency).

4.4.4 Engineering Characterisation

The engineering characterisation phase continues on from the geoscience characterisation (Figure 4.1). Short-term numerical simulation models of the injection phase are needed to provide data on the injection strategy required to achieve the desired injection rates (e.g. number of wells, well design and injection pattern). Post-injection phase numerical simulations evaluate the long-term storage behaviour, modelling the likely migration, distribution and form of the CO_2 in the subsurface. Coupled simulation models, such as geochemical reactive transport, can also be developed to further evaluate the CO_2 storage potential of a site.

4.4.5 Socio-Economic Characterisation

The final stage in a detailed site evaluation is the socio-economic characterisation (Figure 4.1). This includes aspects such as economic modelling, risk and uncertainty analysis and the design of a monitoring and verification program. The economic modelling is necessary to establish the likely capital and operating costs, as well as the cost per tonne of CO_2 avoided. Risk and uncertainty analysis is crucial to establish whether a selected site can be classed as a safe and effective storage site for thousands of years, which is particularly important for public acceptability of a site. The design of a monitoring and verification program is dependent on the geological characteristics of the selected site and needs be carefully evaluated to produce an optimum program both in terms of efficiency and cost.

4.5 SUMMARY

Site characterisation is an important process to describe a site such that a decision can be made as to its potential suitability for CO_2 storage. Site characterisation can be undertaken at different scales of investigation depending on the level of maturity of the project. At each stage of investigation, screening and ranking techniques can help identify the sites with more favourable characteristics to aid prioritisation and selection for further analysis. At the detailed site-specific stage, a potential site can be accurately appraised by applying a comprehensive workflow to analyse the detailed geological and geophysical characteristics of the site. In particular, potential CO_2 storage sites need to be evaluated geologically in terms of their injectivity, containment and capacity. The nature of geological variability means that each potential storage site needs to be assessed individually; however, a similar workflow can be applied to all site evaluations. The geological complexity of any potential CO_2 storage site

is best addressed by a multidisciplinary research effort, which can provide an integrated and comprehensive site characterisation for geological storage of CO_2.